Addis Ababa University

Addis Ababa Institute of Technology

Department of Mechanical Engineering

Thermal Analysis, Design and Experimental Investigation of Parabolic Trough Solar Collector

By

Yidnekachew Messele

Advisor: Dr.-Ing. Abebayehu Assefa

A thesis submitted to the School of Graduate Studies of Addis Ababa University in partial fulfillment of the Degree of Master of Science in Mechanical Engineering (Thermal Engineering Stream)

February 2012

Declaration

I hereby declare that the work which is presented in this thesis entitled "**Thermal Analysis, Design and Experimental Investigation of Parabolic Trough Solar Collector**" is original work of my own, has not been presented for a degree of any other university and that all sources of material used for the thesis have been duly acknowledged.

_____ _____

Yidnekachew Messele Date

This is to certify that the above declaration made by the candidate is correct to the best of my knowledge.

_____ _____

Dr.-Ing. Abebayehu Assefa (Advisor) Date

Acknowledgement

First and foremost, I would like to thank my Lord Jesus Christ for he has made this research a success.

Secondly, I would like to pass my gratitude to my advisor Dr.-Ing. Abebayehu Assefa, Associate Professor of Thermal Engineering staff member, for his continuous support, patience, help, suggestion and courage he has given me for the successful completion of the research. As a mentor he taught me a lot more than the research at hand.

I would like to extend my sincerely appreciation to the staff members of Mechanical Engineering Workshop: AtoTassew, Ato Kassaye and Ato Masresha.

I am very grateful the invaluable support and comment of Yared, Ermias, Addis, Jemal, Tewodros, and colleagues.

Next, I would like to express my cordial thanks to my family for their encouragement and support throughout the study.

Yidnekachew Messele

February 2012

Abstract

Energy is one of the building blocks of modern society. The growth of the modern society has been fueled by cheap, abundant energy resources. Solar energy is a form of renewable energy which is available abundantly and collected unreservedly. In this thesis the application of solar energy using parabolic trough is analyzed. Parabolic trough technology is currently the most extended solar system for electricity production or steam generation for industrial processes. It is basically composed of a collector field which converts solar irradiation into thermal energy and a conventional thermal to electric conversion Rankine cycle.

The prototype of the parabolic trough concentrating solar is collector manufactured using the available materials and equipment in the workshop of Mechanical Engineering Department at AAiT. The prototype is designed using SolidWorks and analyzed in Cosmos software. The thesis work elaborates in detail the steps undertaken in the fabrication of the parabolic trough and other accessory parts used in the experimental setup such as heat exchanger design and pump selection.

An experimental setup has been developed to investigate the performance of the parabolic trough. Measurements of total direct radiation on the plane of the collector, ambient temperature, wind speed, water flow rate, inlet and outlet temperatures of the water inside the absorber tube are collected and employed in studying the performance of the parabolic trough.

A data logger and a computer were employed for data acquisition and the outputs of the experiment are illustrated with the help of graphs plotted using the data logger data import-wizard and Matlab software.

Finally, the efficiency which is used as a measure of performance is calculated. In addition, the experimental results are compared with the result obtained using a mathematical model.

Table of Contents

List of Figures

List of Tables

Nomenclature

$\dot{m}$	Mass flow rate
C_P	Specific heat of the water
T_1	Inlet temperature
k	Thermal conductivity of the water
ρ	Density of the water
ν	Viscosity of the fluid
Pr	Prantle number
ID_t	Internal diameter of the tube
N_P	Number of pass
OD_t	Outer diameter of the tube
N_t	Number of tube
D_S	Shell inside diameter
B	Baffle spacing
N_b	Number of baffles
P_T	Tube pitch
C_T	Clearance between adjacent tubes
A_t	Flow areas in the tube side
A_s	Flow areas in the shell side
V_t	Fluid velocities in the tube side
V_s	Fluid velocities in the shell side
D_e	Shell equivalent diameter
Re_t	Reynolds numbers in the tube side
Re_s	Reynolds numbers in the shell side

Nu_t	Nusselt numbers in the tube side
Nu_s	Nusselt numbers in the shell side
h_t	Convection coefficients in the tube side
h_o	Convection coefficients in the shell side
U_o	Over all heat transfer coefficient of the heat exchanger
A_o	Outer surface temperature of the pipes
S	Temperature Factor
LMTD	Log mean temperature difference
$\dot{Q}_t$	Heat balance in the tube side
$\dot{Q}_s$	Heat balance in the shell side
f_t	Friction factors in the tube side
f_s	Friction factors in the shell side
ΔP_t	Pressure drop in tube side
ΔP_s	Pressure drop in shell side
P_1	Inlet pressure
P_2	Exit pressure
P	Pump Power
g	Acceleration due to gravity
z	Elevation
L	Length of pipe
Δh	Energy loss in the pipe
A	Area of the pipe
$\dot{Q}$	Volume flow rate of the fluid
μ	Dynamic viscosity of the fluid
ε	Pipe roughness
L_{eff}	Equivalent lengths

K	Friction loss factor for fitting
P_m	Electrical motor power input
C	Concentration ratio
W_a	Aperture width
A_a	Aperture area
A_r	Receiver area
F_R	Heat removal factor
F'	Collector efficiency factor
U_L	The sum of convection and radiation heat loss from the heat collecting tube
$\dot{q}'_{3SolAbs}$	Solar irradiation absorption from incident solar irradiation to outer absorber pipe surface
$\dot{q}'_{23Cond}$	Conduction heat flux from outer absorber pipe surface to inner absorber pipe surface
$\dot{q}'_{12Conv}$	Convection heat flux from inner absorber pipe surface to heat transfer fluid.
$\dot{q}'_{35Conv}$	Convection heat from outer absorber pipe surface to ambient
$\dot{q}'_{34rad}$	Heat radiation from outer absorber pipe surface to sky
h_1	Convection heat transfer coefficient inside the tube at T_1
σ	Stefan-Boltzmann constant
ε_3	Emissivity of the outer surface tube
U_L	The sum of convection and radiation heat loss from the heat collecting tube
$\dot{q}'_{used}$	Useful energy gained by HTF
T_a	Ambient temperature
T_t	Receiver tube temperature
I_t	Solar intensity
α_O	Absorptivity of the tube

T_{fo}	The exit temperature of the water in the heat collecting tube
η_{th}	Efficiency
$Q_{collect}$	Amount of solar thermal energy collected
Q_{solar}	Amount of solar radiation from the sun

List of Acronym

ASHRAE	American Society of Heating, Refrigerating and Air Conditioning Engineers
CSP	Concentrated Solar Power
DAQ	Data Acquisition
DNI	Direct Normal Irradiance
DSG	Direct Steam Generation
DNR	Direct Normal Radiation
ECO	Energy Coordination Office Ethiopia
GIZ	Deutsche Gesellschaft fuer Intenationale Zusammenarbeit
HCE	Heat Collecting Element
HTF	Heat Transfer Fluid
LabVIEW	Laboratory Virtual Instrument Engineering Workbench
NI	National Instruments
PTCs	Parabolic-Trough Collectors
SEGS	Solar Electric Generating System
USB	Universal Serial Bus
VI	Virtual Instruments

Chapter One

Background

1.1. Introduction

Energy is one of the crucial inputs for socio-economic development. The rate at which energy is being consumed by a nation often reflects the level of prosperity that it could achieve and total energy consumption has increased along with economic and population growth and, at the same time, various environmental problems associated with human activities have become increasingly serious.

In addition to an increase in price of fossil fuel products and resources will be exhausted in a relatively short period of time. The current high prices of fossil fuel resources are affecting economic and social development worldwide. The impact of energy crises is particularly felt in less developed countries where a high percentage of national budgets for development must be diverted to the purchase of fossil fuel products. To reduce the dependency on imported fuels with high price, most countries have initiated programs to develop alternative energy sources based on domestic renewable resources.

In order to achieve the goals of sustainable development, it is essential to minimize the consumption of finite natural resources and to mitigate the environmental burden to within nature's restorative capacity.

There is now a global consensus that the new sources of energy have to be renewable to satisfy the global energy demand in the long term. Solar thermal power plants are one of the most promising options for renewable electric power production. Unlike traditional power plants, concentrating solar power systems provide an environmentally friendly source of energy, produce virtually no emissions, and consume no fuel other than sunlight.

Ethiopia is one of the countries which are found around the equator in which a better solar radiation exists that creates favorable condition for the exploitation of solar energy. This can make parabolic trough solar power generation system optional for power production in the country.

1.2. Statement of the Problem

Ethiopia, in addition to the persistent food insecurity, is suffering from energy supply. It is observed through studies and recent data, energy consumption increases proportionally to the gross national product. One of the possible methods of overcoming energy crisis is by increasing the use of renewable energy sources such as solar energy, which is freely available.

Because of the proximity to the equator, Ethiopia receives adequate sunshine throughout the year. The annual average daily radiation in Ethiopia reaching the ground is 5.2 kWh/m^2/day. The minimum annual average radiation for the country as a whole is estimated to be 4.5 kWh/m^2/day in July to a maximum of 5.55 kWh/m^2/day in February and March.[1]

Many industries in the country use fuel for water heating process. However, energy costs for heating water is increasing at considerable rate by increasing operating costs and reducing profitability due to continuous escalating of fuel price. Hence, this research explores solar energy as a sustainable alternative for large scale water heating and power generation and it is a step forward to reduce dependency on imported oils.

1.3. Objective of the Study

The general objective of this research is to design, manufacture and experimentally investigate the performance of the prototype parabolic trough solar power generation system. The experimental investigation determines the temperature variations of the circulating fluid, the solar energy absorption rate, the temperature variations of the ambient temperature and the instantaneous efficiency of the system as a function of time.

The specific objectives of the project are:

- Design, modeling and simulation of Parabolic Trough Solar Power Generation System using appropriate software.
- Manufacturing the system using appropriate materials.
- Experimental investigation of the system considering different parameters.

1.4. Methodology

The methods employed to achieve the objectives of the research are:

- **Literature Survey**: Books, journals and articles are reviewed in solar technology, performance improvement and the current solar technology practice of different countries.
- **Prototype Design**: A prototype of the parabolic trough is designed with some specified dimensions. To simplify the design process, appropriate software is used. The applied software also helps to visualize the prototype before manufacturing.
- **Manufacturing prototype**: After the design process is completed, the prototype is manufactured. Based on the design parameters and design materials, the prototype of the parabolic trough is manufactured in the Mechanical Engineering Department workshop of AAiT.
- **Installing the Prototype**: The prototype of the parabolic trough is installed at a site very close to the Mechanical Engineering Department workshop
- **Experimental Investigation**: After the prototype is installed, experimental investigation were conducted by recording data, at least two data for each parameter under consideration.
- **Analysis and Interpreting the Result**: The test results are compiled and compared with the results obtained using a mathematical model to check the validity of the result.

1.5. Significance of the Study

Energy is one of the current issues of the Country. There is a large energy demand in the Country and to fulfill this demand the government is working on different sources of energy.

The result from the study explores solar energy as a sustainable alternative for large scale water heating and power generation and it is a step forward to reduce dependency on imported oils.

The study benefits different industries in reducing the cost related to fuel and other high cost energy sources. This in turn develops the energy alternatives for the industry as well as the Country. In addition, this research can be used as a reference for further study in the area.

1.6. Scope and Limitation of the Project

The scope of this thesis work is to design, manufacture and test the prototype of the parabolic trough based on the design specification and available materials. After the experimental investigation, some conclusion will be drawn based on the test results.

The limitation of this thesis work is that the test is conducted only in Addis Ababa, and does not cover the whole Country. Materials employed for the investigation are those available in the market. Better results would have been obtained if selected materials for improved performance were available in the market.

1.7. Organization of the Study

This study encompasses seven main chapters. The first chapter discusses briefly the background of the study. At the same time, the expected results, the scope and limitation of the research has been stated in this chapter. The second chapter dedicatedly converse literatures related to solar and solar technology and the status of different countries are reviewed. The third chapter mainly focuses on design and manufacturing of the prototype. The installation of the prototype is also discussed in this chapter. The test standards and test equipments implemented in the investigation are identified in the fourth chapter. The mathematical modeling of the parabolic trough has been presented in the fifth chapter. The test results, discussion and the comparison of analytical and experimental results are presented in chapter six. The last chapter, chapter seven, outlines the conclusion, recommendations and future works.

Chapter Two

Literature Review

2.1 Solar Energy

2.1.1 The solar resource

Solar radiation, often called the solar resource, is a general term for the electromagnetic radiation emitted by the sun. Solar radiation can be captured and turned into useful forms of energy, such as heat and electricity, using a variety of technologies. However, the technical feasibility and economical operation of these technologies at a specific location depends on the available solar resource.

Every location on Earth receives sunlight at least part of the year. The amount of solar radiation that reaches any one spot on the Earth's surface varies according to:

- Geographic location
- Time of day
- Season
- Local landscape
- Local weather

Because the Earth is round, the sun strikes the surface at different angles, ranging from 0° (just above the horizon) to 90° (directly overhead). When the sun's rays are vertical, the Earth's surface gets all the energy possible. The more slanted the sun's rays are, the longer they travel through the atmosphere, becoming more scattered and diffuse. Because the Earth is round, the frigid Polar Regions never get high energy from the sun, and because of the tilted axis of rotation, these areas receive no sun at all during part of the year.[2]

From the rays of the sun, which pass through the earth’s atmosphere to the ground, a portion is scattered by particles or clouds. The intensity of solar radiation outside the atmosphere is about 1.3 kW/m². Even though only a fraction of this actually hits the earth’s surface, the magnitude of the energy from this source is enormous. For example, utilizing only 1% of the earth’s deserts and applying a conversion efficiency of 15% to produce electric energy would develop more

electricity than is currently produced worldwide by fossil fuels. [3] This is not practical given the need to distribute the electricity to users around the world, but it does highlight the magnitude of this resource.

Global radiation is radiation energy incident on a surface, which is comprised of a diffuse (scattered) component and a direct normal component (the part coming undisturbed directly from the sun). Figure 2.1 illustrates the definitions of Global, Diffuse and Direct Normal Radiation (DNR).

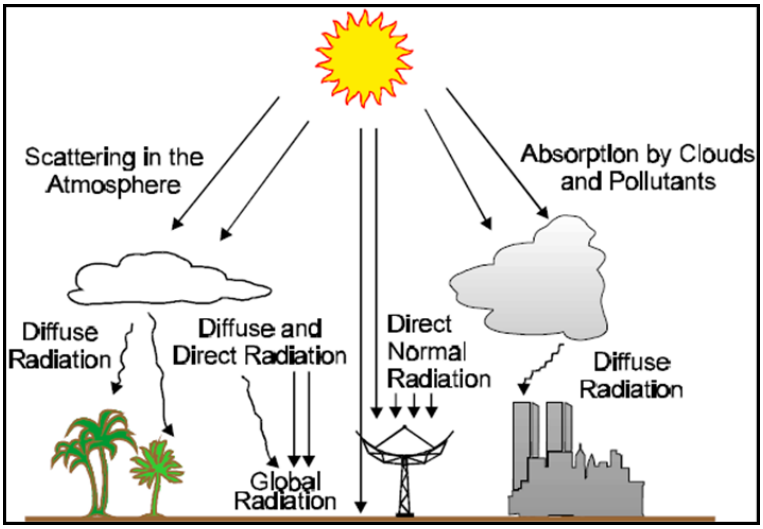

Figure 2.1 Direct normal, diffuse and global radiation [3]

Because the sun is an intermittent resource, its energy is not available throughout the day and seasonally with the same intensity. The angle of the sun's rays relative to the earth's surface changes during the day and with the seasons. The sun is low in the sky in winter, which results in a lower energy flux and causes air temperatures to drop. In summer, the sun is over head and the energy flux is high. Radiation levels are affected by both weather conditions and the length of the path traveled by rays through the atmosphere.

2.1.2 Solar thermal electric power

Classical optical theory predicts that light rays travelling parallel to the axis of a spherical mirror will reflect off the mirror and pass through the focus of the mirror located a distance R/2 from the mirror, where R is the radius of the mirror. [4] The energy of all incident light rays combine

at this point, effectively concentrating the light energy. This concentration produces heat, hence the name: Concentrated Solar Power (CSP). So, in short, CSP systems use different mirror or reflector configurations to convert the sun's energy into high temperature heat. This heat can then be used directly or converted into electricity.

The main components of a CSP system are:

i. The solar collector field

This is the array of mirrors or reflectors that actually collect the solar radiation and focuses it on to the solar receiver. The field is usually quoted in square meters which represents the surface area of the array, not the land use area.

ii. The solar receiver

The solar receiver is the part of the system that transforms the solar radiation into heat. Sometimes this receiver is an integral part of the solar collector field. A heat transfer medium, usually water or oil, is used in the solar receiver to transport the heat to the energy conversion system.

iii. The energy conversion system

The final component in the system converts the heat into usable forms of energy, in the form of electricity or heat.

There are three solar thermal power systems currently being developed: parabolic troughs, power towers, and dish systems. Because these technologies involve a thermal intermediary, they can be readily hybridized with fossil fuel and in some cases adapted to utilize thermal storage. The primary advantage of hybridization and thermal storage is that the technologies can provide dispatch able power and operate during periods when solar energy is not available. Hybridization and thermal storage can enhance the economic value of the electricity produced and reduce its average cost.

These systems can be used for different applications as the concentrated heat they produce is at different temperatures, partly due to the size of the focal area. In the parabolic trough, the focus is the focal axis of the trough collector. In the parabolic dish, the focal area is dependent upon the

radius of the dish and is usually an area of a few hundred m^2. In a central tower, the focal area is much larger, several m^2. [4]

The average level of solar insolation is 1 kW/m^2; the amount of solar energy available on the Earth's surface. This can be concentrated several thousand times using CSP systems. The efficiency with which this radiation can be transformed into thermal energy is dependent up on a combination of optical efficiency and heat conversion efficiency. The optical efficiency of the system is defined by accuracy of the reflective shape of the solar collectors. Heat conversion efficiency is defined by the physical characteristics of the solar receiver to convert solar radiation to thermal energy. Optical efficiencies of up to 98% have been achieved along with heat conversion efficiencies of between 70 and 95%. [4]

In CSP systems that produce electricity, the concentrated heat is used to produce steam, either directly or indirectly, which is then used to produce electricity. The efficiency of this system, solar to electric, is dependent upon the combination of radiation to thermal efficiency and of the steam cycle efficiency. Experimental installations have shown peak efficiencies of up to 29% for parabolic dish systems. [4]

2.1.3 The different concentrated solar power systems

The main concentrated solar power systems are the parabolic trough system, the parabolic dish system and the central tower system.

i. The parabolic dish

A parabolic dish system, or solar dish, as they are sometimes known, is composed of a single structure supporting a parabolic dish covered in mirrors that reflect light on to a solar receiver located at the focal point of the dish, as shown in Figure 2.2.

Solar dishes are being developed mainly for electricity generation and, therefore, the solar receiver is combined with the energy conversion element which is usually a thermal engine, such as a Stirling engine or a Brayton cycle engine.[3]

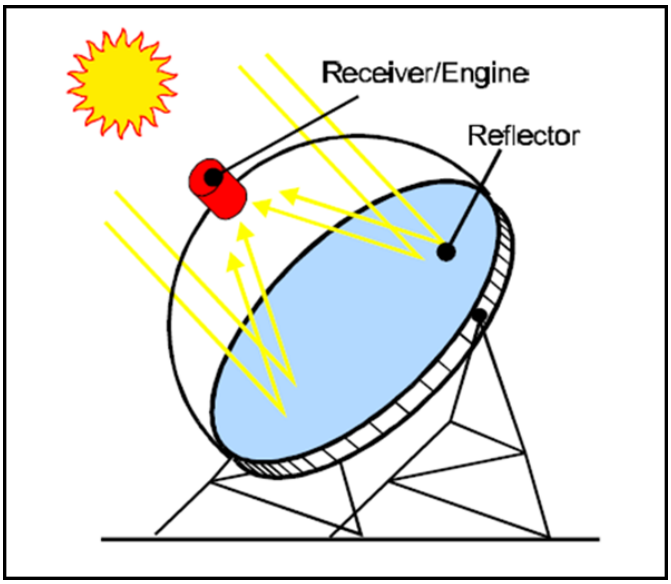

Figure 2.2 Parabolic dish [3]

ii. The central tower system

The central tower system is somewhat different in that the solar collector field is composed of several hundred individual, large sun tracking flat plane mirrors, called heliostats. These heliostats track the path of the sun throughout the days and focus the rays on to the solar receiver, see Figure 2.3. In these systems, a working fluid, either high temperature synethic oil or molten salt is pumped through the receiver. The heated fluid can then be used to generate steam to produce electricity.[3]

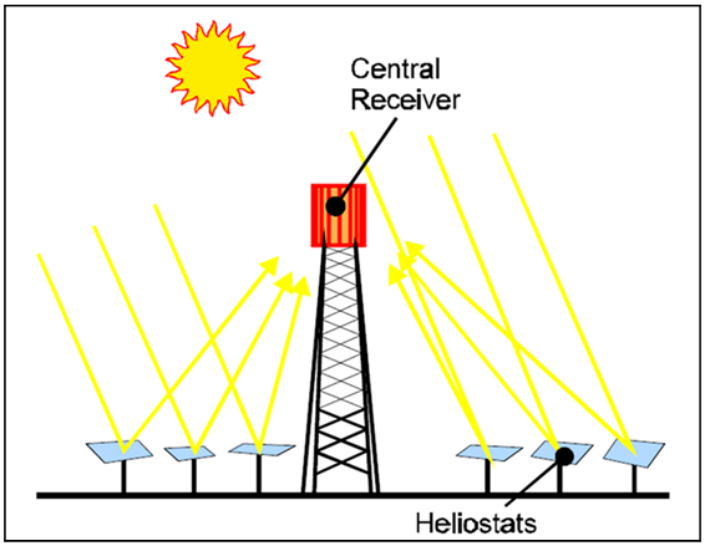

Figure 2.3 Central tower system [3]

iii. The parabolic trough

This is the simplest form of CSP system, [3] where the solar collector field is composed of rows of trough shaped solar collector elements, usually mirrors, with an integral receiver tube, as shown in Figure 2.4. They are parabolic in one dimension only and form a long parabolic shape. The collectors are usually installed in rows and the total solar field is composed of several parallel rows. The collectors are connected to a single motor, controlled by a solar tracking control system, which ensures that the maximum amount of sunlight enters the concentrating system throughout the day. The solar receiver is a black-coated, vacuum glass tube containing the heat transfer fluid, either oil or water. The concentrated sunlight heats the heat transfer fluid, which can then be used to generate electricity using a turbine and an electrical generator.

In this thesis more emphasis is given for parabolic trough technology and discussed in detail.

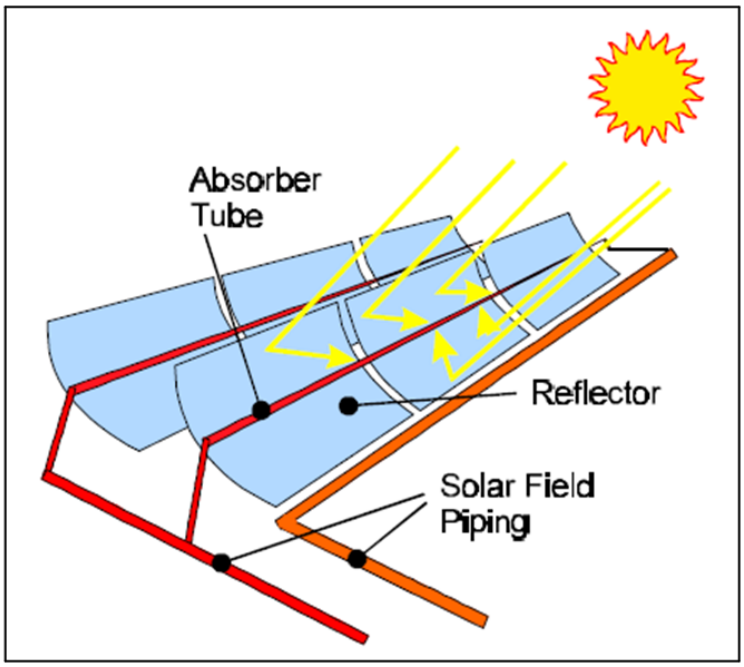

Figure 2.4 Parabolic trough [3]

Comparison of Major Solar Thermal Electric Technologies

Each solar thermal option has its own characteristics, advantages and disadvantages. Table 2.1contrasts the three choices with respect to typical applications, current state of development and special features.[3]

Table 2.1: Comparison of major solar thermal concentrating technologies [3]

	Tower	Dish	Trough
Applications	Grid connected plants, high temperature process heat	Stand alone applications or small power systems	Grid connected plants, process heat
Status	Test and demo units; maximum 10 MWe: commercial status about 1999; designs for integration with combined cycles.	Test and demo units: stand alone systems ≤50 kWe and farms ≤5 MWe; commercial status about 1998.	Commercial size 80 MWe units, total354 MWe operating; designs for integration with combined cycles
Advantages	Good long-term perspective for high efficiencies and storage through high temperatures, hybrid operation possible.	Very high conversion efficiencies, modularity, hybrid operation in development	Commercially available, with 4500 GWh operational experience, hybrid concept proven, storage capability
Disadvantages	Capital cost projections not yet proven; heliostats re-quire very high tracking accuracy; air receiver has reached prototype stage; promising salt receiver system not yet proven	Fossil back-up not yet proven, storage a problem, high cost an issue, development has reached prototype stage	Lower temperatures restrict output to moderate steam qualities through temperature limits of oil

2.2 Parabolic Trough Technology Development

i. Earlier developments

In 212 BC, Archimedes is said to have used mirrors for the first time to concentrate the power of the Sun's rays. In 1615, Salomon De Caux invented a small "solar powered motor" which was the first recorded mechanical application of the Sun's energy. His device consisted of glass lenses, a supporting frame and an airtight metal vessel containing water and air. It produced a small water jet when the air heated up and expanded during operation. [3]

In the mid-1800s a French engineer and math instructor named Auguste Mouchout was granted a patent for solar technology that used the sun to make steam. Mouchout used a dish to concentrate the sun's rays. His invention was an early version of the dish system. He began working on the

project in 1860 in part because he was concerned that his country was too dependent on coal as an energy source.[6]

Mouchout's invention led to innovations on the dish system by other scientists. One of them was John Ericsson. Ericsson came up with a different version of Mouchout's means of using the sun to make power. In 1868, John Ericsson submitted a thesis on "The Use of Solar Heat as a Mechanical Motor-Power", to the Swedish University in Lund.[7] Ericsson attempted to improve on Mouchout's design. He first replaced the dish with a reflector shaped like a combination of a conical dish. Ericsson later replaced this conical dish shape with a parabolic trough. This trough looked like an oil drum cut in half lengthwise. The trough reflected the sun's radiation in a line across the open side of the reflector. What Ericsson came up with evolved into the trough system that is currently used to convert solar energy into electricity.[6]

Ericsson's creation was simple to make. It tracked the sun in a single direction: either north to south or east to west. The trough could not produce the same temperatures or work as efficiently as the dish-shaped reflector. However, Ericsson's design was functional from the beginning. Until his death, he continued to try to improve his design with lighter materials for the reflector.[6]

From 1906 to 1911, an American engineer, Frank Shuman, built and tested a number of solar engines. He used different types of non-concentrating and low-concentrating solar collectors (an absorber with flat reflector wings). Some of them were used for pumping irrigation water in Tacony, Pennsylvania (United States). In 1912, with the knowledge and experience gained in these preliminary tests, Shuman designed and installed a large irrigation pumping plant in Meadi, a small agricultural village south of El Cairo, near the Nile River (Egypt). Shuman worked with Charles Vernon Boys, an English consultant, who suggested substantial changes in the construction of the collectors. Glass-covered boiler tubes were placed along the focal axis of a PTC. These solar collectors produced 0.1-MPa saturated steam directly inside the absorber tube. Each of the five north–south-facing PTC rows was 62.17 m long and 4.1 m wide, providing a total collecting surface of about 1250 m^2 and occupying nearly 4047 m^2 of land. The absorber tubes were 8.9 cm in diameter and had a concentration ratio of 4.6 which resulted in an overall peak absorber efficiency of 40.7% [8][9].

In 1936, C.G. Abbot converted solar energy into mechanical power by using a PTC and a 0.37-kW steam engine. The author claimed an overall system efficiency of 15.5%. A single-tube flash boiler encased in a double-walled evacuated glass sleeve to reduce heat loss was installed along the focal axis. The system was designed to raise full steam pressure within five minutes of exposure to the Sun's rays, producing saturated steam at 374 ^{0}C [8]. In1938 he used a similar boiler in Florida to power a 0.15 kW steam engine. As quoted by Spencer, ''Abbot suggested that a system using this boiler to produce steam at 225 ^{0}C should obtain a theoretical overall efficiency of 15.5% and a real efficiency of 11.7%''[10].

ii. Current parabolic trough developments

Solar radiation is a high-temperature, high-exergy energy source at its origin, the Sun, where its irradiance is about 63 MW/m2. However, Sun–Earth geometry dramatically decreases the solar energy flow down to around 1 kW/m2 on the Earth's surface [11]. However, under high solar flux, this disadvantage can be overcome by using concentrating solar systems which transform solar energy into another type of energy (usually thermal).

Solar radiation is converted into thermal energy in the focus of solar thermal concentrating systems. These systems are classified by their focus geometry as either point-focus concentrators (central receiver systems and parabolic dishes) or line-focus concentrators (parabolic-trough collectors (PTCs) and linear Fresnel collectors).

PTCs focus direct solar radiation onto a focal line on the collector axis. A receiver tube with a fluid flowing inside that absorbs concentrated solar energy from the tube walls and raises its enthalpy is installed in this focal line. The collector is provided with one-axis solar tracking to ensure that the solar beam falls parallel to its axis. PTCs can only use direct solar radiation, called beam radiation or Direct Normal Irradiance (DNI), i.e., the fraction of solar radiation which is not deviated by clouds, fumes or dust in the atmosphere and that reaches the Earth's surface as a parallel beam.

PTC applications can be divided into two main groups. The first and most important is Concentrated Solar Power (CSP) plants. There are currently several commercial collectors for such applications that have been successfully tested under real operating conditions. Typical

aperture widths are about 6 m, total lengths are from 100 to 150 m and geometrical concentrating ratios are between 20 and 30. Temperatures are from 300 to 400 ^{0}C [12]. CSP plants with PTCs are connected to steam power cycles both directly and indirectly. Although the most famous example of CSP plants is the SEGS plants in the United States, a number of projects are currently under development or construction worldwide.

The other group of applications requires temperatures between 100 and 250^{O}C. These applications are mainly industrial process heat (IPH), low-temperature heat demand with high consumption rates (domestic hot water, DHW, space heating and swimming pool heating) and heat-driven refrigeration and cooling. Typical aperture widths are between 1 and 3 m, total lengths vary between 2 and 10 m and geometrical concentrating ratios are between 15 and 20[12]. Most of the facilities are located in the United States, although some have recently been built in other countries. There are also some projects and facilities for other applications such as pumping irrigation water, desalination and detoxification.

Parabolic trough solar fields can supply steam to power plant systems, essentially fulfilling the role of a solar boiler in contrast to fossil fuel-fired boilers. The nature of the intermittent solar energy source is such that the maximum full load operating hours to be expected is about 2,400 hours annually [3]. For this reason it makes good technical land economic sense to choose a power plant configuration that can run on fossil fuel for many additional hours in the year. Plants with the capability to run on solar energy and fossil fuel, called hybrid plants, are described in this section.

iii. Further parabolic trough developments

In an effort to further improve performance and reduce costs in the solar steam generation system, engineering development plans have been formulated for advances in collector design and the solar field system. Work is actively underway in Europe and the US. These plans take several paths.

First, a number of improvements to specific components or subsystems in the parabolic trough solar field of the oil-based SEGS system - the unique element in a solar plant -have been developed. Advances include mirror washing techniques and mirror pad design, transportation methods, installation and replacement of both reflectors and receivers (heat collection elements),

improved optical efficiency and new components e.g., rotating joints instead of flex hoses and redesign of the structural framework. The advanced oil-based system can be viewed as another evolutionary series of improvements to a well-tested technology. In addition, design improvements to lower costs and improve reliability in controls, the power block and balance-of-plant were identified. These included such items as improved mechanical seals on the HTF pumps, upgraded solar field and power block control systems, a single train of solar heat exchangers in contrast to dual trains, optimization of pump groups to reduce parasitic and lower capital costs, and optimization of foundation designs for major equipment.

Second, it was recognized that a dramatic reduction in plant heat rate was required for a solar plant which would operate in a mid- to base-load mode. To achieve this, conceptual designs were envisaged to utilize a parabolic trough solar field with a combined-cycle combustion turbine or steam turbine facility. Progress in this area has been described in the paragraphs above.

Third, a major change was conceived in which steam would be directly generated in the absorbing tubes of the heat collecting element of the solar field (termed direct steam generation, or DSG).This latter approach has the advantage of eliminating the costly synthetic heat transport fluid, intermediate heat transport piping loop and solar-to-steam heat exchangers, as well as offering the potential of better turbine inlet steam conditions.

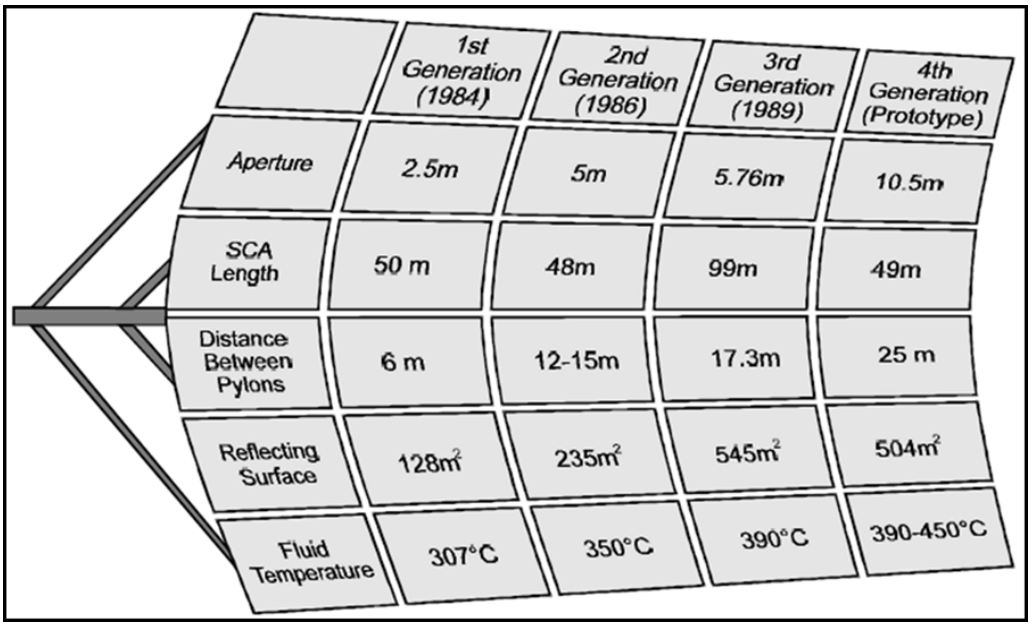

Figure 2.5 Evolutions of solar collector assemblies [3]

2.3 Integration of Parabolic Troughs with Other Energy Systems

2.1.1 Integrated with steam power plants - the SEGS technology

As discussed earlier, the Solar Electric Generating System (SEGS) is fundamentally a steam turbine power plant in which the main fuel is solar radiation. Figure 2.6 shows a schematic diagram of a typical plant configuration.[3]

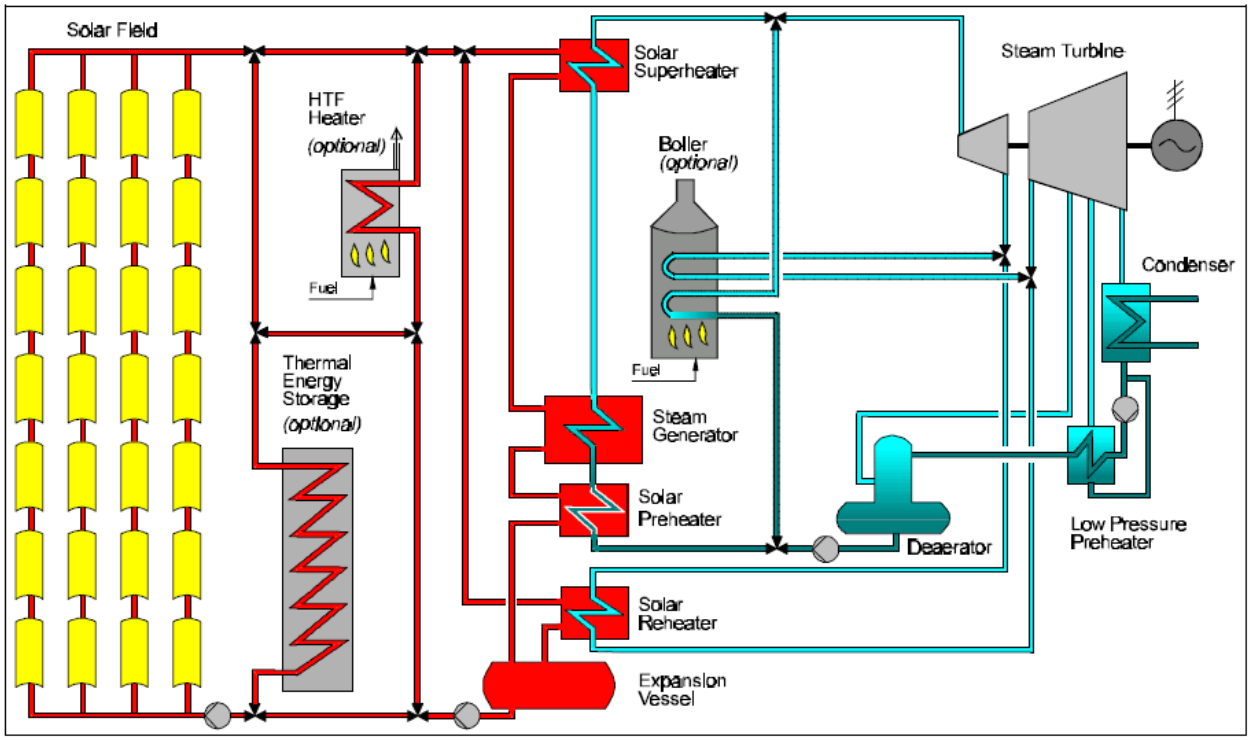

Figure 2.6 Parabolic troughs integrated with steam power plants [12]

The solar field is comprised of parallel rows of Solar Collector Assemblies (SCAs). SCAs supply thermal energy to produce steam to drive a steam turbine or generator. The collectors are single-axis tracking and aligned on a north-south line, thus tracking the sun from east to west. An individual sun sensor device controls the position and tracking of each SCA. All of the SCAs are controlled by a main process computer, the Field Supervisory Controller.[3]

In a parabolic trough solar field of current design heat is transported to the power block via an intermediate loop using synthetic oil (biphenyl-diphenyl oxide) for the Heat Transfer Fluid (HTF). The HTF passes through a heat exchanger system to generate, superheat, and reheat the

steam entirely with solar energy in the solar operating mode. Superheated steam generated by the heat-transfer fluid is then fed to a conventional steam turbine. Spent steam is condensed into water, which returns to the heat exchangers, where it reverts back to steam. After passing through the heat exchangers, the cooled heat-transfer fluid circulates once again through the solar field, thus repeating the process.

2.1.2 Integration of thermal energy storage

For sites where there is a moderate and consistent rise in electrical demand in early evening, an attractive design option is the use of thermal energy storage. Excess solar energy can be collected and stored during the day, and its utilization shifted to the evening to produce electricity. With a corresponding increase in the capacity of the solar field, thermal storage can also be used to increase the capacity factor of a solar power plant without the use of a fossil backup system where fuel is costly or its availability restricted. In either case, thermal storage improves the operation of a solar plant by buffering any rapid changes in solar radiation during the day. The integration of a thermal storage system into a SEGS configuration is shown as an option in Figure 2.6.

2.1.3 Parabolic troughs integrated with other power plants

i. Combined cycles

Conventional combined cycle power plants fired by natural gas are a very cost effective configuration due to excellent performance, cost and emission characteristics. The combined cycle plant consists of a combustion (gas) turbine, heat recovery steam generator and steam turbine. Fuel is combusted in the gas turbine in the normal way, and the hot exhaust gases pass through the heat recovery steam generator and steam turbine. Here the energy from the gases generates and superheats steam to be used in the steam turbine bottoming cycle. Hence, the energy in the gas, or other fossil fuel, is used much more efficiently than in a gas turbine alone. Modern cycles can achieve overall thermal to electric efficiencies of 55% or higher.[3]

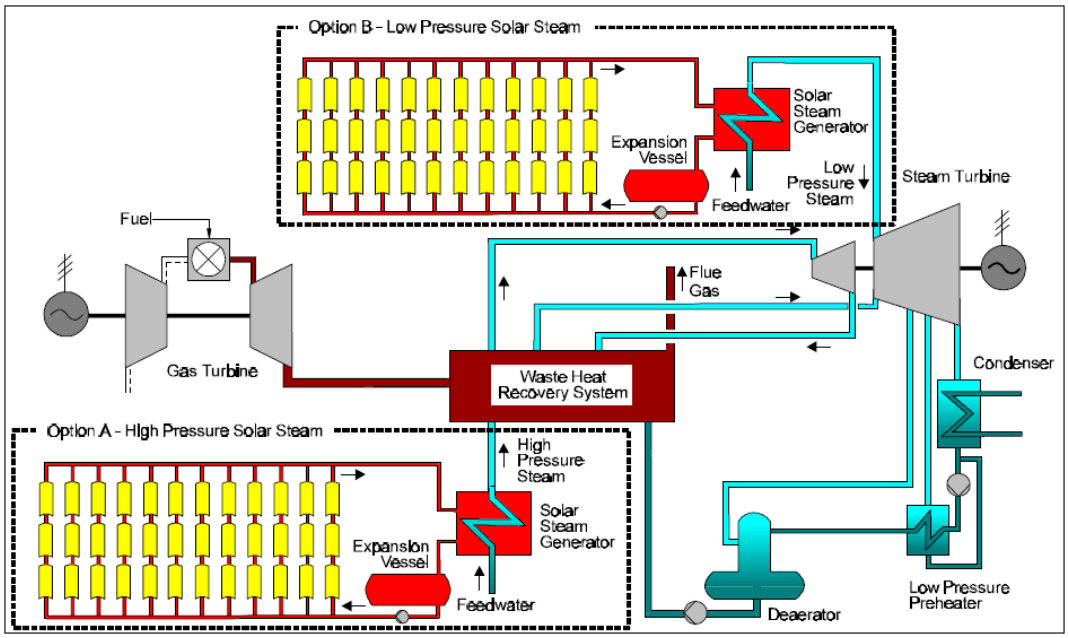

Figure 2.7 Combined cycle system [12]

ii. Coal-fired steam Rankine cycles

Solar steam can also be integrated into a base-load coal-fired Rankine cycle plant. For example, solar steam can be integrated in the lower pressure steam turbine casing. High pressure solar steam can also be fed into the steam drum of the coal-fired boiler, where hot combustion gases would then provide high temperature superheat and reheat. An interesting aspect of integration into a coal fired plant is that solar steam would be displacing or supplementing steam which would be otherwise generated by firing coal, and the unit cost per unit of plant emissions reductions would be more significant than for the case of solar integration in a gas-fired combined cycle.

Chapter Three

Design, Simulation and Manufacturing of the Prototype

3.1 Introduction

Production of a parabolic trough prototype is the major work of this thesis work. The analyses of the test results are dependent on reliable measurements. However, if all the right procedures of design as well as automated production methods are thoroughly followed, the accuracy of the test will converge to the theoretical expectation. Standard design procedures have been implemented to come up with an accurate design, as much as possible, as discussed below.

As far recent tools in design and simulation, the prototype is designed using SolidWorks, which provides both modeling and finite element analysis on its platform (Cosmo work) and far more on that the integration of the mobility on the developed mechanism to the structural architecture is simulated using SolidWork animation.

Production of the prototype needed a coordinated step that will inferred to the limited recourse available in the workshop of the Mechanical Engineering Department – AAiT, available machines, work force, both skilled and labor, and consumable materials. Financial constraints are the major hindrance that induced an inevitable consideration on the production plan starting from the infancy.

The major components of the designed and manufactured parabolic trough system consist of the stand, the trough support and parabolic trough. Each of these components is briefly discussed, with regards to their use, working mechanisms and methods implemented on the production.

3.2 Components of the Prototype

3.2.1 Stand

The stand, four legged, holds all the components up right: parabolic trough support, the ratchet mechanism and tracing mechanism, up from the floor. It has three parts; the lower part of the stand is connected to the concrete foundation using anchoring bolts. The stand is linked to the

upper part of the trough by a mechanism that allows 360-degree (the actual angle of rotation need to trace the sun's position 47.30) rotation of the trough to trace the sun's monthly position.

A ratchet and pinion mechanism is used to fix the trough at one position depending on a pre-determined sun's position on a given month. Both the ratchet and pinion are located at the middle part of the stand. The stand is used as a support as well as contains a mechanism that allows a movement in two axes, one perpendicular to the ground and the other parallel to the direction of the trough axis and the ground.

Figure 3.1 Stand of the parabolic trough

3.2.2 Trough support

This part of the parabolic trough connects the lower part of the support to the upper part of the trough. The parabolic troughs are connected to this support using bearings so that it is free to rotate from east to west to trace the solar position. This part also gives a rigid structural support of the trough with the stand. The connection between the stand and trough support is contact connection so that the trough support can rotate through 360^0 over the stand.

3.2.3 The parabolic trough

The parabolic trough is the most important part of the assembly. The solar radiation strikes the surface of the trough reflected to the focal point. The parabolic trough structure is made from RHS metal and angle iron and the reflecting material is aluminum sheet.

Figure 3.2 Trough support

The development of the concentrator takes the maximum effort for the whole efficiency of the object depends on the capability of the reflector to focus the radiation emanating from the surface. For the development of the concentrator, first, the size of the parabola is determined. Then its focal point position is evaluated which is accessed from the curve mathematical relation given as:

$$y = \frac{x^2}{4P} \qquad (3.1)$$

where: P is the focal point of the parabola

In Equation (3.1), three unknown variables exist that take the equation to indeterminate state, on which the number of unknowns exceeds the number of equations. Therefore, at least two of the unknowns should be defined to have the third variable and take out the equation from indeterminate state. To get a better shape of a parabolic curve some interpolations are done to have a better focal point that best sizes the curve. The interpolation is done by varying the value of the focal point (P) for some interval values of x and y-axis. At most, the selection criterion is manufacturability of the parabola in the workshop using the available machines.

Table 3.1 Iteration of the parabolic curve

Y	-85	-80	-75	-70	-65	-60	-55	-50	-45	-40	-35	-30	-25	-20	-15	-10	-5
X	45.2	40	35.2	30.6	26.4	22.5	18.9	15.6	12.7	10	7.7	5.6	3.9	2.5	1.4	0.6	0.2

Y	5	10	15	20	25	30	35	40	45	50	55	60	65	70	75	80	85
X	0.2	0.6	1.4	2.5	4	5.6	7.7	10	12.7	15.6	18.9	22.5	26.4	30.6	35.2	40	45.2

$$y = \frac{x^2}{4p}$$

P	40

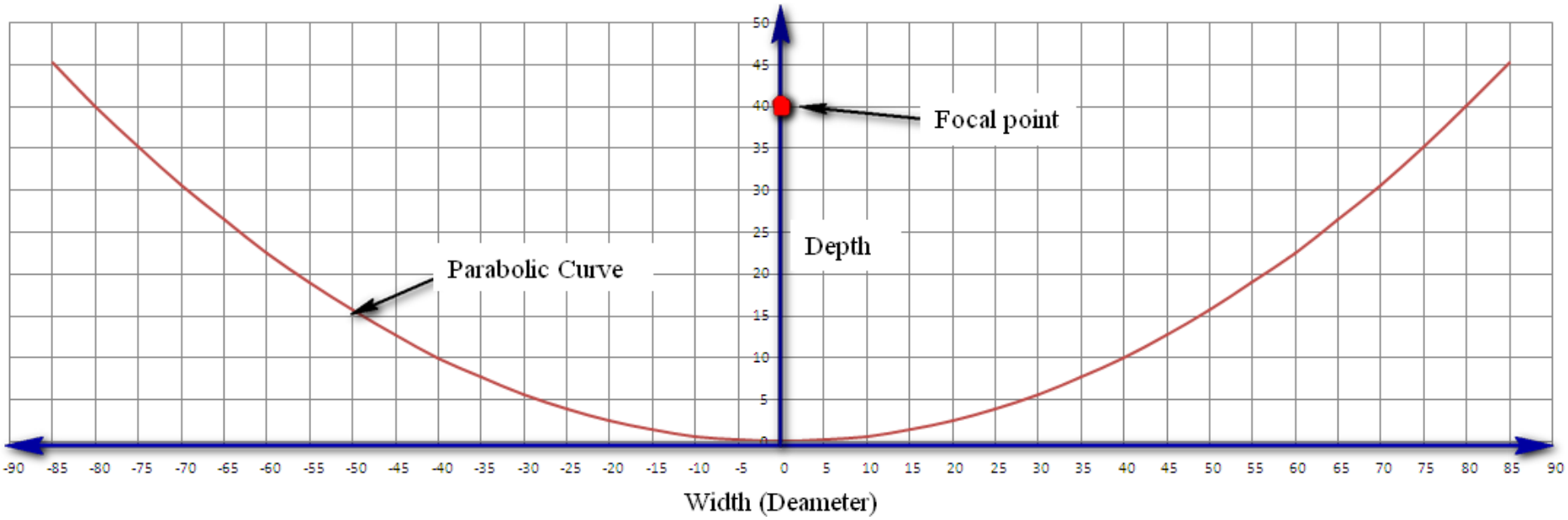

Figure 3.3 The iterated parabolic curve

The above iterated results are checked by using Parabola Calculator version 2.0 software. The software is a Freeware program written to help the designing of solar collector or wifi projects using parabolic reflectors. Weather improving the signal strength of a wifi antenna, or designing a satellite antenna or solar trough program calculates the focal length and (x, y) coordinates for a parabola of any diameter and depth. It can help to determine what size and shape to make a parabola very quickly.

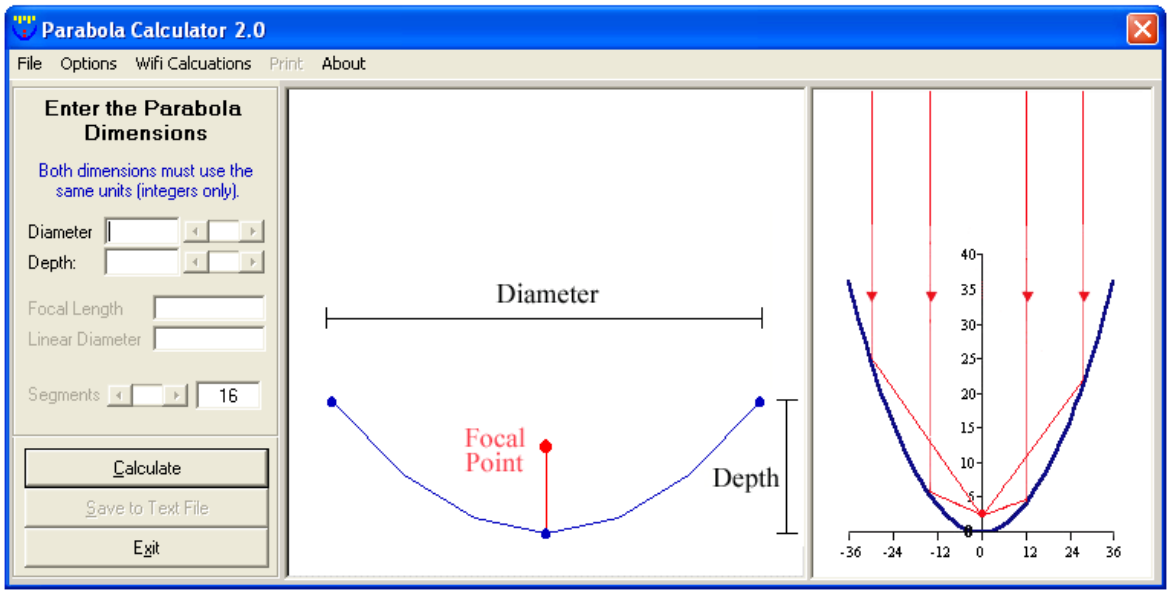

Figure 3.4 Parabola calculator value input window

On the software interface, values of the parabolic curve diameter and depth are fed, then the software calculates the values of focal length, volume, linear diameter and area of the parabolic curve. For this case, from the above iteration the diameter of the parabola is 170 cm and the depth is 45.2 cm. After feeding these values to the software, the result is the same as the result that is obtained from the excel iteration. See the comparison of the two results in the Appendix.

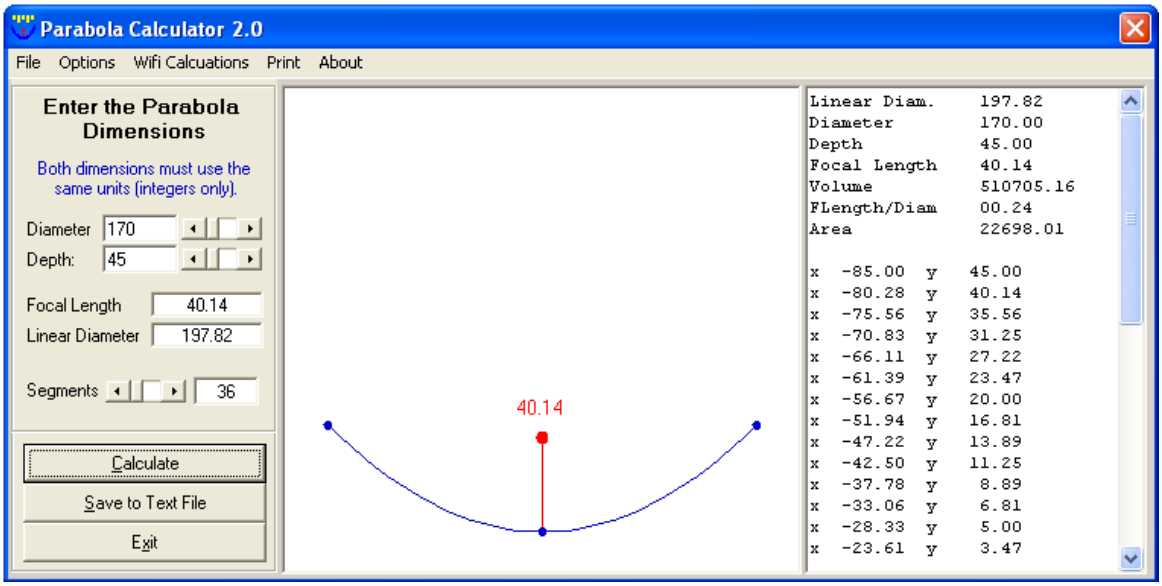

Figure 3.5 Parabola calculator output window

After the parabolic curve is obtained, the next step is to manufacture the curve using the RHS metal frame. First, the RHS metal frame is curved into the obtained parabolic curve, using rolling machine available in the workshop as shown in the figure below.

Figure 3.6 Rolling the metal frame in to parabola curve

To make 5m long and 1.7m diameter parabolic trough, 6 curved RHS are used. These 6 curved RHS components are then connected together with angle iron metals, with interval of 1m between them, as shown in Figure 3.7.

Figure 3.7 The parabolic trough structure

After the structure part is assembled, 2m x 1m x 0.5mm aluminum sheet metals are used to cover the upper part of the parabolic structure. The aluminum reflector sheets are riveted to the structure.

Figure 3.8 The parabolic trough structure covered with aluminum reflector

Two parabolic troughs are connected together using RHS metal frame structure and this RHS metal frame structure also helps to connect the parabolic troughs to the trough support.

Figure 3.9 Connecting structure of the two parabolic troughs

3.2.4 Heat exchanger

Heat exchanger is one of the components of this experimental setup. After the working fluid is heated by the solar radiation, the heat should be rejected at some point in the experiment setup because the working fluid will circulate again through the collector tube. The heat exchanger that is selected for this purpose is shell and tube heat exchanger.

A shell and tube heat exchanger is a class of heat exchanger designs [13] [14]. In their various construction modifications, they are probably the most widespread and commonly used basic heat exchanger configurations in the process industries. As its name implies, this type of heat exchanger consists of a shell (a large pressure vessel) with a bundle of tubes inside it. One fluid runs through the tubes, and another fluid flows over the tubes (through the shell) to transfer heat between the two fluids.

The shell and tube heat exchanger provides a comparatively large ratio of heat transfer area to volume and weight. It provides this surface in a form which is relatively easy to construct in a wide range of sizes and which is mechanically rugged enough to withstand normal shop

fabrication stresses, shipping and field erection stresses, and normal operating conditions. There are many modifications of the basic configuration, which can be used to solve special problems. The shell and tube exchanger can be reasonably easily cleaned, and those components most subject to failure, gaskets and tubes, can be easily replaced.

3.2.4.1 Basic components of shell and tube heat exchangers

While there is an enormous variety of specific design features that can be used in shell and tube exchangers, the number of basic components is relatively small. These are shown and identified in Figure 3.9.

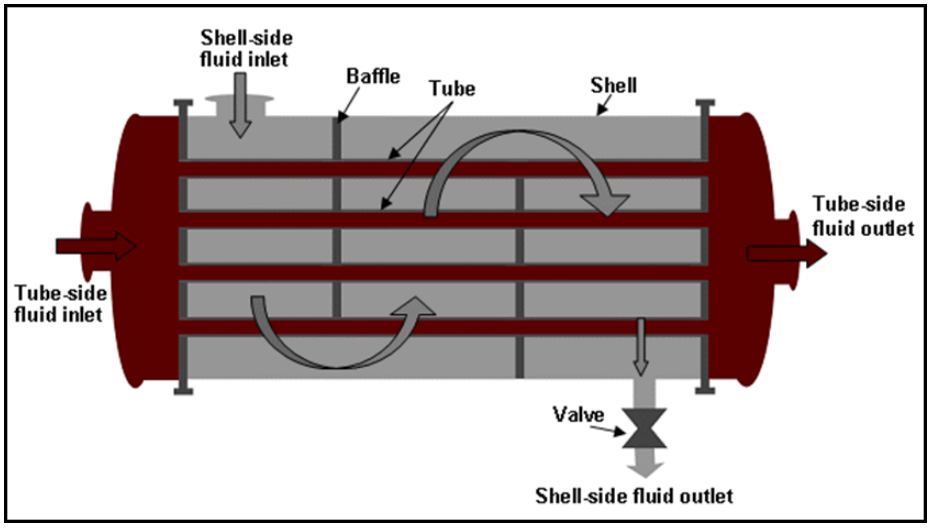

Figure 3.10 Shell and tube heat exchanger

i. Tubes

The tubes are the basic component of the shell and tube exchanger, providing the heat transfer surface between one fluid flowing inside the tube and the other fluid flowing across the outside of the tubes. The tubes may be seamless or welded and most commonly made of copper or steel alloys. Other alloys of nickel, titanium, or aluminum may also be required for specific applications.

ii. Tube sheets

The tubes are held in place by being inserted into holes in the tube sheet and there either expanded into grooves cut into the holes or welded to the tube sheet where the tube protrudes from the surface. The tube sheet is usually a single round plate of metal that has been suitably drilled and grooved to take the tubes (in the desired pattern), the gaskets, the spacer rods, and the bolt circle where it is fastened to the shell.

iii. Nozzles

Shell and shell-side nozzles (flanges)

The shell is simply the container for the shell-side fluid, and the nozzles (flange) are the inlet and exit ports. The shell normally has a circular cross section and is commonly made by rolling a metal plate of the appropriate dimensions into a cylinder and welding the longitudinal joint ("rolled shells"). Small diameter shells (up to around 24 inches in diameter) can be made by cutting pipe of the desired diameter to the connect length ("pipe shells"). The roundness of the shell is important in fixing the maximum diameter of the baffles that can be inserted and therefore the effect of shell-to-baffle leakage

Tube-side channels and nozzles (flange)

Tube-side channels and nozzles simply control the flow of the tube-side fluid into and out of the tubes of the exchanger. Since the tube-side fluid is generally the more corrosives, these channels and nozzles will often be made out of alloy materials (compatible with the tubes and tube sheets, of course). They may be clad instead of solid alloy.

iv. Baffles

Baffles serve two functions: Most importantly, they support the tubes in the proper position during assembly and operation and prevent vibration of the tubes caused by flow-induced eddies, and secondly, they guide the shell-side flow back and forth across the tube field, increasing the velocity and the heat transfer coefficient.

The most common baffle shape is the single segmental, shown in Figure 3.11. The segment sheared off must be less than half of the diameter in order to insure that adjacent baffles overlap

at least one full tube row. For liquid flows on the shell side, a baffle cut of 20 to 25 percent of the diameter is common; for low pressure gas flows, 40 to 45 percent (i.e., close to the maximum allowable cut) is more common, in order to minimize pressure drop.

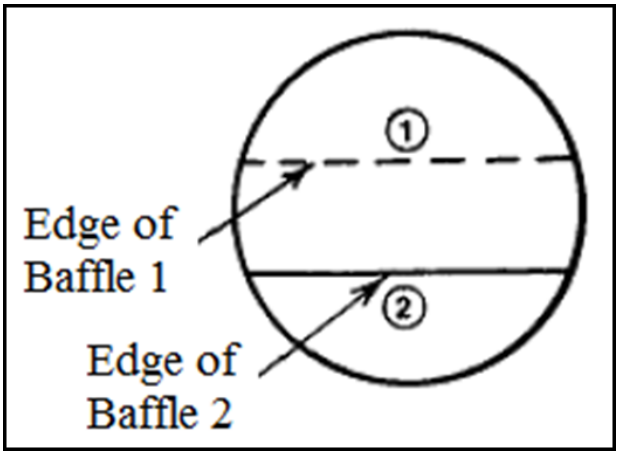

Figure 3.11 Sketch of typical segmental baffle arrangements.

3.2.4.2 Analysis of Shell and Tube Heat Exchangers

Before starting the analysis, first the fluid properties should be determined from table.

Fluid Properties

The fluid properties are read from Table 3.3 based on the inlet temperature.

Assumptions:

- Steady-state conditions exist
- Fluid properties remain constant and are evaluated at the inlet temperature

The warmer fluid properties:

$\dot{m}_t = 1000 liter/hr$; $T_1 = 80^O C$; $\rho_t = 960.63 kg/m^3$

$C_{pt} = 4216.1\ J/kgK$; $k_t = 0.680 W/mK$; $v_t = 0.294 x 10^{-6} m^2/s$

$\Pr_t = 1.74$

Assumptions:

- Steady-state conditions exist
- Fluid properties remain constant and are evaluated at the inlet temperature

The Cooler fluid properties:

$\dot{m}_s = 1200 liter/hr$; $t_1 = 20^O C$; $\rho_s = 1000.52 kg/m^3$

$C_{ps} = 4181.8\ J/kgK$; $k_s = 0.597 W/mK$; $v_s = 1.006x10^{-6} m^2/s$

$\Pr_s = 7.02$

where

$\dot{m}_t$ =mass flow rate C_{pt} = specific heat

T_1 = inlet temperature k_t = thermal conductivity

ρ_t =density v_t = viscosity of the fluid

$\Pr_t$ = prantle number

Tubing Sizes

$ID_t = 0.017m$; $OD_t = 0.02m$;

$N_t = 32$; $N_P = 1$;

where

ID_t =internal diameter of the tube, N_P = number of pass

OD_t = outer diameter of the tube, N_t = number of tube

Shell Data

$D_S = 0.320m$; $B = 0.3m$;

$N_b = 4$; $P_T = 0.04m$;

$C_T = P_T - OD_t = 0.023m$;

where

D_S = Shell inside diameter, B = Baffle spacing

N_b = Number of baffles, P_T = Tube pitch

C_T =Clearance between adjacent tubes

Flow Areas

Tube Side:

$$A_t = \frac{N_t \pi ID_t^2}{4N_p} = 0.01m^2 \quad (3.2)$$

Shell side:

$$A_s = \frac{D_S C_T B}{P_T} = 0.0552m^2 \quad (3.3)$$

Fluid Velocities (Route the fluid with the higher flow rate through the flow cross section with the greater area)

Tube Side:

$$V_t = \frac{\dot{m}_t}{\rho_t A_t} = 0.0278m/s \quad (3.4)$$

Shell side:

$$V_s = \frac{\dot{m}_s}{\rho_s A_s} = 0.0063m/s \quad (3.5)$$

Shell Equivalent Diameter

$$D_e = \frac{3.64P_T^2 - \pi OD_t^2}{\pi OD_t} = 0.093m \quad (3.6)$$

Reynolds Numbers

Tube Side:

$$Re_t = \frac{V_t ID_t}{\nu_t} = 1891.156 \quad (3.7)$$

Shell side:

$$Re_s = \frac{V_s D_e}{\nu_s} = 582.4 \quad (3.8)$$

Nusselt Numbers

Tube Side:

$$Nu_t = \frac{h_i ID_t}{k_t} = 0.023 Re_t^{0.8} Pr_t^n = 11.357 \quad (3.9)$$

where

$n = 0.4$ if fluid is being heated

$n = 0.3$ if fluid is being cooled

Shell side:

$$Nu_s = \frac{h_o D_e}{k_s} = 0.36 Re_s^{0.55} Pr^{1/3} = 22.871 \quad (3.10)$$

Convection Coefficients

Tube Side:

$$h_i = \frac{Nu_t k_t}{ID_t} = 386.138 W/m^2K \quad (3.11)$$

$$h_t = h_i \frac{ID_t}{OD_t} = 328.22 W/m^2K \quad (3.12)$$

Shell side:

$$h_o = \frac{Nu_s k_s}{D_e} = 145.09 W/m^2K \quad (3.13)$$

Exchanger Coefficient

$$\frac{1}{U_o} = \frac{1}{h_t} + \frac{1}{h_o} \Rightarrow U_o = 100.6136 W/m^2K \quad (3.14)$$

Outlet Temperature Calculations

$$R = \frac{\dot{m}_c C_{pc}}{\dot{m}_w C_{pw}} = 0.8 \quad (3.15)$$

$$A_o = N_t \pi OD_t L = 3.02 m^2 \quad (3.16)$$

$$\frac{U_o A_0}{\dot{m}_c C_{pc}} = 0.25 \quad (3.17)$$

Using the values of R and $\frac{U_o A_0}{\dot{m}_c C_{pc}}$, the values of S (temperature factor) can be obtained from Figure 3.12.

$$S = 0.518$$

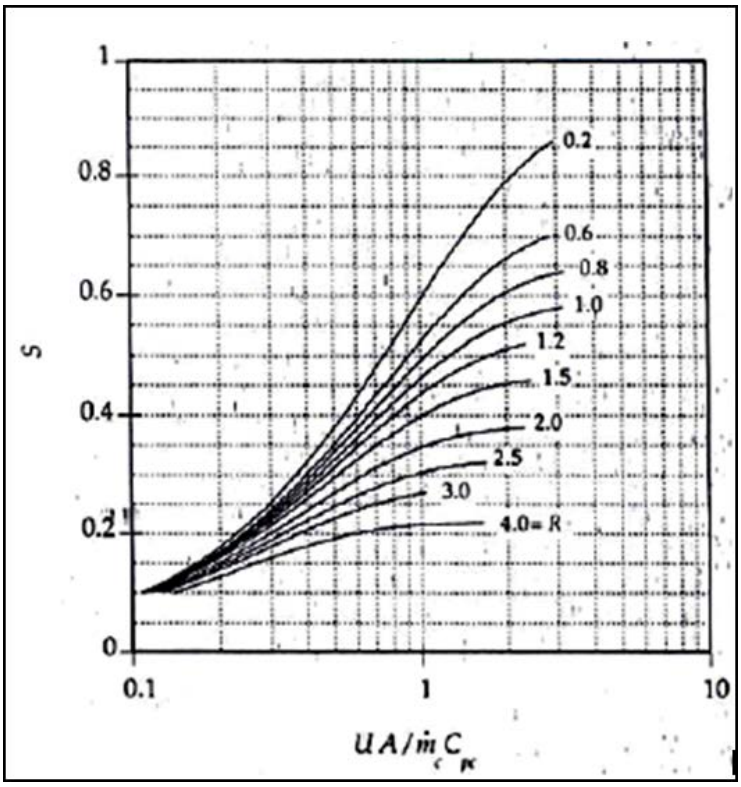

Figure 3.12 Graph of equation

$$t_2 = t_1 + S(T_1 - t_1) = 51.08^O C \tag{3.18}$$

$$T_2 = T_1 - R(t_2 - t_1) = 30.4^O C \tag{3.19}$$

Log Mean Temperature Difference (LMTD)

$$LMTD = \frac{(T_1 - t_2) - (T_2 - t_1)}{ln\left[\frac{T_1 - t_2}{T_2 - t_1}\right]} = 11.96^O C \tag{3.20}$$

Heat Balance

$$\dot{Q}_t = \dot{m}_t c_{pt}(T_1 - T_2) = 55.8346kW \qquad (3.21)$$

$$\dot{Q}_s = \dot{m}_s c_{ps}(t_2 - t_1) = 53.283kW \qquad (3.22)$$

Overall Heat Balance for the Exchanger

Using the values of R and S the value of correction factor can read from Figure 3.13 Graph of Correction Factor for a Shell and Tube Heat Exchanger with 1 Shell Pass and 2 or More Tube Passes.

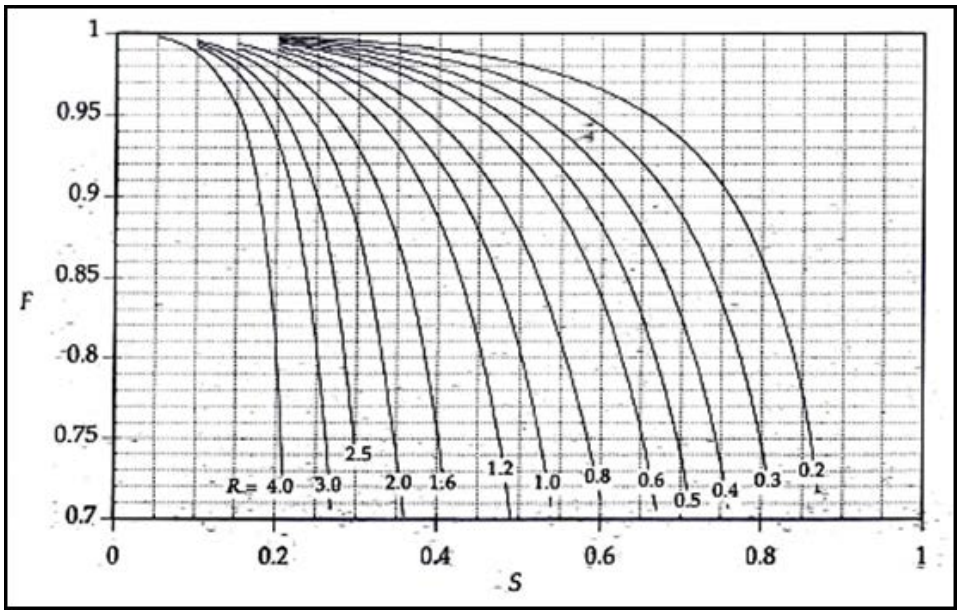

Figure 3.13 Graph of correction factor for a shell and tube heat exchanger with 1 shell pass and 2 or more tube passes

$$F = 0.76$$

$$\dot{Q} = U_o A_o F(LMTD) = 2.761kW \qquad (3.23)$$

Fouling factors and design coefficient

Table 3.2 Water - fouling Factors in [m^2K/W] [15]

Conditions	cooling water < 50 ° C cooled fluid < 120 ° C		cooling water > 50 ° C cooled fluid > 120 ° C	
Water velocity	v < 1 m/s	v > 1 m/s	v < 1 m/s	v > 1 m/s
Type of water	m^2 K/W			
Sea	0.00009	0.00009	0.00018	0.00018
Brackish	0.00035	0.00018	0.00053	0.00035
Cooling tower with inhibitor	0.00018	0.00018	0.00053	0.00053
Cooling tower without inhibitor	0.00053	0.00053	0.00088	0.00070
City grid	0.00018	0.00018	0.00035	0.00035
River minimum	0.00018	0.00018	0.00035	0.00035
River average	0.00053	0.00035	0.00070	0.00035
Engine jacket	0.00018	0.00018	0.00018	0.00018
Demineralized or distilled	0.00009	0.00009	0.00009	0.00009
Treated Boiler Feed water	0.00018	0.00009	0.00018	0.00018
Boiler blow down	0.00035	0.00035	0.00035	0.00035

$$R_{di} = 0.00018 m^2 k / W ; \qquad R_{do} = 0.00018 m^2 k / W$$

$$\frac{1}{U} = \frac{1}{U_o} + R_{di} + R_{do} \Rightarrow U = 97.096 W / m^2 K \qquad (3.24)$$

Friction Factors

$$\text{Tube Side: } f_t = (0.79 \ln Re_t - 1.64)^{-2} = 0.05357 \qquad (3.25)$$

$$\text{Shell side: } f_s = \exp(0.576 - 0.19 \ln Re_s) = 0.53 \qquad (3.26)$$

Pressure Drop Calculations

$$\text{Tube Side: } \Delta P_t = N_p \left(\frac{f_t L}{ID_t} + 4 \right) \frac{\rho_t V_t^2}{2} = 3.239 kPa \qquad (3.27)$$

$$\text{Shell side: } \Delta P_s = f_s (N_b + 1) \frac{D_s \rho_s V_s^2}{2 D_e} = 0.181 kPa \qquad (3.28)$$

From the above analysis the tube and shell pressure drops are bellow the maximum allowable pressure drop that is 70kPa.

Table 3.3 Properties values of liquid in a saturated state [16]

t (^oC)	ρ (kg/m3)	C_P (J/kg.K)	ν (m^2/s)	K (W/m.K)	α (m^2/s)	Pr	β (K^{-1})
Water, H_2O							
0	1002.28	4.2178×	l.788× 10^{-6}	0.552	1.308×10^{-7}	13.6	
20	1000.52	10^3	1.006	0.597	1.430	7.02	0.18×10^{-3}
40	994.59	4.1818	0.658	0.628	1.512	4.34	
60	985.46	4.1784	0.478	0.651	1.554	3.02	
80	974.08	4.1843	0.364	0668	1 636	2.22	
100	960.63	4.1964	0.294	0.680	1.680	1.74	
120	945.25	4.2161	0.247	0.685	1.708	1.446	
140	928.27	4.250	0.214	0.684	1.724	1.241	
160	909.69	4.283	0.190	0.680	1.729	1.099	
180	889.03	4.342	0.173	0.675	1.724	1.004	
200	866.76	4.417	0.160	0.665	1.706	0.937	
220	842.41	4.505	0.150	0.652	1.680	0.891	
240	815.66	4.610	0.143	0.635	1.639	0.871	
260	785.87	4.756	0.137	0.611	1.577	0.874	
280.6	752.55	4.949	0.135	0.580	1.481	0.910	
300	714.26	5.208	0.135	0.540	1.324	1.019	
		5.728					

Based on the above analysis the heat exchanger is manufactured in Vonall.com Company.

Figure 3.14 Heat exchanger manufacturing

3.2.2 Pump

Pump is the driving force of the circulating fluid on this experimental set up. The selection of the pump is done considering the layout of the setup and the availability of the pump in the market.

The theoretical power to circulate fluid in the system is the liquid power P and is calculated as

$$P = \dot{m}\int_{P_1}^{P_2} v dp \qquad (3.29)$$

where:

$\dot{m}$ - mass flow rate of the fluid, kg/s

P_2 - exit pressure, Pa

P_1 - inlet pressure, Pa

v - specific volume, m^3/kg

Since the specific volume of a liquid experiences a negligible changes as it pass the pump, v can be moved outside the integral sign and combined with $\dot{m}$ to give $\dot{Q}$, the volume flow rate. The expression become:

$$P = \dot{Q}(P_2 - P_1) \qquad (3.30)$$

The power required in the actual pumping process by assuming the efficiency of the pump, η_p =45%

$$P = \frac{\dot{Q}(\Delta p)}{\eta_p} \qquad (3.31)$$

The basis for selecting the pump flow rate lies on the standard test procedure suggestion, ASHRAE Standard 93 suggests that testing be done at 2 mL/s per square meter of gross collector area for liquid systems and that the test fluid is water. While it is acceptable to use lower flow rates or a heat transfer fluid other [17].

$$\dot{m} = 0.002 kg/sm^2 \times A$$
$$\dot{m} = 0.034 kg/s \qquad (3.32)$$

where: A- the gross collector area

The volume flow rate is given by

$$\dot{m} = \rho \dot{Q} \tag{3.33}$$

Taking the working fluid density of water 1000kg/m^3

$$\dot{Q} = \frac{\dot{m}}{\rho} = 0.00034 m^3 / s$$

Pump head and pipe loss friction calculation

The head of the pump is calculated using both the Bernoulli equation and Darcy- Weisbach equation. The Bernoulli equation represents pressure content of the fluid at any location in the system: Assuming constant fluid density within the system the Bernoulli equation given by:

$$\frac{V_1^2}{2} + \frac{P_1}{\rho_1} + gz_1 = \frac{V_2^2}{2} + \frac{P_2}{\rho_2} + gz_2 = e \tag{3.34}$$

where:

V - streamline (local) velocity, m/s

P -absolute pressure, Pa (N/m^2)

ρ -density, kg/m^3

g = acceleration due to gravity, m/s^2

z = elevation, m

Pressure drop caused by fluid friction in fully developed flows of all “well-behaved” (Newtonian) fluids is described by the Darcy- Weisbach equation:

$$\Delta p = f\left(\frac{L}{D}\right)\left(\frac{\rho V^2}{2}\right) \tag{3.35}$$

where:

Δp = pressure drop, Pa

f = friction factor, dimensionless (from Moody chart)

L = length of pipe, m

D = internal diameter of pipe, m

ρ= fluid density at mean temperature, kg/m^3

V = average velocity, m/s

This equation is often presented in specific energy form as

$$\Delta h = \frac{\Delta p}{\rho g} = f\left(\frac{L}{D}\right)\left(\frac{V^2}{2g}\right) \tag{3.36}$$

where:

Δh = energy loss, m

g = acceleration of gravity, m/s^2

Based on the layout of the experimental setup lets calculate the head first let start from the pipe friction (layout of the experimental setup shown in Figure 3.16 and Figure 3.17).

From point 1 to 2:

$$A = \frac{\pi d^2}{4} = 5.067 \times 10^{-4} m^2 \tag{3.37}$$

where:

A - Area of the pipe (m^2)

d - Diameter of the pipe (m)

$$V = \frac{\dot{Q}}{A} = 0.671 m/\sec \tag{3.38}$$

where:

V - Velocity of the fluid (m/s)

$\dot{Q}$ - Volume flow rate of the fluid

The friction factor is a function of pipe roughness ε inside diameter d and parameter Re, the Reynolds number.

$$Re = \frac{\rho V d}{\mu} = 16958.438 \tag{3.39}$$

where:

ρ - Density of the fluid (kg/m^3)

μ - Dynamic viscosity of the fluid (N ·s/m^2)

Table 3.4 Density, dynamic and kinematic viscosity of water [18]

$T, {}^0C$	ρ, kg/m^3	μ, $N \cdot s/m^2$	ν, m^2/s
0	1000	1.788×10^{-3}	1.788×10^{-6}
10	1000	1.307×10^{-3}	1.307×10^{-6}
20	998	1.003×10^{-3}	1.005×10^{-6}
30	996	0.799×10^{-3}	0.802×10^{-6}
40	992	0.657×10^{-3}	0.662×10^{-6}
50	988	0.548×10^{-3}	0.555×10^{-6}
60	983	0.467×10^{-3}	0.475×10^{-6}
70	978	0.405×10^{-3}	0.414×10^{-6}
80	972	0.355×10^{-3}	0.365×10^{-6}
90	965	0.316×10^{-3}	0.327×10^{-6}
100	958	0.283×10^{-3}	0.295×10^{-6}

The friction factor is frequently presented on a moody chart giving f as a function of Re with $\frac{\varepsilon}{D}$ as a parameter.

The value of the pipe roughness (ε) is obtained from Ttable 3.5.

Table 3.5 Duct roughness factors [19]

Duct Material	**Roughness Category**	**Absolute Roughness ε ,mm**
Uncoated carbon steel, clean (Moody 1944) (0.05 mm) PVC plastic pipe (Swim 1982) (0.01 to 0.05 mm) Aluminum (Hutchinson 1953) (0.04 to 0.06 mm)	Smooth	0.03
Galvanized steel, longitudinal seams, 1200 mm joints (Griggs et al. 1987) (0.05 to 0.10 mm) Galvanized steel, continuously rolled, spiral seams, 3000 mm joints (Jones 1979) (0.06 to 0.12 mm) Galvanized steel, spiral seam with 1, 2, and 3 ribs, 3600 mm joints (Griggs et al. 1987) (0.09 to 0.12 mm)	Medium smooth	0.09
Galvanized steel, longitudinal seams, 760 mm joints (Wright 1945) (0.15 mm)	Average	0.15
Fibrous glass duct, rigid Fibrous glass duct liner, air side with facing material (Swim 1978) (1.5 mm)	Medium rough	0.9

Fibrous glass duct liner, air side spray coated (Swim 1978) (4.5 mm) Flexible duct, metallic (1.2 to 2.1 mm when fully extended) Flexible duct, all types of fabric and wire (1.0 to 4.6 mm when fully extended) Concrete (Moody 1944) (1.3 to 3.0 mm)	Rough	3.0

The pipe material is galvanized iron from standard table $\varepsilon = 0.09mm$

$$\frac{\varepsilon}{D} = 3.54 \times 10^{-3} \qquad (3.40)$$

Using the value of Re and $\frac{\varepsilon}{D}$, from moody chart the value of friction factor f is 0.026

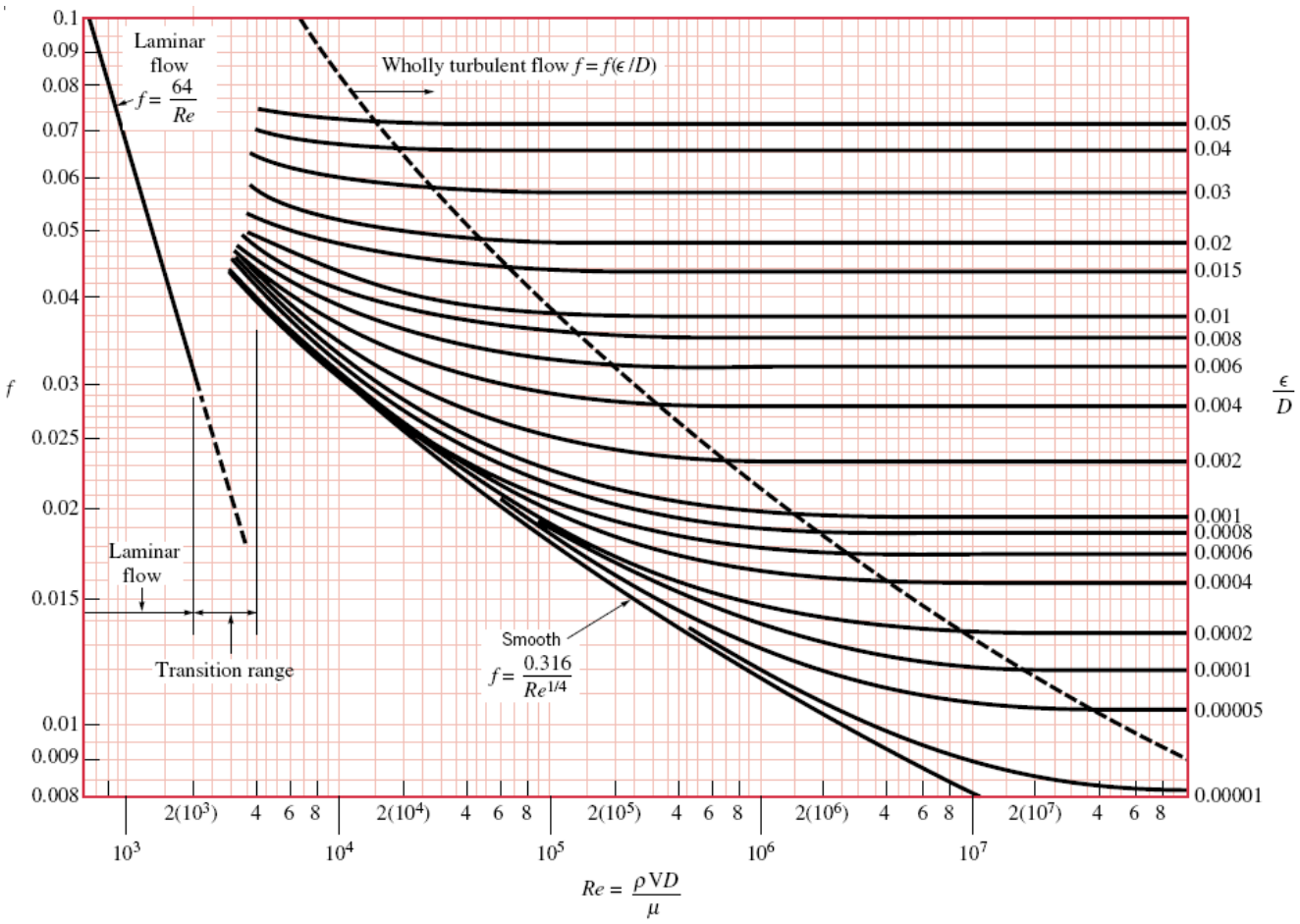

Figure 3.15 Relation between friction factor and Reynolds Number (Moody 1944)[19]

The total head loss for a piping system is determined by adding the equivalent lengths (The effective length) for the fitting and the valves to the pipe length to obtain the total length of the pipe.

Thus this is calculated as:

$$L_{eff} = \frac{KD}{f} \qquad (3.41)$$

where:

L_{eff} = equivalent lengths (m)

K = friction loss factor for fitting

f = friction factor

D = pipe diameter

From point 1 to 2 there is one 90^0 elbow, one check valve and one tee-branch the friction loss factors are listed in table 3.6.

Table 3.6 K factors—pipe fittings [19]

Nominal Pipe Dia., mm	90° Ell Reg.	90° Ell Long	45° Ell	Return Bend	Globe Valve	Gate Valve	Angle Valve	Swing Check Valve	Tee-Branch
10	2.5	-	0.38	2.5	20	0.40	-	8.0	2.7
15	2.1	-	0.37	2.1	14	0.33	-	5.5	2.4
20	1.7	0.92	0.35	1.7	10	0.28	6.1	3.7	2.1
25	1.5	0.78	0.34	1.5	9	0.24	4.6	3.0	1.8
32	1.3	0.65	0.33	1.3	8.5	0.22	3.6	2.7	1.7
40	1.2	0.54	0.32	1.2	8	0.19	2.9	2.5	1.6
50	1.0	0.42	0.31	1.0	7	0.17	2.1	2.3	1.4
65	0.85	0.35	0.30	0.85	6.5	0.16	1.6	2.2	1.3
80	0.80	0.31	0.29	0.80	6	0.14	1.3	2.1	1.2
100	0.70	0.24	0.28	0.70	5.7	0.12	1.0	2.0	1.1

After substituting the values, the equivalent length of elbow is 1.465 and gate valve is 0.234 and the tee-branch is 1.758.

After substituting the values in pressure drop equation, $\Delta P_{(1to3)} = 1142.28Pa$

Using the same procedure the rest pressure losses calculated

$$\Delta P_{(3to5)} = 713.121Pa \quad ; \qquad \Delta P_{(6to7)} = 1028.9Pa$$

$$\Delta P_{(7to8)} = 3239.4Pa \quad ; \qquad \Delta P_{(8to9)} = 1035.8Pa$$

Total pressure loss:

$$\Delta P_{loss} = 6131.501Pa$$

The maximum height that the fluid elevates above the pump is at point 5 and at that point the maximum pump work is required to elevate the fluid. Thus, the pressure required to raise the fluid at point 5 can calculate using Bernoulli equation

$$\frac{V_{\mathrm{Re}}^{\ 2}}{2} + \frac{P_{\mathrm{Re}}}{\rho_{\mathrm{Re}}} + gz_{\mathrm{Re}} = \frac{V_5^{\ 2}}{2} + \frac{P_5}{\rho_5} + gz_5 \qquad (3.42)$$

$$P_5 = 46490Pa$$

The pressure that required by the pump to exert on the fluid (ΔP) is the pressure at point 5 and the sum of all pressure losses in the fluid path

$$\Delta P = P_5 + \Delta P_{loss} = 52621.501Pa$$

The power output of a pump:

$$P = \frac{\dot{Q}(\Delta P)}{\eta_p} = 39.75W \qquad (3.43)$$

The electrical motor power input will be (assuming η_e=90%)

$$P_m = \frac{P}{\eta_e} = 44.17W \qquad (3.44)$$

Based on this result the pump is selected and purchased from the market.

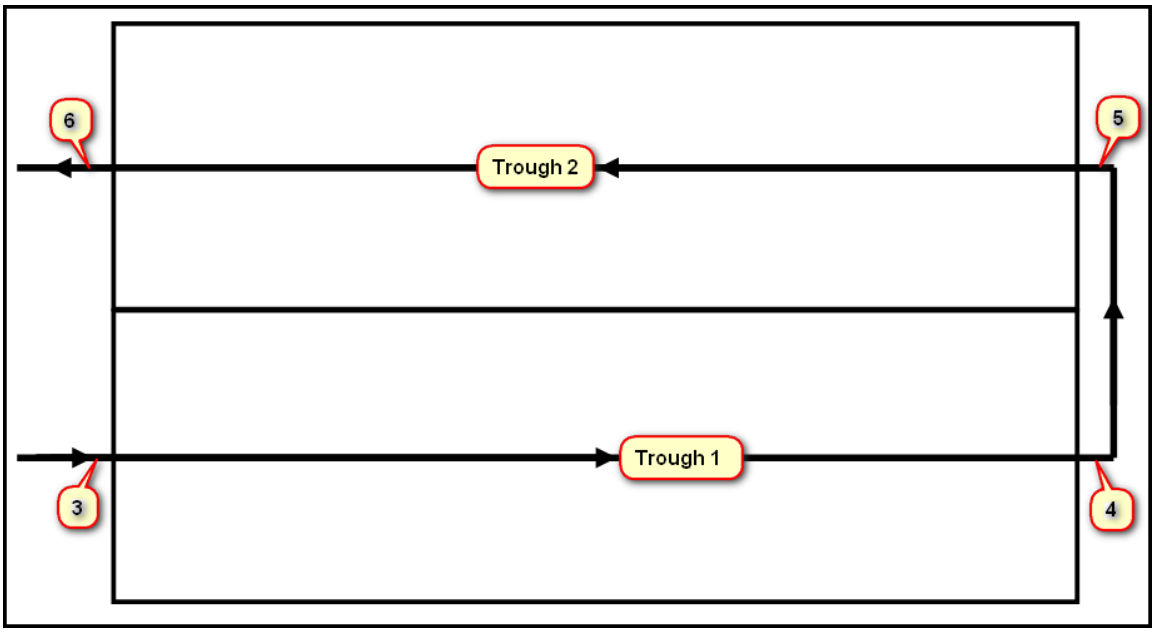

Figure 3.16 Top view of the experimental setup layout

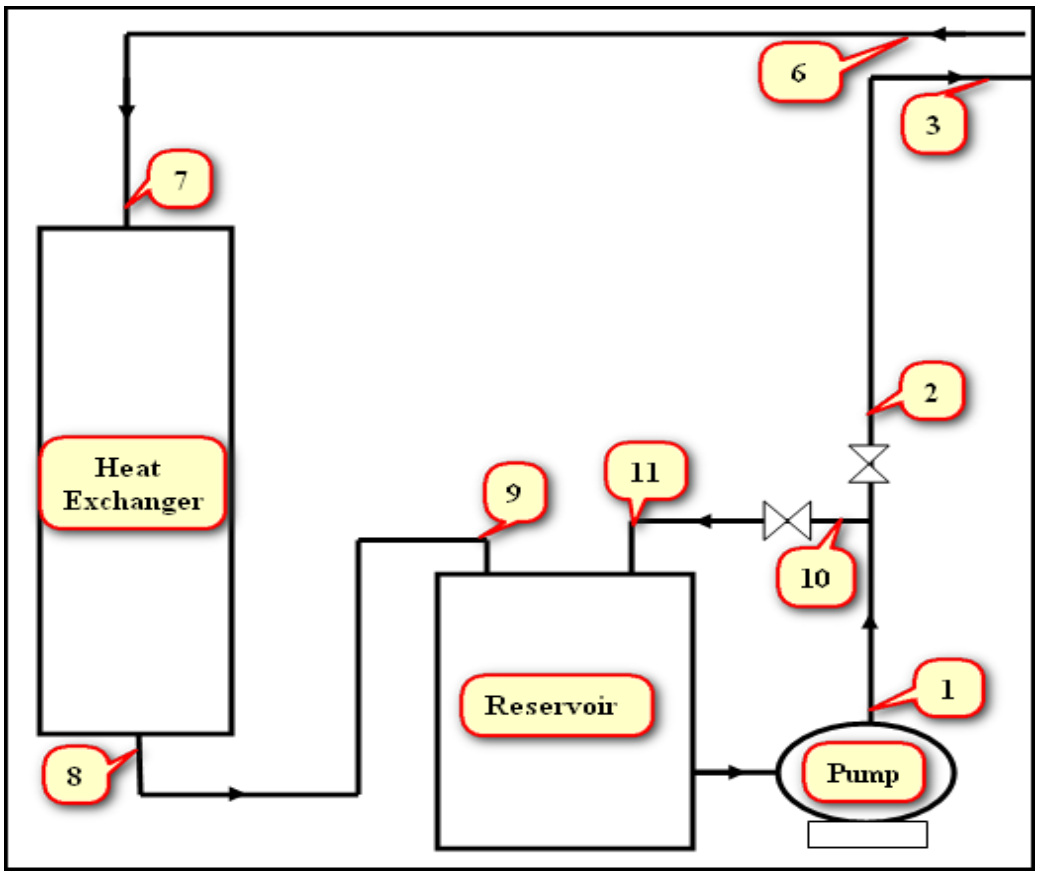

Figure 3.17 Front view of the experimental setup layout

3.2 Installing the Prototype at the Selected Site

Before installing the prototype, the appropriate site is selected for the test. The selection criteria were free from shadow and the availability of wide area that would facilitate the testing procedure. The selected site is free from building shadow starting from 2:30 in the morning up to 10:30 in the afternoon. Hence, for eight testing hours the site clear is from any shadow.

Figure 3.18 Satellite view of the selected site

The first work of the installation is to fence the selected site with the appropriate material that would help test the prototype without any interference and it secures the testing site from any other damages.

Figure 3.19 Fencing the selected site

To install the parabolic trough, first the foundation has to be done. The foundation holds the stand of the parabolic trough with j-bolt connection (the foundation has 2 m length, 1.35 m width, 0.3 m depth below the ground and 0.3 m height above the ground. It is build using the standard concrete materials with the assistance of Civil Engineering Department staff members). The parabolic trough has to face east direction to get the maximum solar radiation by maintaining the trough perpendicular the sun. To find the east direction magnetic compass was utilized.

Figure 3.20 Foundation work of the parabolic trough

After the foundation is dry and ready for installing the parabolic trough, the rest of the parabolic trough components are assembled one by one as shown in the Figure 3.18.

Figure 3.21 Installation of the parabolic trough

The other experimental set up accessories, like heat exchanger, pump, flow controlling valves, flexible hose, flanges and gaskets are installed as shown in the Figure 3.19

Figure 3.22 Experimental set up accessories installation

The parabolic trough is designed to track the sun in any direction. There are two rotational axes to make the tracking system easy. The first rotational axis allows the trough to track the sun from east to west during the day and the second rotational axis allows the trough to rotate in the vertical rotational axis and it tracks seasonal sun direction change from east to northeast and east to southeast.

Figure 3.23 Rotational directions from east to west

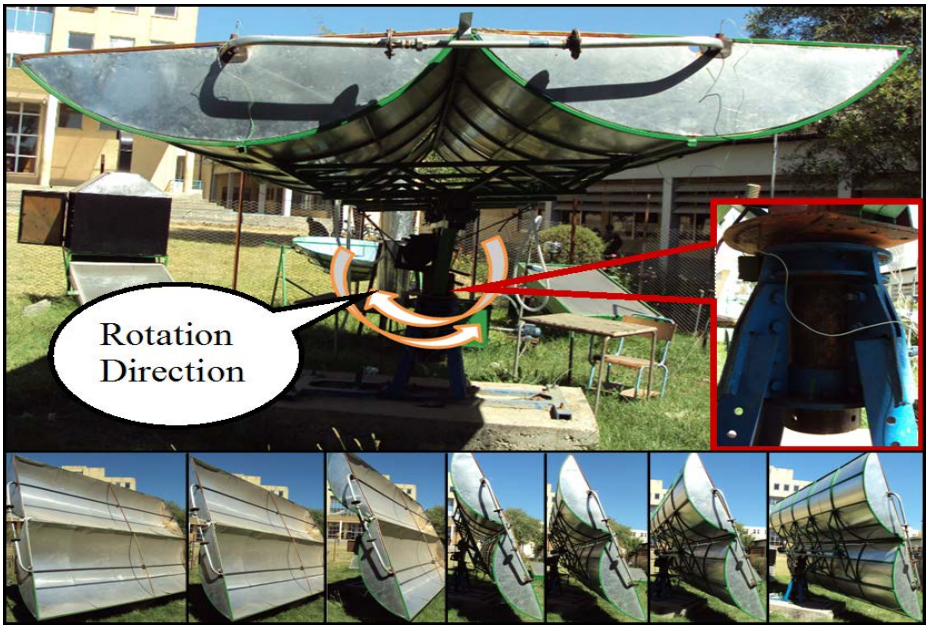

Figure 3.24 Rotational Direction with vertical rotational axis

Chapter Four

Test Standards and Testing Equipment

4.1 Introduction

In recent times major changes in the technology of testing solar collectors have been created. Many new items have come into common use and many older ones are now out of date. ASHRAE Standard 93 gives information on testing solar energy collectors using single-phase fluids and no significant internal storage. The data can be used to predict performance in any location and under any conditions where load, weather, and insolation are known.[19]

To be able to compare the thermal performance of different collectors, a standard test method must be followed.

Requirements

- Testing of full-scale modules is preferred. The size of the collector to be tested shall be large enough so that the performance characteristics determined will be indicative of those that would occur when the collector is part of an installed system. If the collector is modular and the test is being done on one module, it should be mounted and insulated in such a way that the back and edge losses will be characteristic of those that will occur during operation on a structure.
- For tests conducted outdoors to determine thermal efficiency, the collector shall be mounted in a location such that there will be no significant energy reflected or reradiated onto the collector from surrounding buildings or any other surfaces in the vicinity of the test stand for the duration of the test period. Care shall be taken to conduct the tests in a location or manner such that a condition of high ground reflectance is avoided. If significant reflection can occur, provision shall be made to shield the collector by the use of a non reflective shield. In addition, the test stand shall be located so that no shadow will be cast onto the collector by any obstacle at any time during the test period.

- The heat transfer fluid used in the solar collector during testing shall be the same fluid as recommended by the collector manufacturer and shall be the same fluid used throughout the entire test and shall have a known temperature dependence for its density and specific heat over the temperature range of the fluid during the test period. The mass flow rate of the heat transfer fluid shall be the same throughout the test sequence used to determine a thermal efficiency curve, time constant, and incident angle modifiers for a given collector.[17]

4.2 Instrumentation (Apparatus) and Methods of Testing

4.2.1 Solar radiation measurement

A pyranometer (Radiometers) is used to measure the global shortwave radiation from both the sun and the sky, and a solar-tracking pyrheliometer is used to measure the direct normal component of the solar irradiance. The instruments have the following minimum characteristics.

- Change of Response Due to Variation in Ambient Temperature During the Test: The change in the instrument's response due to variations in ambient temperature is less than ±1%.
- Variation in Spectral Response: Pyranometers and pyrheliometers have a constant sensitivity to within ±2% over the spectral range from 0.3 to 2.5 microns.
- Variation of Response with Angle of Incidence: Ideally the response of the pyranometer is proportional to the cosine of the incident angle of the direct solar radiation and is constant at all azimuth angles. Unless the pyranometer's deviation from a true cosine response is less than ±1% for the incident angles encountered during the test(s), the pyranometer used is with the latest calibration curve relating the response to the angle of incidence with an accuracy within ± l%.
- Precautions for Effects of Temperature Gradient: The instrument used during the test(s) is placed in its test position and allowed to equilibrate for at least 30 minutes before data taking commences.

The pyranometer is mounted such that its sensor is coplanar with the plane of the collector aperture. It is not to cast a shadow onto the collector aperture at any time during the test period.[17]

Based on the above standard, the appropriate instrument used in the experimental process is MacSolar Global Irradiance Measuring Device, obtained from Deutsche Gesellschaft fuer Intenationale Zusammenarbeit Energy Coordination Office Ethiopia (GIZ ECO Ethiopia).

MacSolar enables primarily an uncomplicated measuring of actual irradiance values. The sensor, an autarkic power supply and the LCD display are integrated in a compact, robust, weatherproof handy device. The user can therewith immediately obtain information about the solar irradiance conditions for a precise location. The irradiance values are measured using mono-Si solar cells, which also assume the device's power supply. Each device is calibrated by means of a solar simulator and a certified reference cell and the initial high accuracy is guaranteed by an internal automatic compensation mechanism.[20]

Figure 4.1 MacSolar – global irradiance measuring device

4.2.2 Temperature measurements

The temperature difference measuring devices are calibrated for the range of temperatures and temperature differences encountered in the test(s). The recommended devices for measuring the temperature difference of the transfer fluid across the solar collector are:

- A type-T thermopile;
- Precision resistance thermometers, separate or connected in two arms of a bridge circuit;
- Precision thermometers;
- Precision thermistors, separate or connected in two arms of a bridge circuit;
- Matched type-T thermocouples; and
- Other devices equal to or better than those listed above.[17]

Based on the above temperature measuring recommendations, general purpose probes (STK1) thermocouples are used to read the inlet and the outlet temperatures of the working fluid.

The STK1 is a general purpose probe utilizing a nickel-chromium (Chromal)/nickel-aluminium (Alumel), K type, thermocouple sensor. This is contained in a stainless steel sheath of 4.8mm nominal outside diameter, 125mm long, which is, in turn, connected to a two core cable, 5m long. The materials used in the construction of the probe allow its use over a temperature range of -50 to 250 °C. [21]

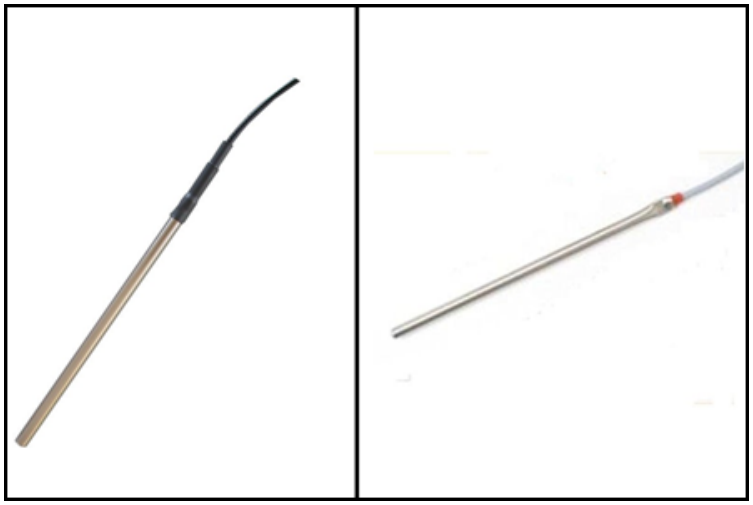

Figure 4.2 STK1 thermocouple

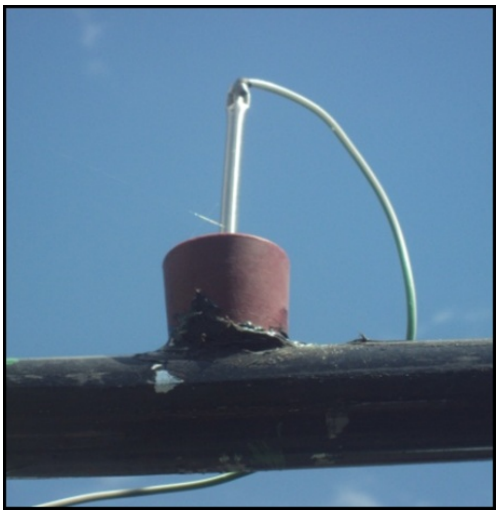

Figure 4.3 Thermocouple connected to the collector pipe to read the temperature

4.2.3 Collector flow measurements

The fluid flow is measured with a turbine type flow meter. The accuracy of the liquid flow rate measurement is equal to or better than ±1.0% of the measured value in mass units per unit time.[17]

The turbine type flow meter is installed for measuring the flow rate water entering the parabolic trough collector. The meter causes a rotor of the small turbine wheel to rotate. In the turbine body a permanent magnet is enclosed so that it rotates with the wheel. The rotation of the magnet energizes the coil in such a way that it produce a signal which is read by the flow meter.

Figure 4.4 Flow rate measurement

4.2.4 Wind velocity

The wind velocity is measured with an instrument and associated readout device that can determine the integrated average wind velocity for each test period to an accuracy of ±0.8 m/s (± 1.8 mph).

The velocity measurement is made in the immediate vicinity of the collector, at a height corresponding to the mid-height of the collector and at a location where the velocity sensor is not shielded from the wind and the sensor does not cast a shadow on the collector during the tests. Wind direction for each test period is also determined and reported.[17]

Figure 4.5 Wind velocity measurement

4.2.5 Ambient temperature

Ambient temperature measurements are representative of the environmental temperature conditions around the collector during testing. The ambient temperature sensor is housed in a well-ventilated instrumentation shelter with its bottom 1.25 m (4.1 ft) above the ground and with its door facing north, so that the sun's direct beam cannot fall upon the sensor when the door is opened. The instrument shelter is painted white outside and is not close to any obstruction than twice the height of the obstruction itself (i.e., trees, fences, building, etc.).[17]

The Delta-T air temperature sensor with a designation of AT2 is a precision thermistor mounted in stainless steel housing. The probe is located within the housing sleeve simply by a piece of

heat shrink sleeve. The housing sleeve fits in the bottom of the solar radiation shield. The AT2 air temperature sensor comprises solar radiation shield that protests the sensor from solar radiation and rain when they are mounted outdoors, bracket, temperature probe with cable attached and housing sleeve.

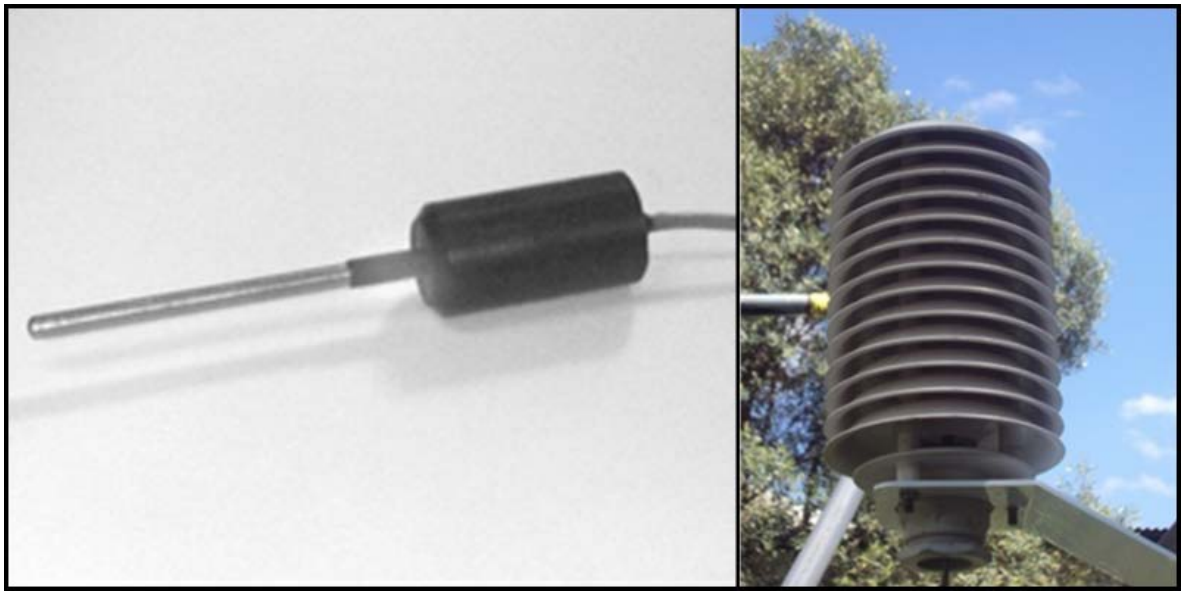

Figure 4.6 Air temperature sensor

4.3 Data Recorders

Analog and digital recorders used have accuracy equal to or better than ±0.5% of the full-scale reading and have a time constant of 1 second or less. The peak signal indication is between 50% and 100% of full scale.[17]

The data recording procedure is under taken using National Instruments NI Compact DAQ data logger with the help of LabView graphical programming environment. The NI cDAQ-9172 is an eight-slot USB chassis designed for use with C Series I/O modules. The NI cDAQ-9172 chassis is capable of measuring a broad range of analog and digital I/O signals and sensors using a Hi-Speed USB 2.0 interface.[22]

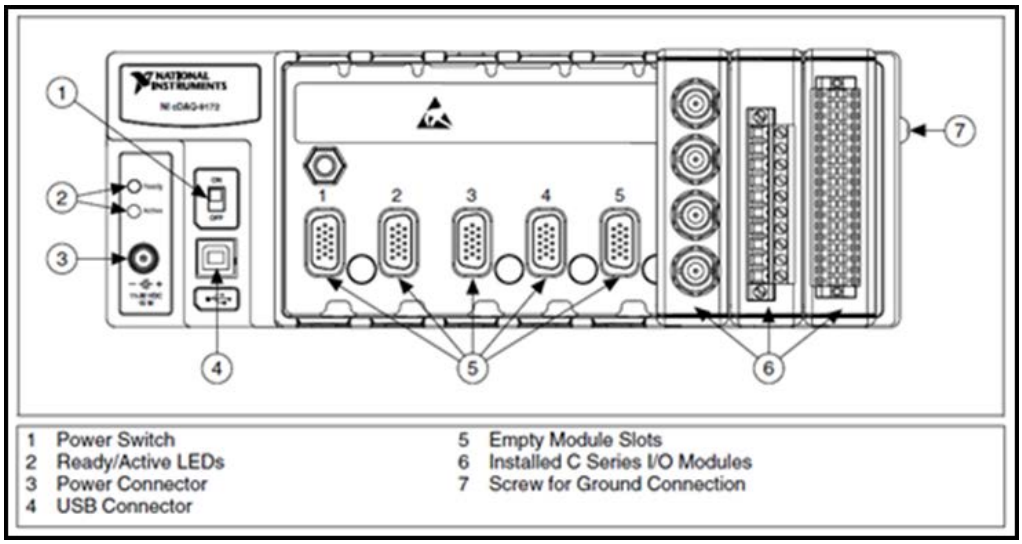

Figure 4.7 NI cDAQ-9172 Chassis [22]

Figure 4.8 NI Compact DAQ USB data acquisition system

i. LabVIEW

LabVIEW (Laboratory Virtual Instrument Engineering Workbench) is a graphical programming language that uses icons instead of lines of text to create applications. In contrast to text-based programming languages, where instructions determine the order of program execution, LabVIEW uses dataflow programming, where the flow of data through the nodes on the block diagram determines the execution order of the VIs and functions. VIs, or virtual instruments, are LabVIEW programs that imitate physical instruments.[23]

In LabVIEW, the user builds a user interface by using a set of tools and objects. The user interface is known as the front panel. The user then adds code using graphical representations of functions to control the front panel objects. This graphical source code is also known as G code or block diagram code. The block diagram contains this code. In some ways, the block diagram resembles a flowchart.

LabVIEW programs are called virtual instruments, or VIs, because their appearance and operation imitate physical instruments, such as oscilloscopes and multimeters. Every VI uses functions that manipulate input from the user interface or other sources and display that information or move it to other files or other computers.[23]

A VI contains the following two components:

- **Front panel**: Serves as the user interface.
- **Block diagram**: Contains the graphical source code that defines the functionality of the VI.

ii. Front panel

The front panel is the user interface of the VI. The user builds the front panel using controls and indicators, which are the interactive input and output terminals of the VI, respectively. Controls are knobs, push buttons, dials, and other input mechanisms. Indicators are graphs, LEDs, and other output displays. Controls simulate instrument input mechanisms and supply data to the block diagram of the VI. Indicators simulate instrument output mechanisms and display data the block diagram acquires or generates. The fig below shows the front panel of the program that used for data recording.

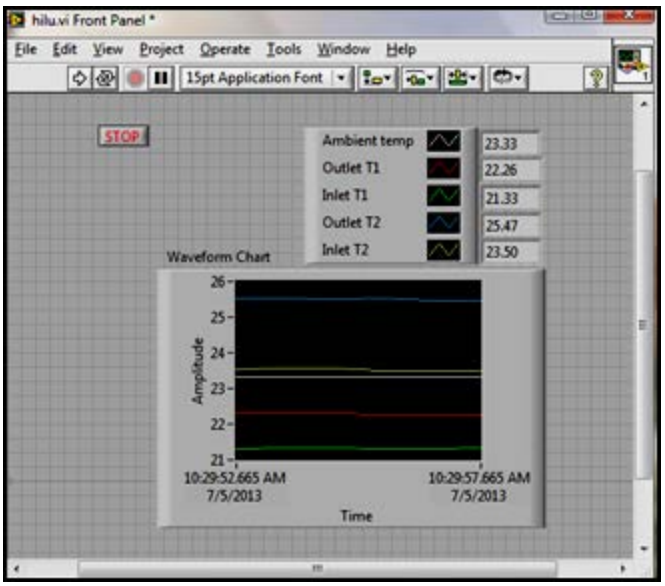

Figure 4.9 Front panel interface

iii. Block diagram

After the user builds the front panel, it adds code using graphical representations of functions to control the front panel objects. The block diagram contains this graphical source code, also known as G code or block diagram code. Front panel objects appear as terminals on the block diagram.

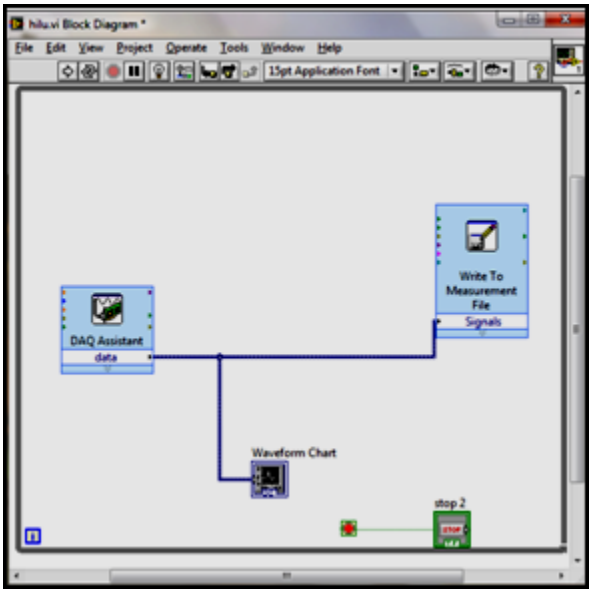

Figure 4.10 Block diagram window

After the front panel and block diagram are generated the next step is to use the USB-6008 and modify the VI to collect samples from it. When the USB cable is connected to the computer the green LED on the device blinks. Using the DAQ assistant window, the type of the thermocouple is seated (like J, K, and T type), the inlet and the outlet sensors are allocated.

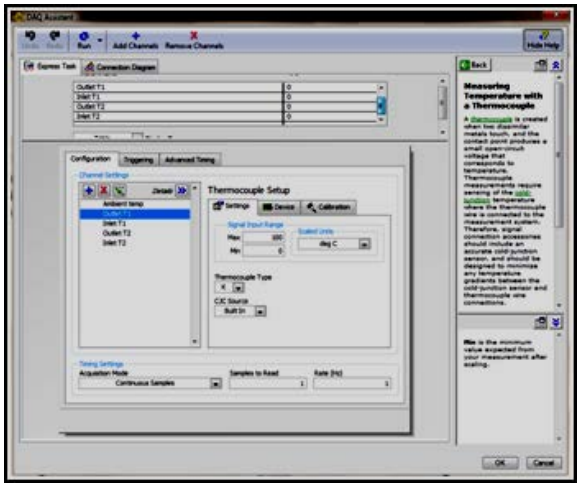

Figure 4.11 DAQ assistant window

4.4 Additional Equipment

A pump and a means of adjusting the flow rate of the heat transfer fluid are provided. The pump is selected based on the Chapter 3 subtopic 3.2.5 procedure. The flow rate is adjusted manually using the flow rate control valves.

Figure 4.12 Water pump

Chapter Five

Mathematical Formulation

5.1 Thermal Analysis of Collector

In analyzing the solar parabolic collector, it is important to identify each and every part of the collector and the terms used on the solar collector. Figure 5.1 briefly describes the solar parabolic collector. In the concept and design of the parabolic collector, the first definition is strictly geometric as ratio of aperture area to receiver area. The ratio of these two areas defines the concentration ratio of the parabolic trough as:[24]

$$C = \frac{A_a}{A_r} \tag{4.1}$$

$$A_a = W_a \times L \tag{4.2}$$

$$A_r = \pi DL \tag{4.3}$$

where:

C = concentration ratio

W_a =aperture width (m)

A_a = aperture area (m^2)

L = aperture length (m)

A_r = receiver area (m^2)

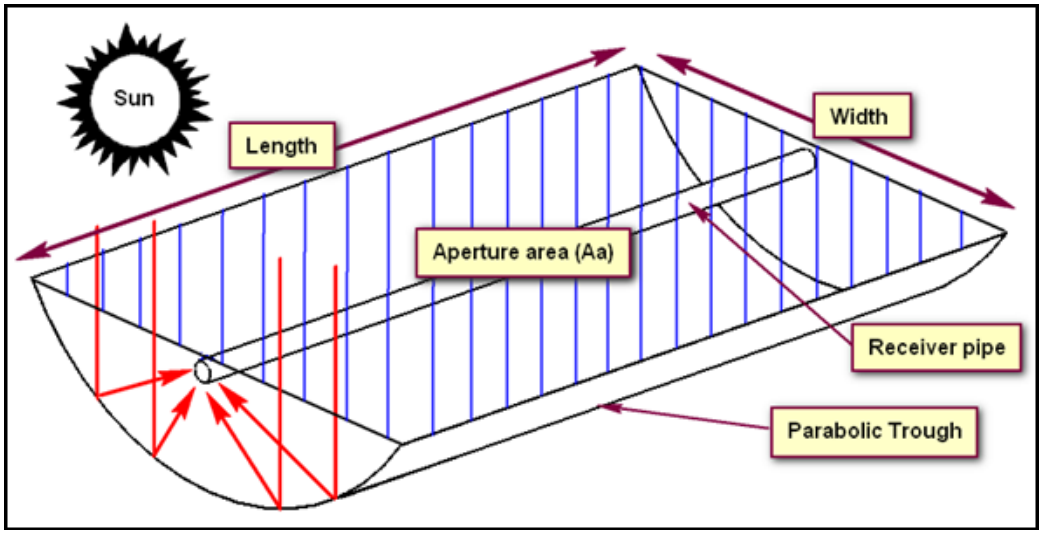

Figure 5.1 Parabolic trough

5.2 Mathematical Modeling of the Parabolic Trough

5.2.1 Heat collecting element (HCE) performance model

The HCE performance model is based on an energy balance on the collector and the HCE. The energy balance includes the direct normal solar irradiation incident on the collector, optical losses from both the collector and HCE, thermal losses from the HCE, and the heat gain into the HTF. Temperature gradient on the receiver can be accounted for by a flow factor F_R to allow the use of inlet fluid temperature in energy balance equation. Thus it is required to drive appropriate expression for the collector efficiency factor F', the loss coefficient U_L, and the heat removal factor F_R to numerically evaluate the outlet temperature.

For short receivers (< 100 m) a one-dimensional energy balance gives reasonable results; for longer receivers a two dimensional energy balance becomes necessary.[25] All the equations and relationships used in one-dimensional HCE performance models are described in the following sections.

5.2.2 One-dimensional energy balance model

The HCE performance model uses an energy balance between the HTF and the atmosphere, and includes all equations and correlations necessary to predict the terms in the energy balance, which depend on the collector type, HCE condition, optical properties, and ambient conditions.

Figure 5.2 shows the one-dimensional steady-state energy balance for a cross-section of an HCE, and Figure 5.3 shows the thermal resistance model and subscript definitions. For clarity, the incoming solar energy and optical losses have been omitted from the resistance model. The optical losses are due to imperfections in the collector mirrors, tracking errors, shading, and mirror and HCE cleanliness. The effective incoming solar energy (solar energy minus optical losses) is absorbed by the selective coating ($\dot{q}'_{3SolAbs}$). Some energy that is absorbed into the selective coating is conducted through the absorber ($\dot{q}'_{23Cond}$) and transferred to the HTF by

convection ($\dot{q}'_{12Conv}$); remaining energy is transmitted back to the environment by convection ($\dot{q}'_{35Conv}$)and radiation ($\dot{q}'_{34rad}$).

The model assumes all temperatures, heat fluxes, and thermodynamic properties are uniform around the circumference of the HCE. Also, all flux directions shown in Figure 5.2(a) are positive. And all the terms in above paragraph are defined in Table 5.1. Dotted variables indicate rates and the prime indicates per unit length of receiver. A double prime will indicate per unit normal aperture area.

Table 5.1 Heat flux definitions

Heat Flux Heat Transfer Path (W/m)	Heat Transfer Mode and Transfer Path
$\dot{q}'_{3SolAbs}$	Solar irradiation absorption from incident solar irradiation to outer absorber pipe surface
$\dot{q}'_{23Cond}$	Conduction heat flux from outer absorber pipe surface to inner absorber pipe surface
$\dot{q}'_{12Conv}$	Convection heat flux from inner absorber pipe surface to heat transfer fluid.
$\dot{q}'_{35Conv}$	Convection heat from outer absorber pipe surface to ambient
$\dot{q}'_{34rad}$	Heat radiation from outer absorber pipe surface to sky

With the help of Figure 5.2, the energy balance equations are determined by conserving energy at each surface of the HCE cross-section.

$$\dot{q}'_{12conv} = \dot{q}'_{23cond} \tag{4.4}$$

$$\dot{q}'_{3SolAbs} = \dot{q}'_{23Cond} + \dot{q}'_{35Conv} + \dot{q}'_{34rad} \tag{4.5}$$

$$\dot{q}'_{HeatLoss} = \dot{q}'_{35Conv} + \dot{q}'_{34rad} \tag{4.6}$$

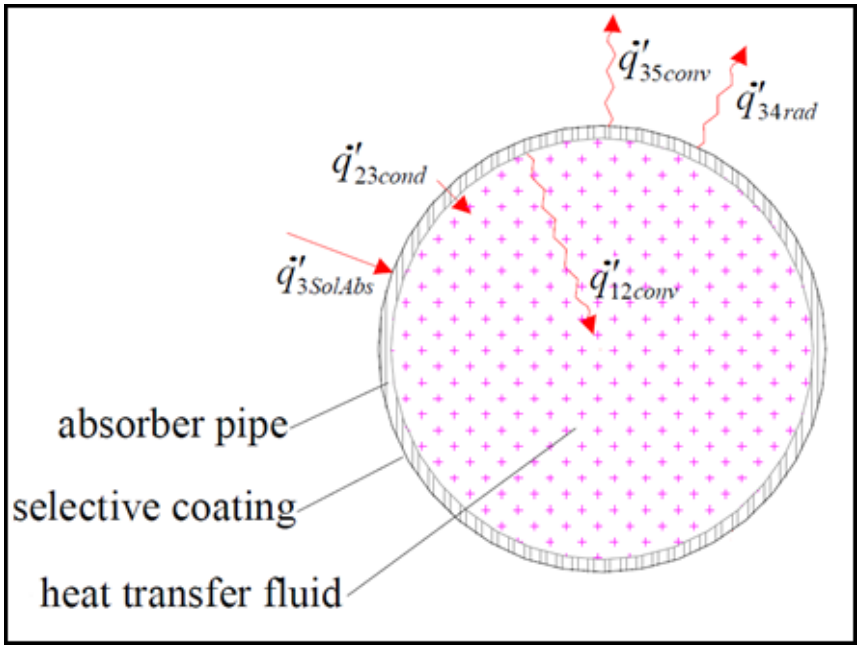

Figure 5.2 One-dimensional steady-state energy balance

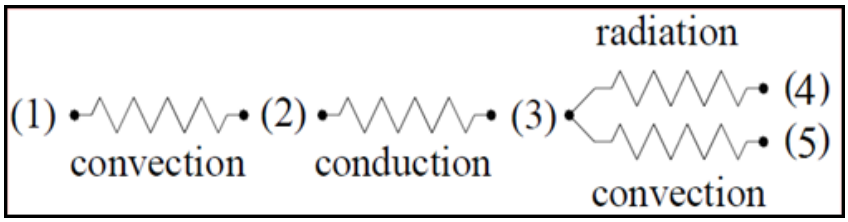

Figure 5.3 Thermal resistance model for a cross-section of an HCE

Where: Point 1 is heat transfer fluid

Point 2 is absorber inner surface

Point 3 is absorber outer surface

Point 4 is sky

Point 5 is surrounding air

i. Convection heat transfer between the HTF and the absorber

From Newton's law of cooling, the convection heat transfer from the inside surface of the absorber pipe to the HTF is

$$\dot{q}'_{12Conv} = h_1 D_1 \pi (T_2 - T_1) \ (\text{W/m}) \qquad (4.7)$$

Or $$\dot{q}'_{12Conv} = h_1 \qquad \left(\mathrm{W/m^2}k\right)$$

With

$$h_1 = Nu_{D1}\frac{k_1}{D_1} \tag{4.8}$$

Where

h_1 =convection heat transfer coefficient inside the tube at T_1 (W/m^2K)

D_1 = inside diameter of the absorber pipe (m)

T_1 = mean (bulk) temperature of the HTF (^oC)

T_2 = inside surface temperature of absorber pipe (^oC)

NuD_1 = Nusselt number based on D_1

k_1 = thermal conductance of the HTF at T_1 (W/mK)

In these equations, both T_1 and T_2 are independent of angular and longitudinal HCE directions, as will be all temperatures and properties in the one-dimensional energy balance model.

The Nusselt number depends on the type of flow through the HCE. At typical operating conditions, the flow in an HCE is well within the turbulent flow region. However, during off-solar hours or when evaluating the HCE heat losses on a test platform, the flow in the HCE may become transitional or laminar because of the viscosity of the HTF at lower temperatures. But for our prototype test the HTF flow rate maintained at minimum level. Therefore, the model heat losses determine at laminar flow type.

When the laminar option is chosen and the Reynolds number is lower than 2300, the Nusselt number will be constant. For pipe flow, the value will be 4.36 [26]

ii. Conduction heat transfer through the absorber wall

Fourier's law of conduction through a hollow cylinder describes the conduction heat transfer through the absorber wall[26].

$$\dot{q}'_{23Cond} = 2\pi k_{23}(T_2 - T_3)/\ln(D_2/D_1)(W/m) \tag{4.9}$$

Or

$$\dot{q}'_{23Cond} = 2k_{23}/\ln(D_2/D_1)(W/m^2k)$$

where:

k_{23} = absorber thermal conductance at the average absorber temperature $(T_2+T_3)/2$ (W/mK)

T_2 = absorber inside surface temperature (K)

T_3 = absorber outside surface temperature (K)

D_1 = absorber inside diameter (m)

D_2 = absorber outside diameter (m)

In this equation the conduction heat transfer coefficient is constant, and is evaluated at the average temperature between the inner and outer surfaces.

iii. Heat transfer from the absorber wall to the atmosphere

The heat will transfer from the glass envelope to the atmosphere by convection and radiation. The convection will either be forced or natural, depending on whether there is wind. Radiation heat loss occurs due to the temperature difference between the glass envelope and sky.

- **Convection heat transfer**

The convection heat transfer from the glass envelope to the atmosphere (q''_{35Conv}) is the largest source of heat loss, especially if there is a wind. From Newton's law of cooling

$$\dot{q}'_{35Conv} = h_{35} D_2 \pi (T_3 - T_5) \ (\mathrm{W/m}) \qquad (4.10)$$

Or

$$\dot{q}'_{35Conv} = h_{35} (T_3 - T_5) \ \left(\mathrm{W/m^2}k\right)$$

With

$$h_{35} = Nu_{D2} \frac{k_3}{D_2} \qquad (4.11)$$

where:

T_3 = glass envelope outer surface temperature (^oC)

T_5 = ambient temperature (^oC)

h_{35} = convection heat transfer coefficient for air at $(T_3 - T_5)/2$ (W/m^2K)

k_3 = thermal conductance of air at $(T_3 - T_5)/2$ (W/mK)

D_2 = glass envelope outer diameter (m)

Nu_{D2} = average Nusselt number based on the glass envelope outer diameter

The Nusselt number depends on whether the convection heat transfer is natural or forced (i.e no wind or with wind). The experiment setup is outside the house, thus convection heat transfer assumed forced convection (with wind).

If there is wind, the convection heat transfer from the outer surface of the tube to the environment will be forced convection. The Nusselt number in this case is estimated with Zhukauskas' correlation for external forced convection flow normal to an isothermal cylinder [26].

$$Nu_{D2} = C\,\mathrm{Re}_{D3}{}^{m}\,\mathrm{Pr}_5{}^{n}\left(\frac{pr_5}{\mathrm{Pr}_3}\right)^{1/4} \qquad (4.12)$$

Table 5.2 Constants for the circular cylinder

$\mathbf{Re_D}$	C	m
1-40	0.75	0.4
40-1000	0.51	0.5
1000-200000	0.26	0.6
200000-1000000	0.076	0.7

This correlation is valid for $0.7 < Pr_5 < 500$, and $1 < Re_{D2} < 106$. All fluid properties are evaluated at the atmospheric temperature, T_5, except Pr_3, which is evaluated at the outer surface of the tube temperature.

5.2 Radiation Heat Transfer

The useful incoming solar irradiation is included in the solar absorption terms. Therefore, the radiation transfer between the outer surface of the tube and sky is caused by the temperature difference between the outer surface of the tube and sky. To approximate this, the outer surface

of the tube is assumed to be a small convex gray object in a large blackbody cavity (sky). The net radiation transfer between the glass envelope and sky becomes [26].

$$\dot{q}'_{34rad} = \sigma\pi D_2 \varepsilon_3 \left(T_3^4 - T_4^4\right) \text{ (W/m)} \qquad (4.13)$$

where: σ = Stefan-Boltzmann constant (5.670E-8) (W/m2-K4)

D_2 = the outer surface tube diameter (m)

ε_3 = emissivity of the outer surface tube

T_3 = the outer surface tube temperature (K)

T_4 = effective sky temperature (K)

Thus after determining the loss coefficient U_L and determining the heat transfer resistance from the outer surface of the receiving tube to the fluid in the tube, the overall heat transfer coefficient (i.e the sum of heat gain and heat loss of the heat collecting tube) which is given by

$$\frac{1}{U_O} = \left[\frac{1}{U_L} + \frac{D_2}{h_1 D_1} + \frac{D_2 \ln\left(\frac{D_2}{D_1}\right)}{2k_{23}} \right] \qquad (4.14)$$

where:

U_L - The sum of convection and radiation heat loss from the heat collecting tube

5.3 Solar Irradiation Absorption

Using basic energy balance equation, the useful energy gained per unit collector length expressed in terms of the local receiver tube temperature and the absorbed solar radiation per unit of the aperture area, which is the difference between the absorbed solar radiation and the thermal loss and is given by:

$$\dot{q}'_{used} = \frac{A_a \dot{q}_{ab} - A_t U_L (T_t - T_a)}{L} \qquad (4.15)$$

$$\dot{q}_{ab} = \alpha_O I_t \qquad (4.16)$$

$$A_t = \pi D_2 L \tag{4.17}$$

where:

$\dot{q}'_{used}$ - Useful energy gained by HTF

A_a - Aperture area

U_L - The sum of convection and radiation heat loss from the heat collecting tube

L - Parabolic trough length

T_t - Receiver tube temperature

T_a - Ambient temperature

I_t - Solar intensity

α_O - absorptivity of the tube

D_2 - Receiver tube outer diameter

In terms of the energy transferred in to the working fluid at local fluid temperature

$$\dot{q}'_{used} = \frac{\left(\frac{A_t}{L}\right)\left(T_t - T_f\right)}{\frac{D_2}{h_1 D_1} + \frac{D_2}{2k}\ln\left(\frac{D_2}{D_1}\right)} \tag{4.18}$$

Rewrite Equation 4.15 in the form of T_t and substituting in Equation 4.18 then it give the following

$$\dot{q}'_{used} = F' \frac{A_a}{L}\left[\dot{q}_{ab} - \frac{A_t}{A_a} U_L (T_f - T_a)\right] \tag{4.17}$$

Where:

F' is collector efficiency factor which is given by

$$F' = \frac{\frac{1}{U_L}}{\frac{1}{U_L} + \frac{D_2}{h_1 D_1} + \frac{D_2}{2k}\ln\left(\frac{D_2}{D_1}\right)} \tag{4.18}$$

This can be rewrite in the form of:

$$F' = \frac{U_O}{U_L} \tag{4.19}$$

The actual useful energy collected by fluid is given by

$$\dot{q}'_{used} = F_R \left[\frac{A_a \dot{q}_{ab} - A_t U_L (T_{fi} - T_a)}{L} \right] \tag{4.20}$$

Where F_R is the collector heat removal factor, defined as the ratio of the actual useful energy gain to the useful energy gain if the entire collector was at the fluid inlet temperature T_{fi} and it is expressed as:

$$F_R = \frac{\dot{m} C_{pf} (T_{fo} - T_{fi})}{\frac{A_a}{L}\left[\dot{q}_{ab} - \frac{A_t}{A_a} U_L (T_{fi} - T_a) \right]} \tag{4.21}$$

After rearranging the above equation including collector efficiency factor it becomes

$$F_R = \frac{\dot{m} C_{pf}}{A_t U_L}\left[1 - \exp\left(- \frac{A_t U_L F'}{\dot{m}_f C_{pf}} \right) \right] \tag{4.22}$$

Where

C_{pf} - Specific heat of the working fluid

$\dot{m}_f$ - Mass flow rate of the working fluid

Finally, rearranging the above equations in the form of T_{fo}, then the exit temperature of the water in the heat collecting tube can be calculated by the following formula,

$$T_{fo} = T_{fi} + \frac{\dot{q}'_{used}}{\dot{m}_f C_{pf}} \tag{4.23}$$

Chapter Six

Result and Discussion

6.1 Introduction

In this section, the thermal performance of parabolic trough solar collector is investigated using the measured data of the inlet and outlet temperature of the working fluid, ambient temperature, wind speed and global radiation around the experimental setup. Plots of the performance parameters are also done using Matlab software from the data logger import wizard to Microsoft excel worksheet.

Generally, in the test setup, water is circulated through the absorber tube, then to the heat exchanger, finally to the reservoir and again it is pumped back to the absorber tube. A regulating mechanism which is a gate valve is used to alter the flow rate in the system. Temperature of water incoming into and outgoing from the absorber tube are logged using data acquisition system. The pump circulates the water throughout the day starting from sunrise up to sunset. This is in line with the general test procedure in all standards.

Two absorber tubes are tested in this project; galvanized still pipe and aluminum pipe. The test results are listed below based on the pipe type. The tests are conducted from November 15 to December 10, 2011. Among different tests, ten representative tests, five for each pipe, are selected and tabulated in Appendix A. Furthermore, among representative tests, two of them are selected from each pipe to demonstrate the different results obtained in the experiment.

6.2 Galvanized Steel Pipe Test Result

The data selected to demonstrate the result of galvanized still pipe is taken on November 21, 2011 and the ambient temperature variation throughout the day is shown in the figure below.

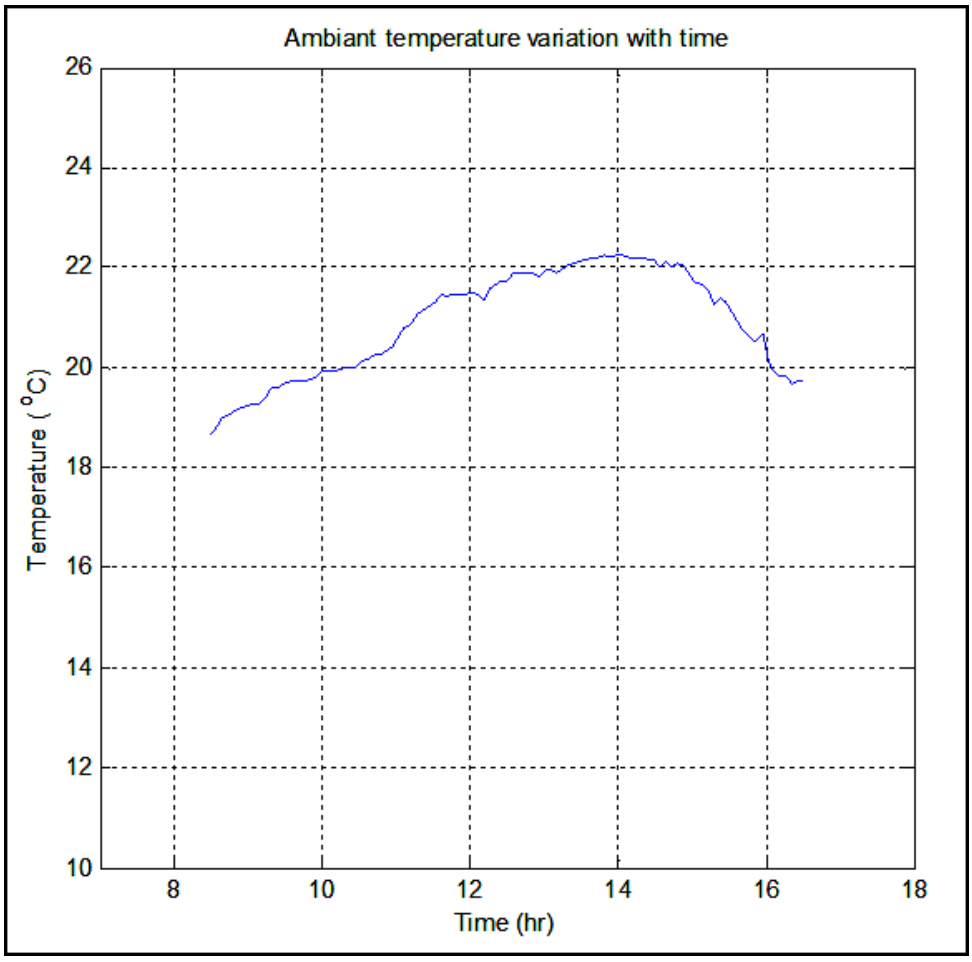

Figure 6.1 Variation of ambient temperature recorded on November 21, 2011

The test was started at 8:30 and ended at 16:30. The maximum ambient temperature measured between 13:57 to 14:05, is found to be 22.25^0C. The minimum temperature measured on the same day was 18.6^0C, at 8:30.

The direct solar radiation variation is shown in the Figure 6.2. The maximum radiation measured is 975.54 W/m^2 and the minimum value is 395.63W/m^2.

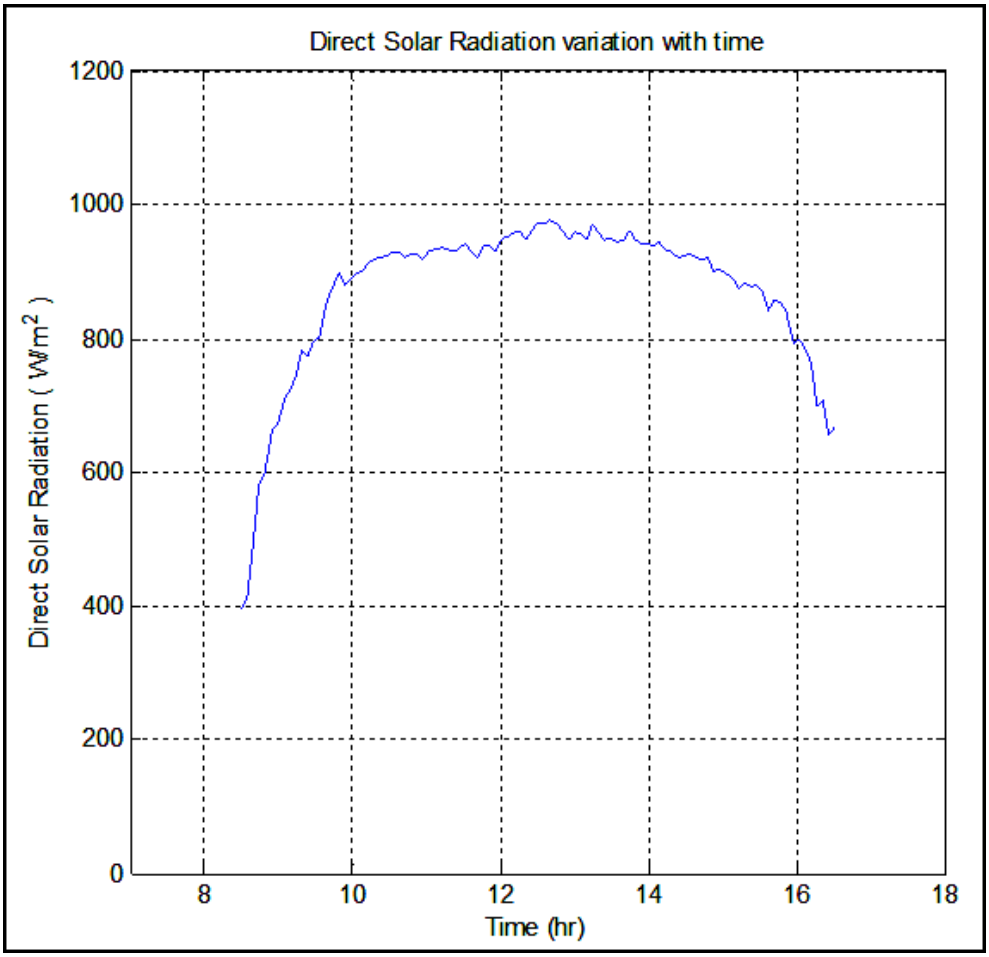

Figure 6.2 Variation of Direct Solar Radiation recorded on November 21, 2011

The temperature variations of the two troughs are shown in the Figure 6.3 and 6.4. The first trough increased the water temperature to a maximum of 40.63 ^{0}C, which remained above 38 ^{0}C for five working hours, starting from 10:30 up to 15:30. The second trough increased the water temperature to a maximum of 51.39 ^{0}C, which remained above 48 ^{0}C for five working hours, starting from 10:30 up to 15:30.

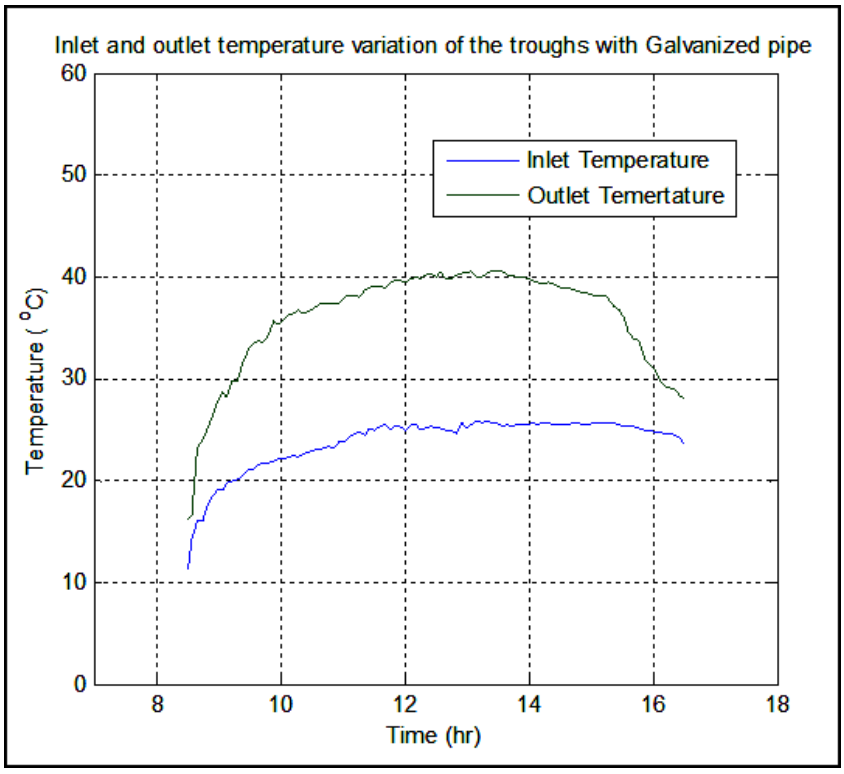

Figure 6.3 Temperature variation of the water in the first trough

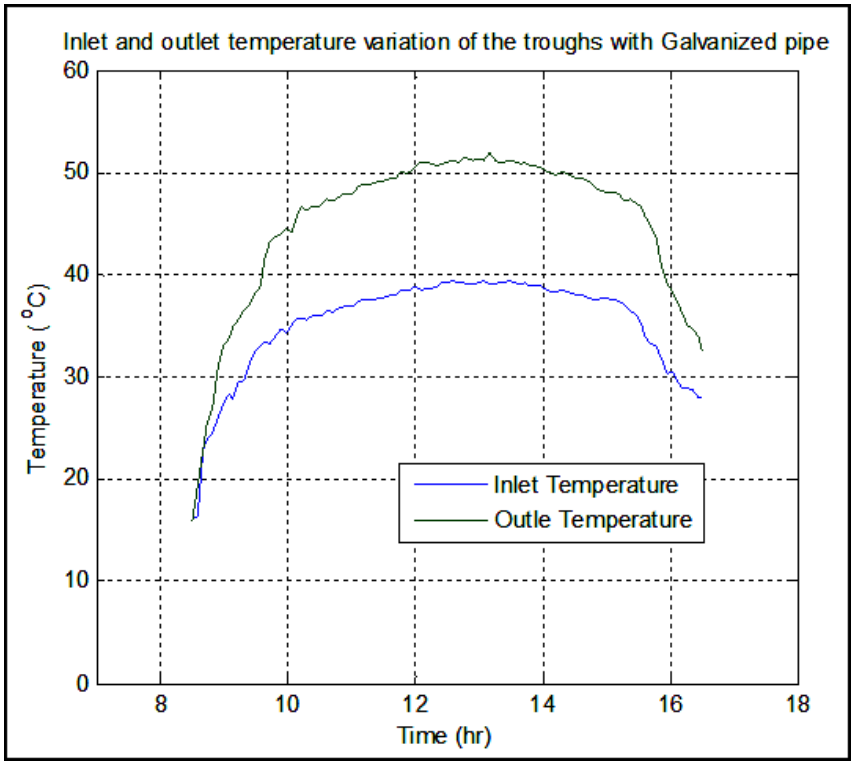

Figure 6.4 Temperature variation of water in the second trough

The total temperature variations of the water in the trough are shown in the Figure 6.5 and Figure 6.6.

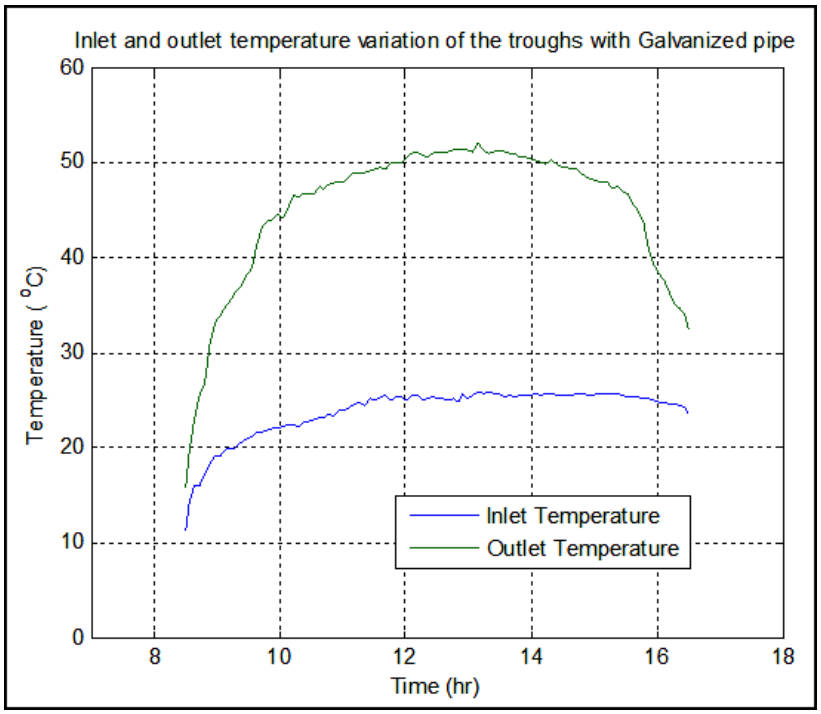

Figure 6.5 Temperature variation of the water

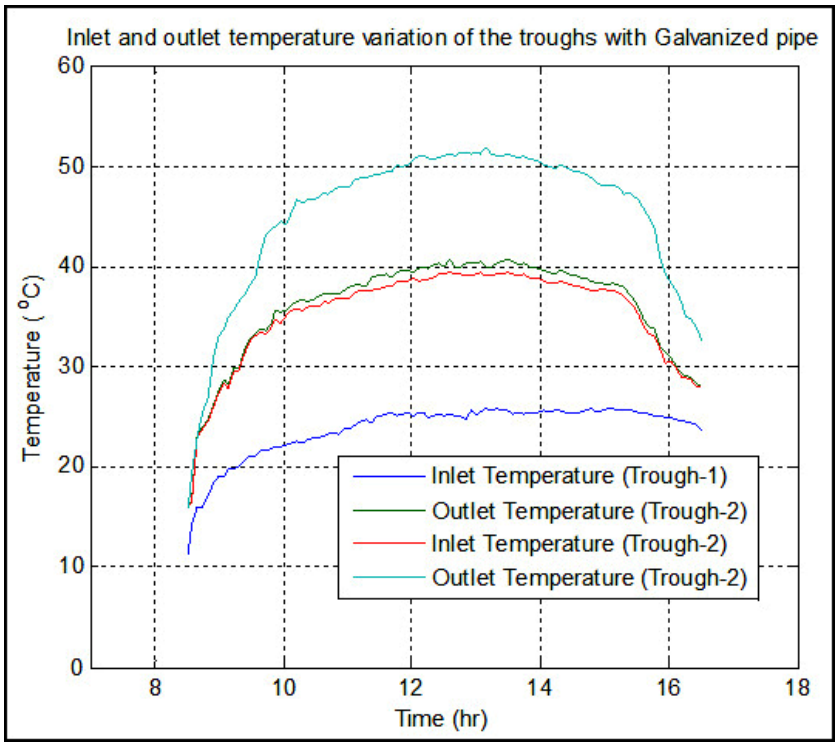

Figure 6.6 Inlet and outlet temperature variation of water

6.3 Aluminum Pipe Test Result

The data selected to demonstrate the result of aluminum pipe was taken on December 2, 2011 and the ambient temperature variation in the trough during the day is shown in the figure below.

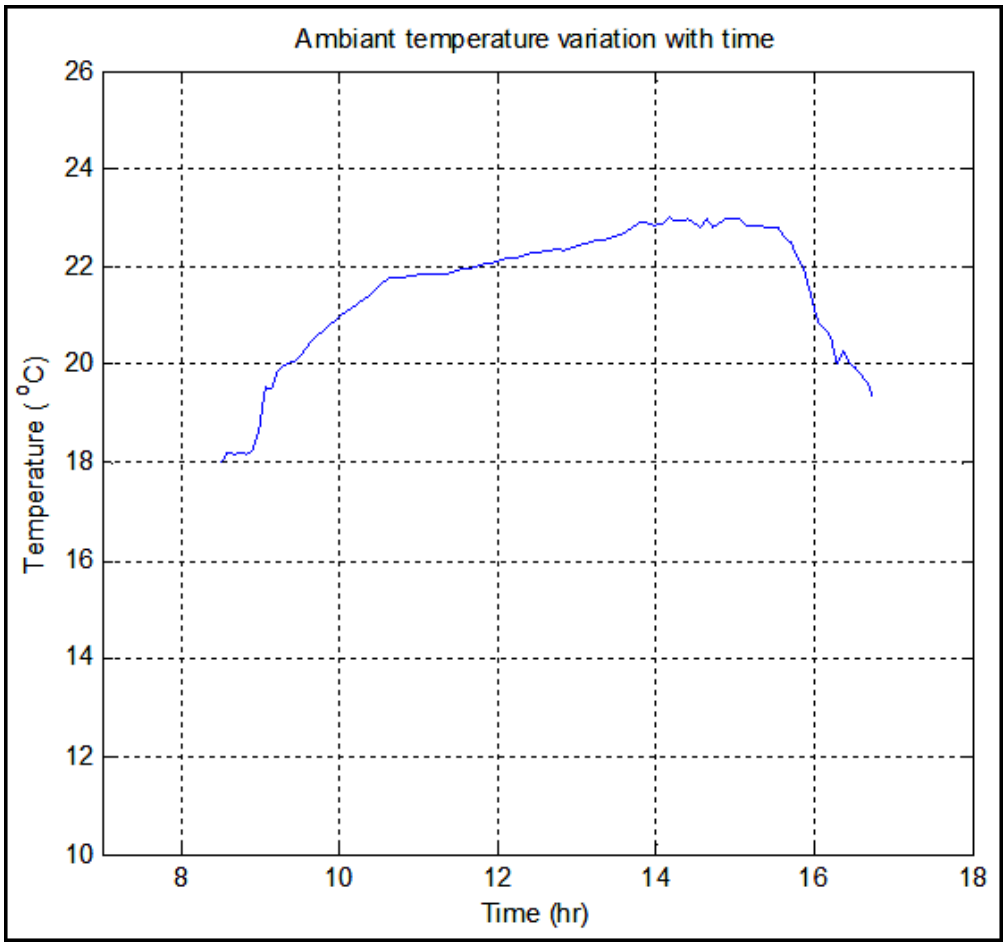

Figure 6.7 Variation of ambient temperature recorded on November 21, 2011

The test started 8:40 in the morning and it ended 4:30 in the afternoon. The maximum temperature measured was 22.99^{0}C between 2:15 to 3:03 in the afternoon and the minimum temperature measured is 17.9 ^{0}C at 8:40 in the morning.

The direct solar radiation variation is shown in the Figure 6.8. The maximum radiation measured is 1049.519W/m^{2}and the minimum value is 302.32 W/m^2.

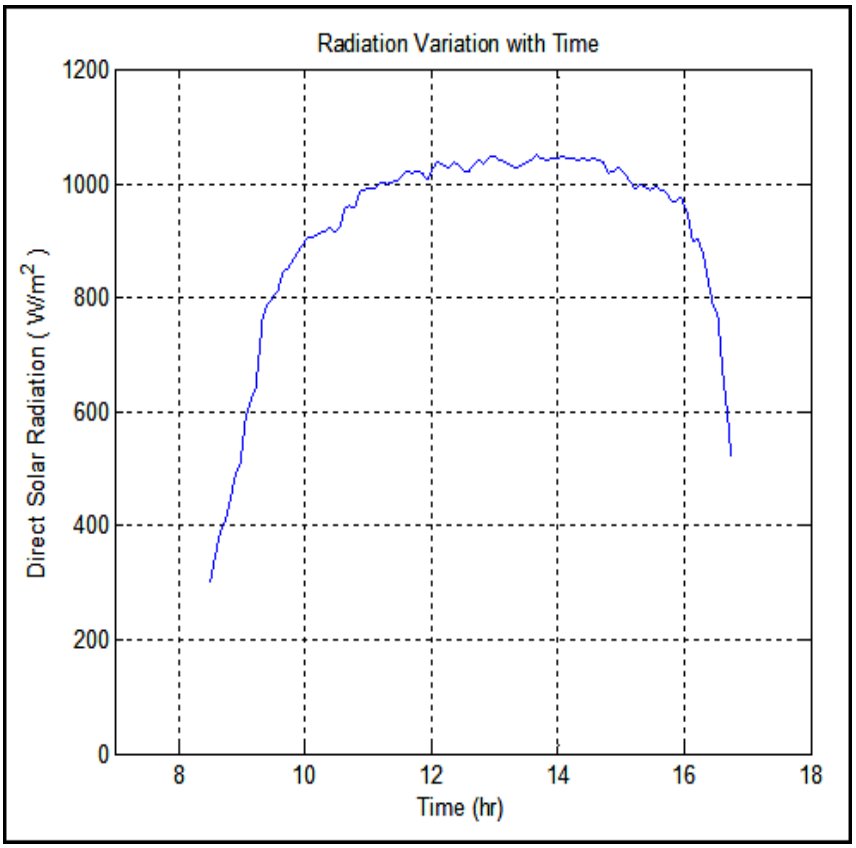

Figure 6.8 Variation of Direct Solar Radiation recorded on December 2, 2011

The temperature variations of the two troughs are shown in Figure 6.9 and 6.10. The first trough increased the water temperature to a maximum of 55.95^{0}C, which remained above 55 ^{0}C for two working hours, starting from 12:15 up to 14:23, and above 50^{0}C for five and a half working hours starting from 10:17 up to 15:42. The second trough increased the water temperature to a maximum of 73^{0}C, raising the temperature above 70^{0}C for about five working hours starting from 10:42 up to 14:30.

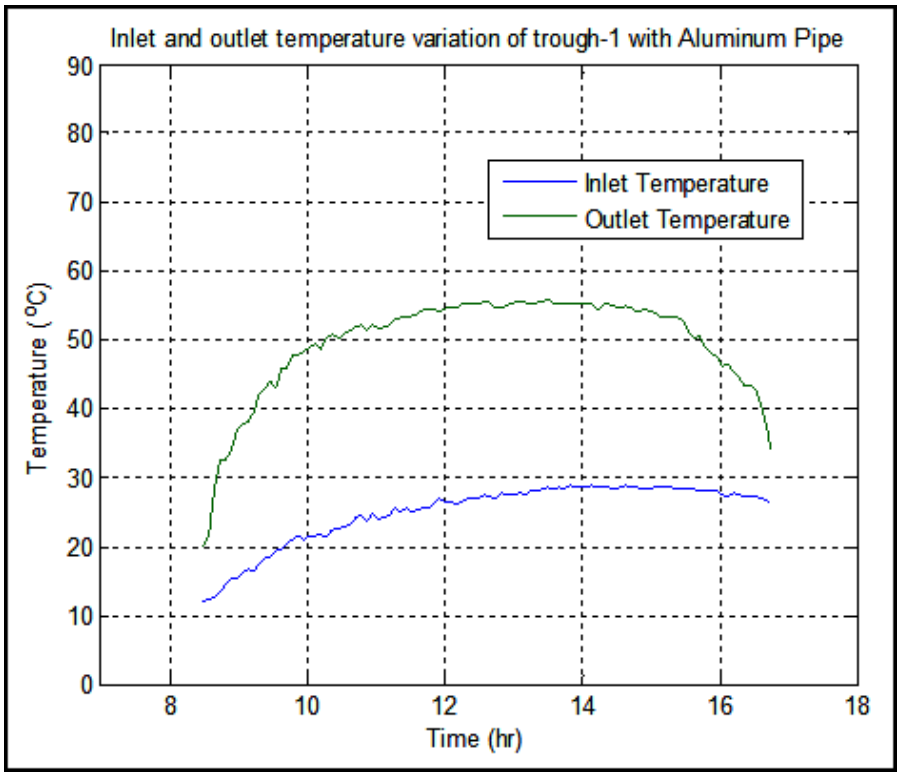

Figure 6.9 Temperature Variation of the water in the first trough

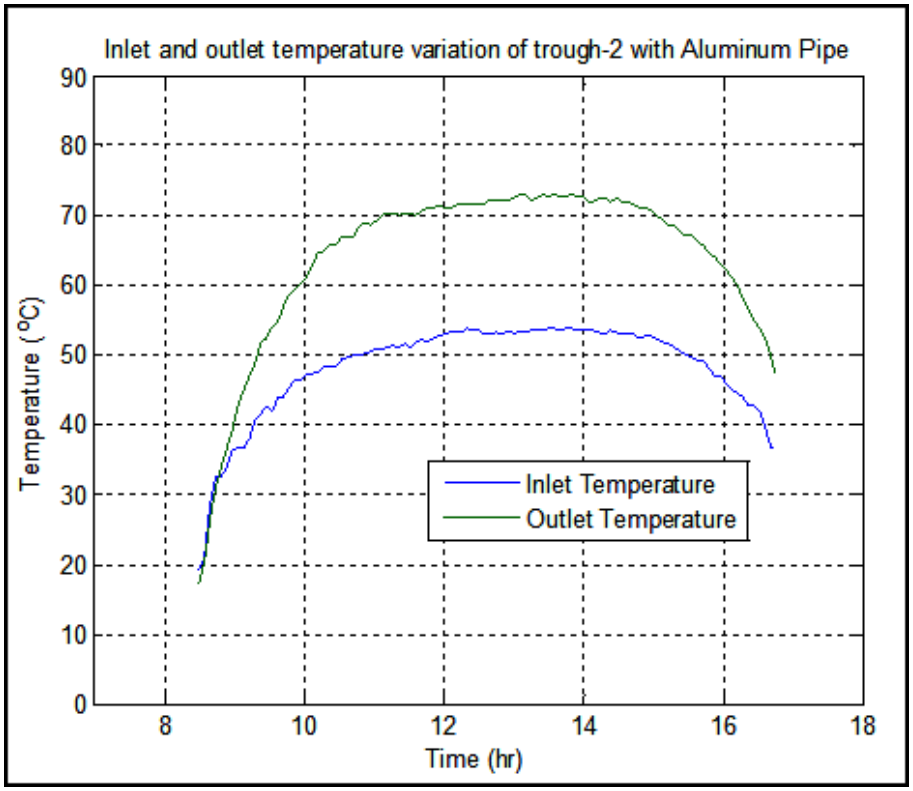

Figure 6.10 Temperature Variation of water in the second trough

Total temperature variations of the water in the trough are shown in Figure 6.11 and Figure 6.12.

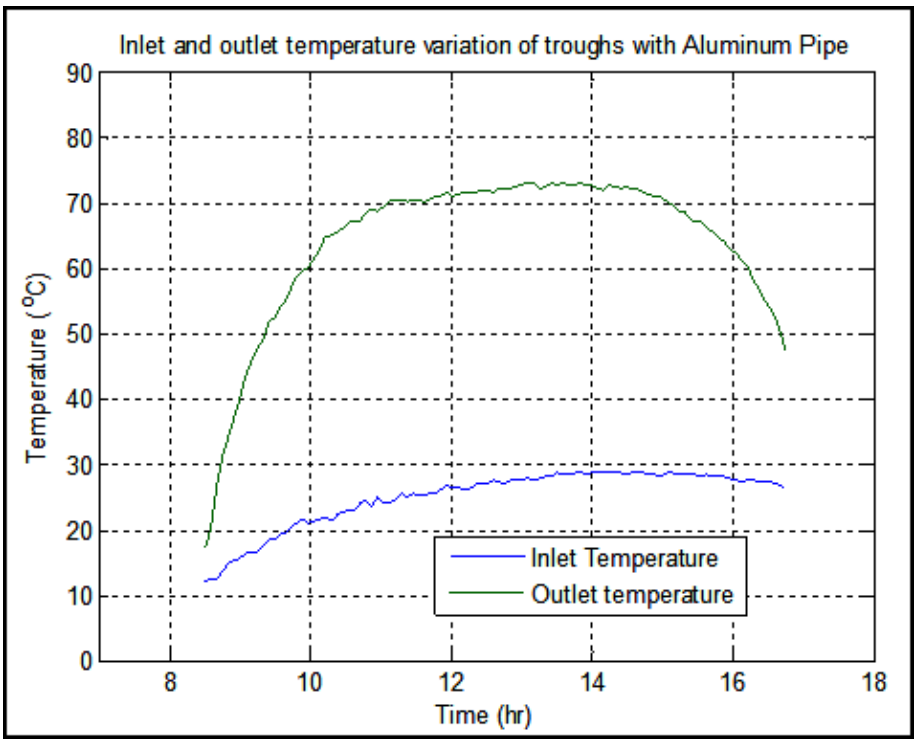

Figure 6.11 Temperature Variation of the water

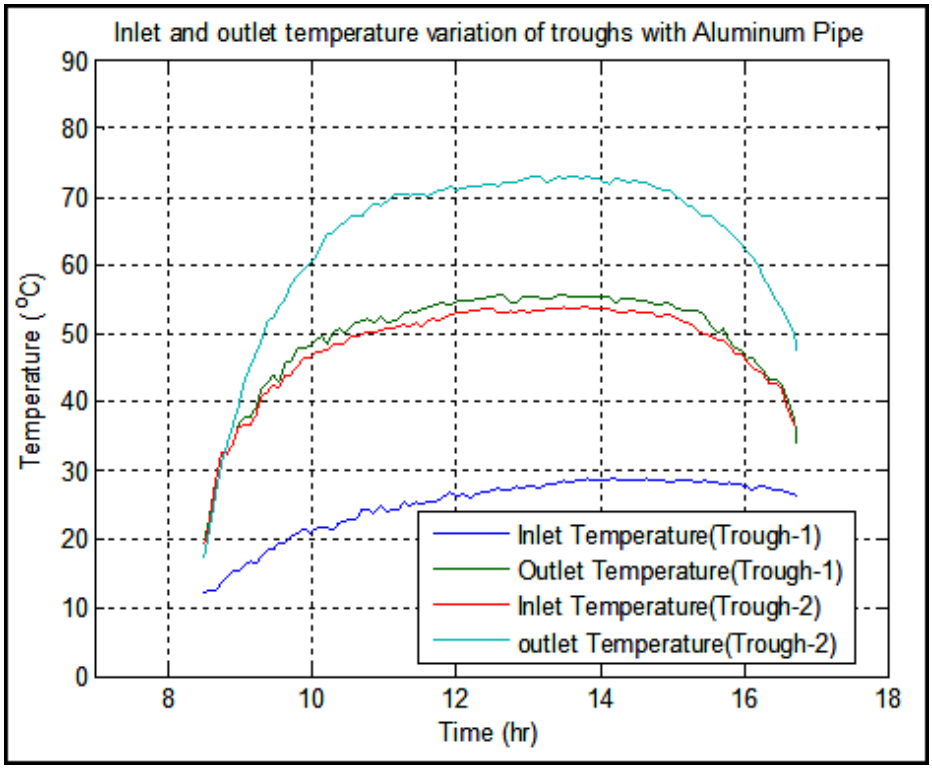

Figure 6.12 Inlet and Outlet Temperature Variation of the water

6.4 Collector Efficiency

Another important aspect in analyzing the solar collector is its efficiency. Basically the thermal efficiency of any solar thermal collector is expressed as:[27]

$$\eta_{th} = \frac{Q_{collect}}{Q_{solar}} \tag{6.1}$$

where:

$Q_{collect}$ = amount of solar thermal energy collected

Q_{solar} = amount of solar radiation from the sun

The useful energy collected by the trough is obtained by the formula

$$Q_{collect} = \dot{m} C_p (T_{out} - T_{in}) \tag{6.2}$$

where:

$\dot{m}$ = mass flow rate of heat transferring fluid (J/s)

C_p =specific heat of the heat transferring fluid (J/kgK)

T_{out} =outlet temperature of the heat transferring fluid (^oC)

T_{in} = inlet temperature of the heat transferring fluid (^oC)

$\dot{Q}_{solar}$ is dependent on the beam irradiance I_b, aperture area of the mirror A_a and the optical efficiency $\eta_{optical}$.

$$\dot{Q}_{solar} = \eta_{optical} \times I_b \times A_a \tag{6.3}$$

The optical efficiency contains complex parameters such as reflectivity, absorption, transmission and spillage of the mirror, the glass envelope and the absorber tube. For aluminum reflective surface field test shows that the optical efficiency is above 60% [28].

Based on the above analysis the efficiency of the trough is evaluated for both pipes, as shown in Figure 6.13 for galvanized still pipe and Figure 6.14 for aluminum pipe.

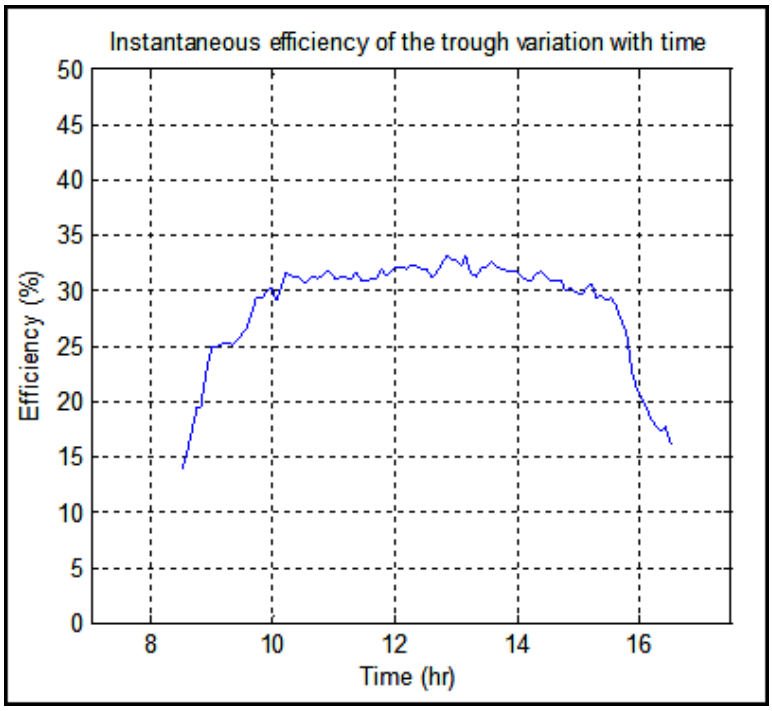

Figure 6.13 Instantaneous efficiency of the galvanized still heat collecting pipe

The efficiency of the galvanized still heat collector pipe fluctuates between 30% - 35% starting from 10:00 up to 15:00; more than five working hours.

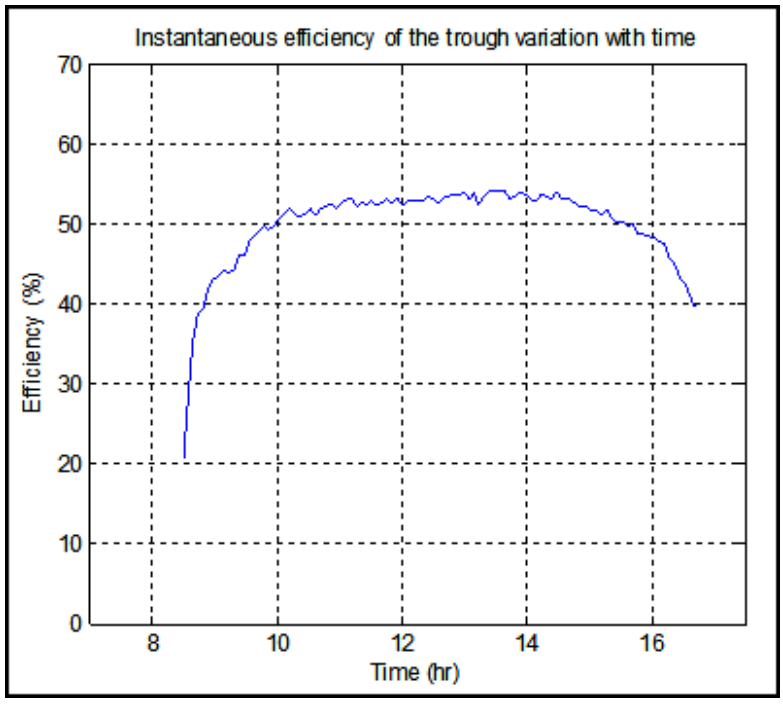

Figure 6.14 Instantaneous efficiency of the aluminum heat collecting pipe

The efficiency of the aluminum heat collector pipe fluctuates between 50% - 60% starting from 10:00 up to 16:00; more than six working hours.

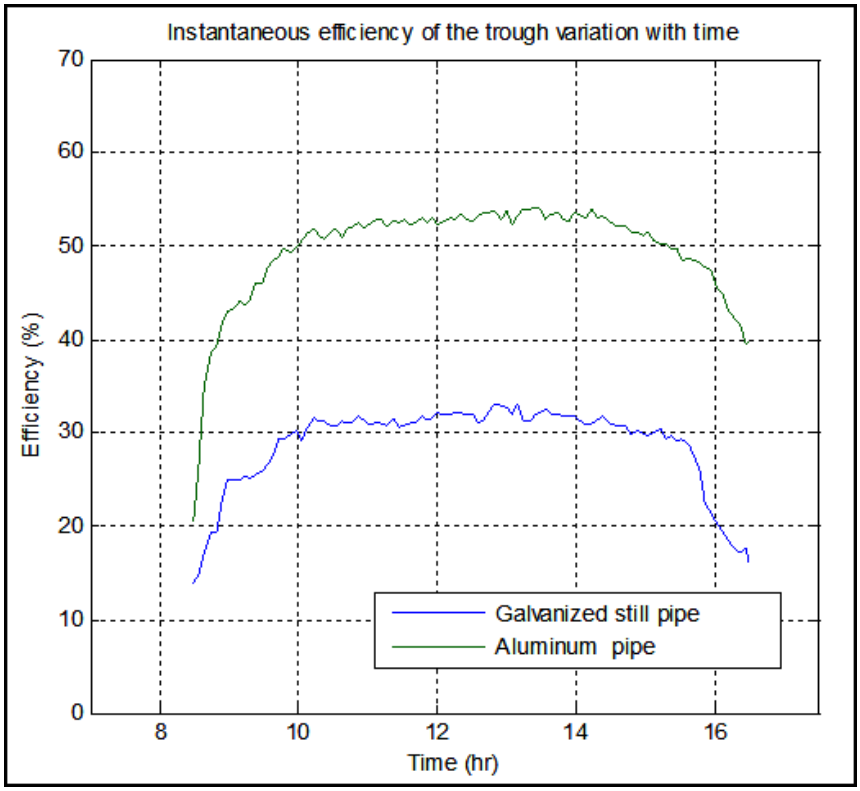

Figure 6.15 Instantaneous efficiency of both (aluminum and galvanized still) pipes

The test results are also compared with the mathematical model analysis that is discussed in Chapter six. For the comparison of the test and mathematical model analyses, the aluminum pipe is selected.

From graphs shown in Figure 6.15 and 6.16, the temperature difference between the analytical model and the actual test results are between seen to lie between 0 and10^0C. These deviations can be accounted for by the manufacturing and test procedures errors.

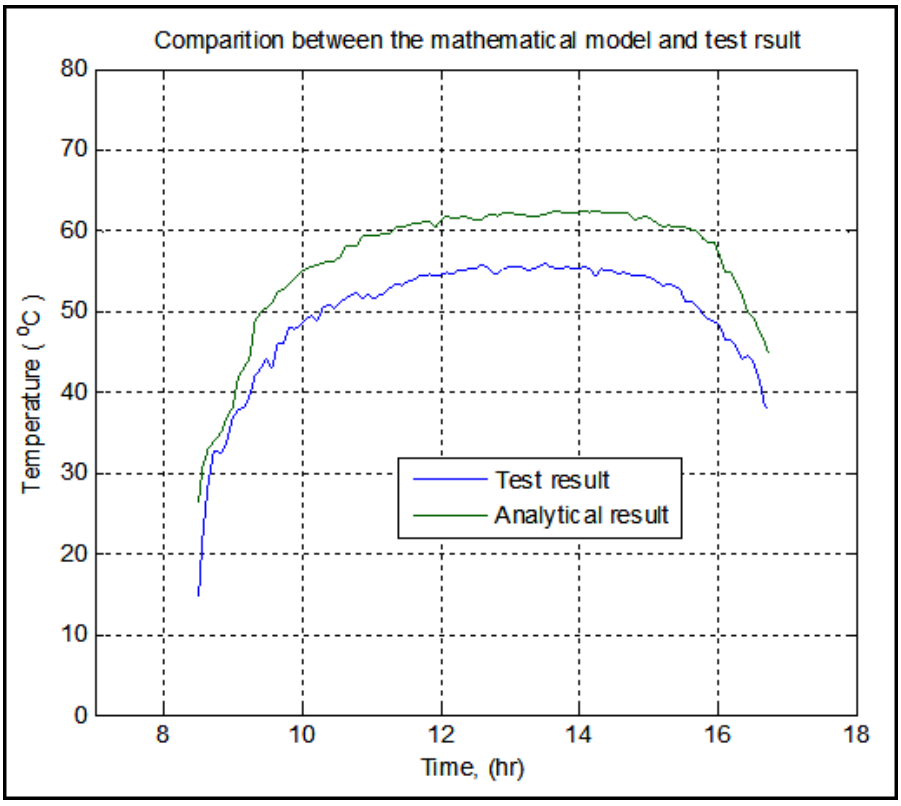

Figure 6.16 Comparisons between the mathematical model and test result (Trough-1)

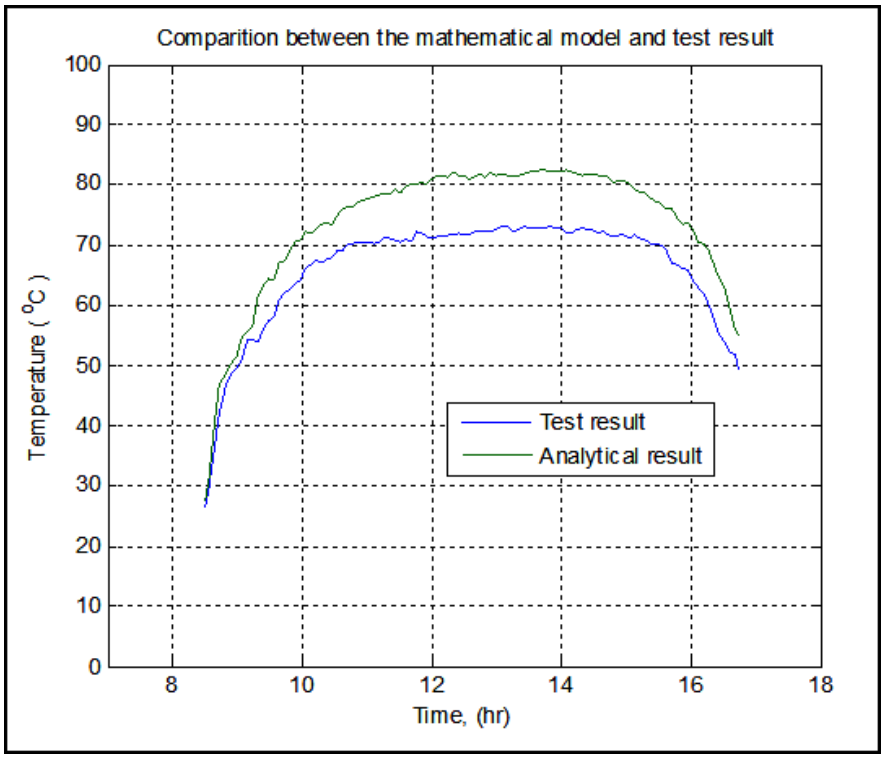

Figure 6.17 Comparisons between the mathematical model and test result (Trough-2)

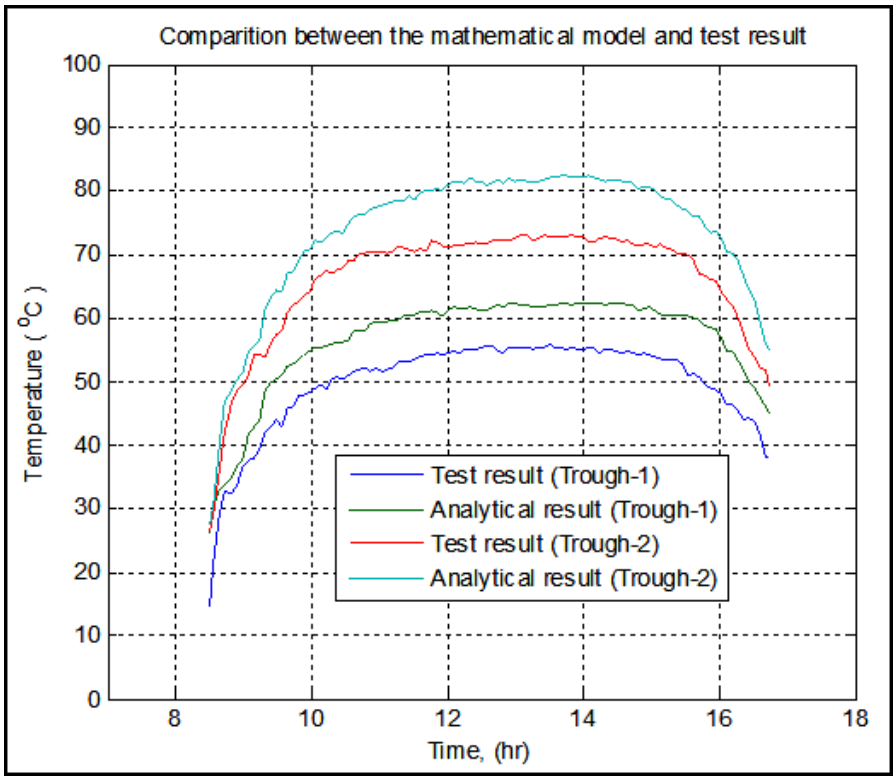

Figure 6.18 Comparisons between the mathematical model and test result (Both Troughs)

Chapter Seven

Conclusion and Recommendation

The major aim of this project work was to design, manufacture and conduct an experimental investigation on the performance of parabolic trough and prepare a mathematical model to verify the results obtained during the test period. In this chapter some basic concluding points and recommendation are indicated.

Conclusion

This paper has attempted to highlight the following issues:

- Based on the current status of the Country a new method of a solar energy application has been tested and new technical and technological opportunities of a solar energy application in water heating and steam generation has been established.
- Aluminum sheet material bends easily into the required parabolic trough shape. Black painted aluminum pipe is used as absorber tube. Temperature sensor thermocouples measure the changing water temperature at inlet and outlet of the central receiver. Daily data were collected from each material used as the absorber. Water temperature does increase in the absorber.
- On a clear sky day, a maximum of 73 ^{0}C and an average of 70 ^{0}C of water temperature were recorded using aluminum pipe absorber tube. However, with the galvanized steel pipe an average of 48 ^{0}C was recorded for water temperature.
- On the average, the efficiency of the aluminum-absorber parabolic trough is about 50% while for the galvanized steel pipe the efficiency is about 30%.
- From the result, it can be observed that the parabolic trough is very efficient generating high temperature water for about five and a half working hours, from 10:00 to 15:30.
- The experimental and the analytical results are very comparable with some acceptable differences.
- The environmental factor plays a major role in the performance analysis of the solar collector. Environmental or weather conditions such as wind and scattered clouds conditions are factors that bring down the efficiency of the solar collector.

- The result of this study gives guidance for the possible use of parabolic trough application for energy generation.

Recommendation

- The parabolic trough is tested using water as heat transfer fluid. For future work, it is recommended that oil be used as heat transfer fluid, if oil pump is available. Replacing the absorber tube with copper tube would result in better performance.
  Improvement is also expected from parabolic troughs covered with glass. Or transparent material. This increases the efficiency of the parabolic trough by reducing convection heat loss from the absorber tube and prevent the reflector from dust particle.

- Mechanical or electrical solar tracking system should be used to reduce the error that is created by manual tracking system.

- The utilization of renewable energy in Ethiopia should be increased, as there is a global concern that the developing nations could be faced with energy crisis and global warming. It is expected that more damage and pollution of the environment will continue. Parabolic trough solar collector is one of the options for renewable energy and this technology should be adopted in industries that utilize fossil fuel for water heating and steam generation.

- The government has to support further research works in this area financially and allocating large area to test large grids of the parabolic trough system for steam generation and power production.

Appendix

A. Ambient Temperature, Direct Solar Radiation, Inlet and Outlet Temperature of the Water and Efficiency Graphs for Galvanized Still Absorber Tube

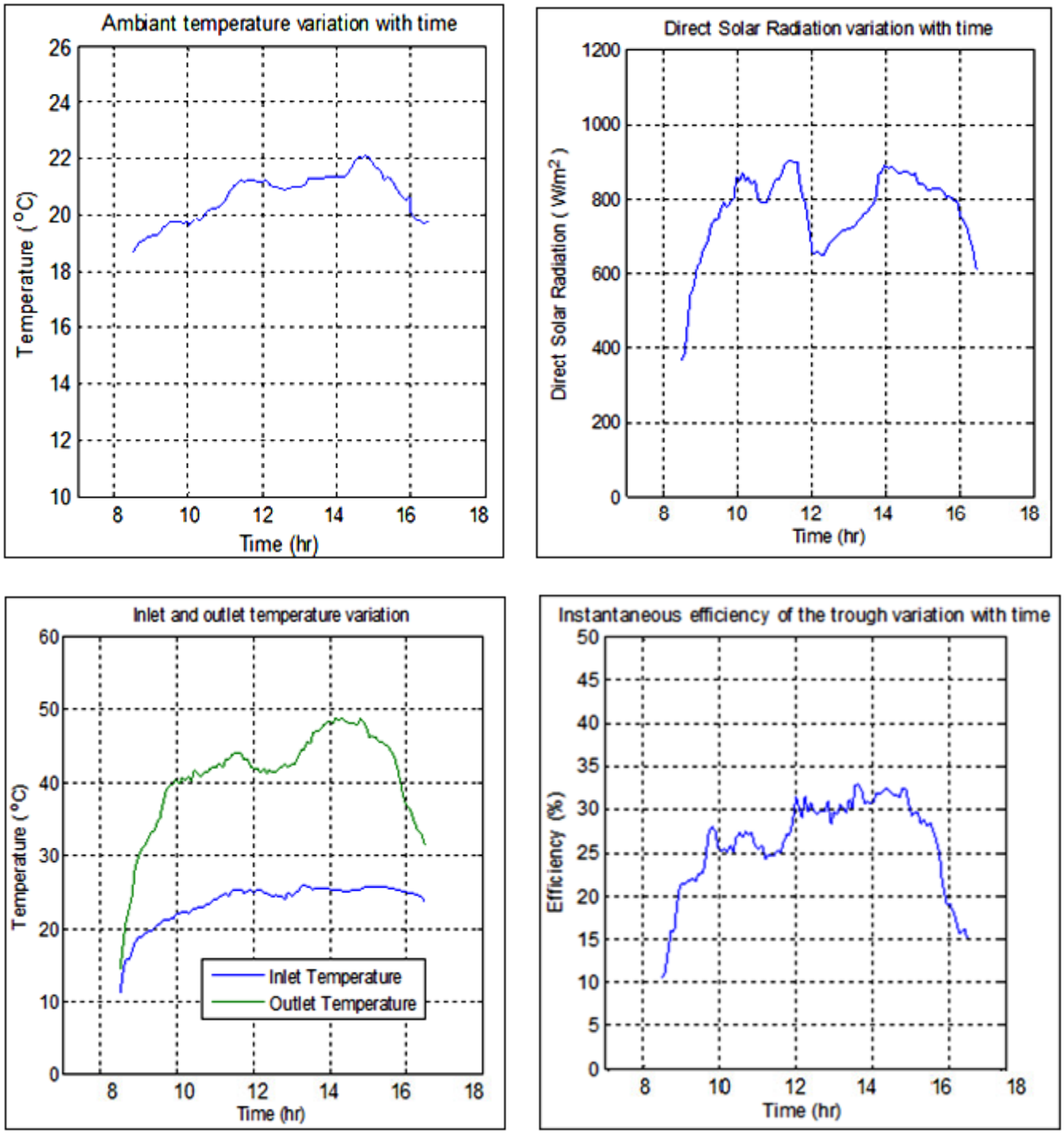

Figure A.2 Graphical representation of the test data collected on November 17, 2011

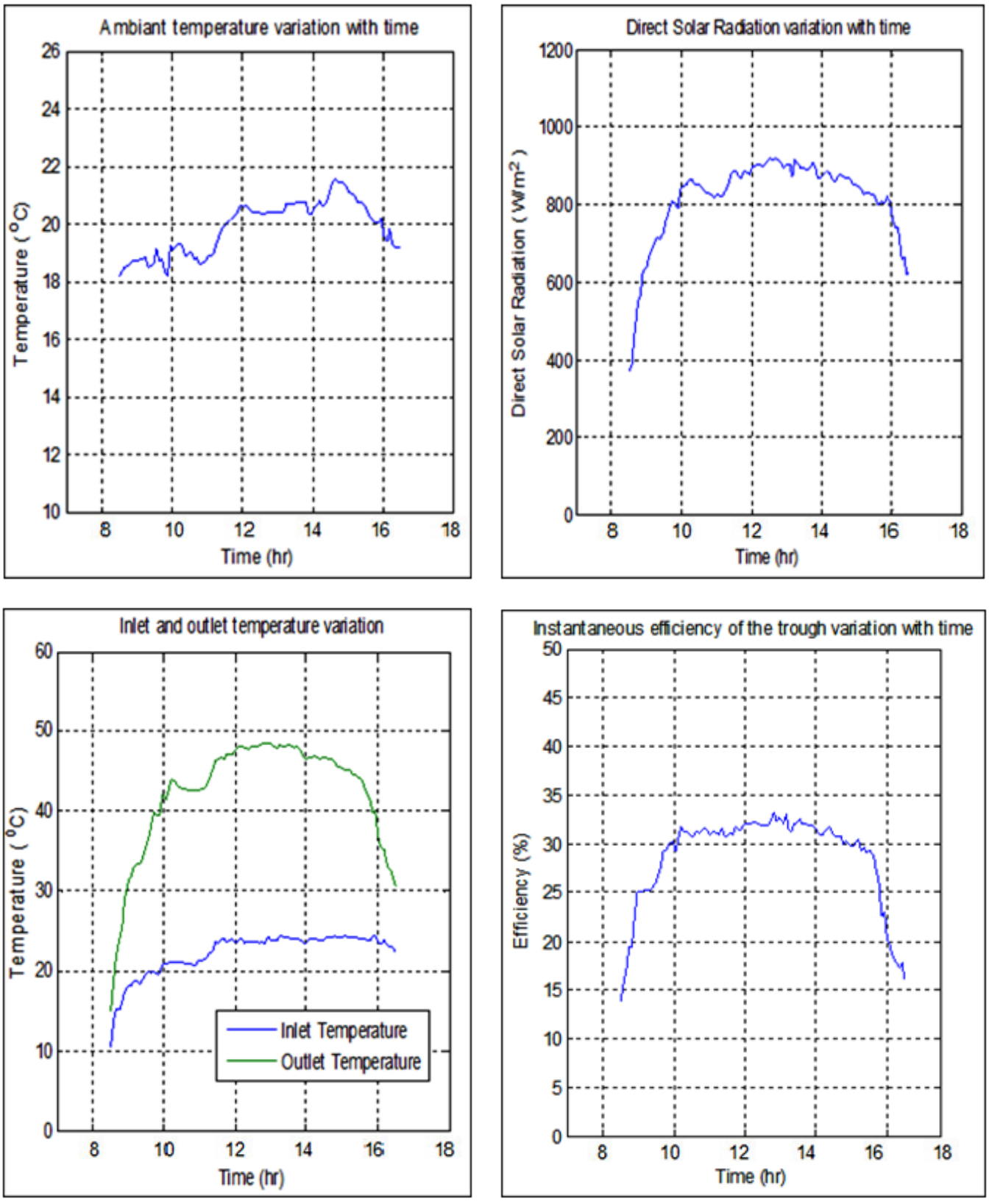

Figure A.2 Graphical representation of the test data collected on November 19, 2011

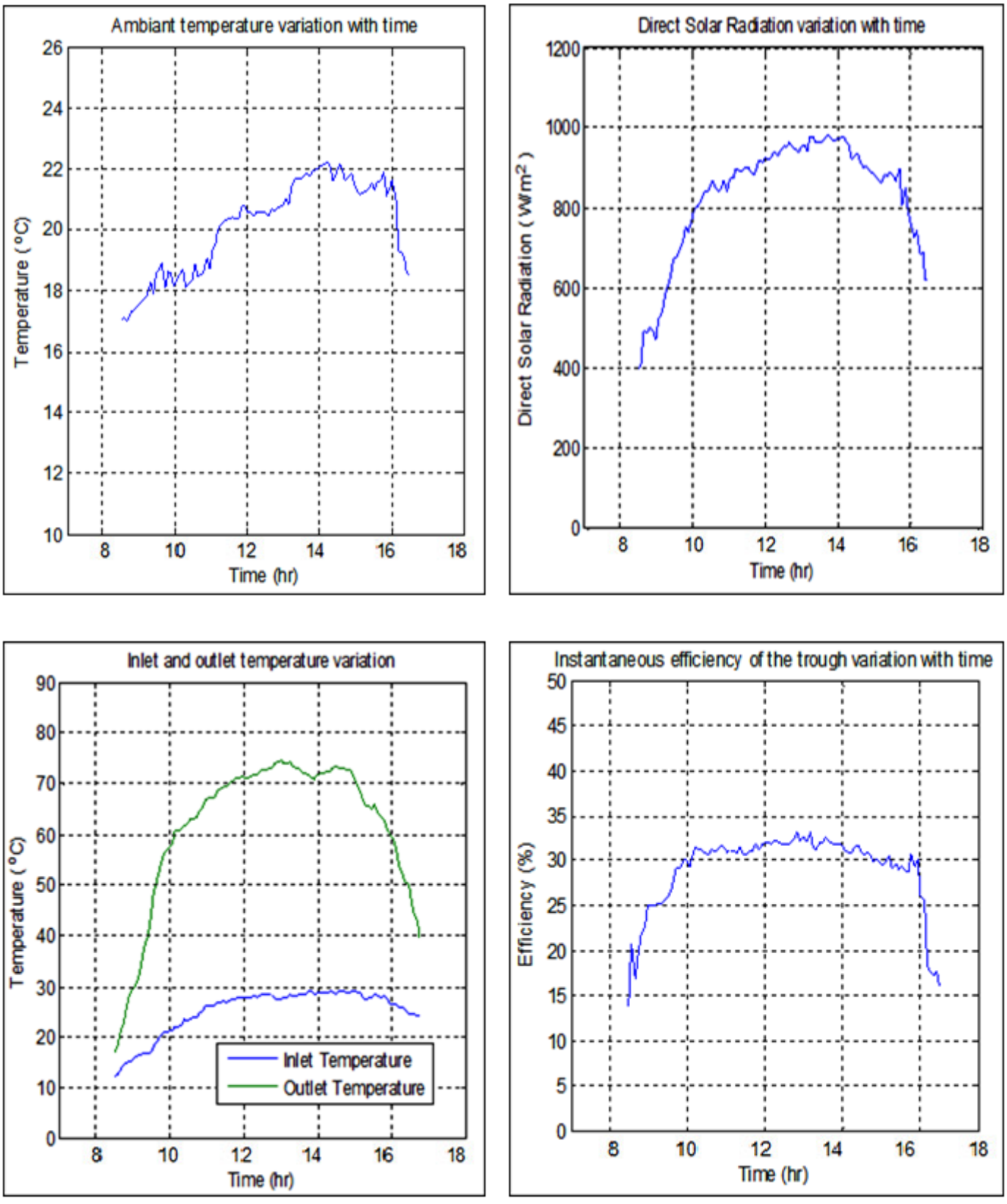

Figure A.3 Graphical representation of the test data collected on November 22, 2011

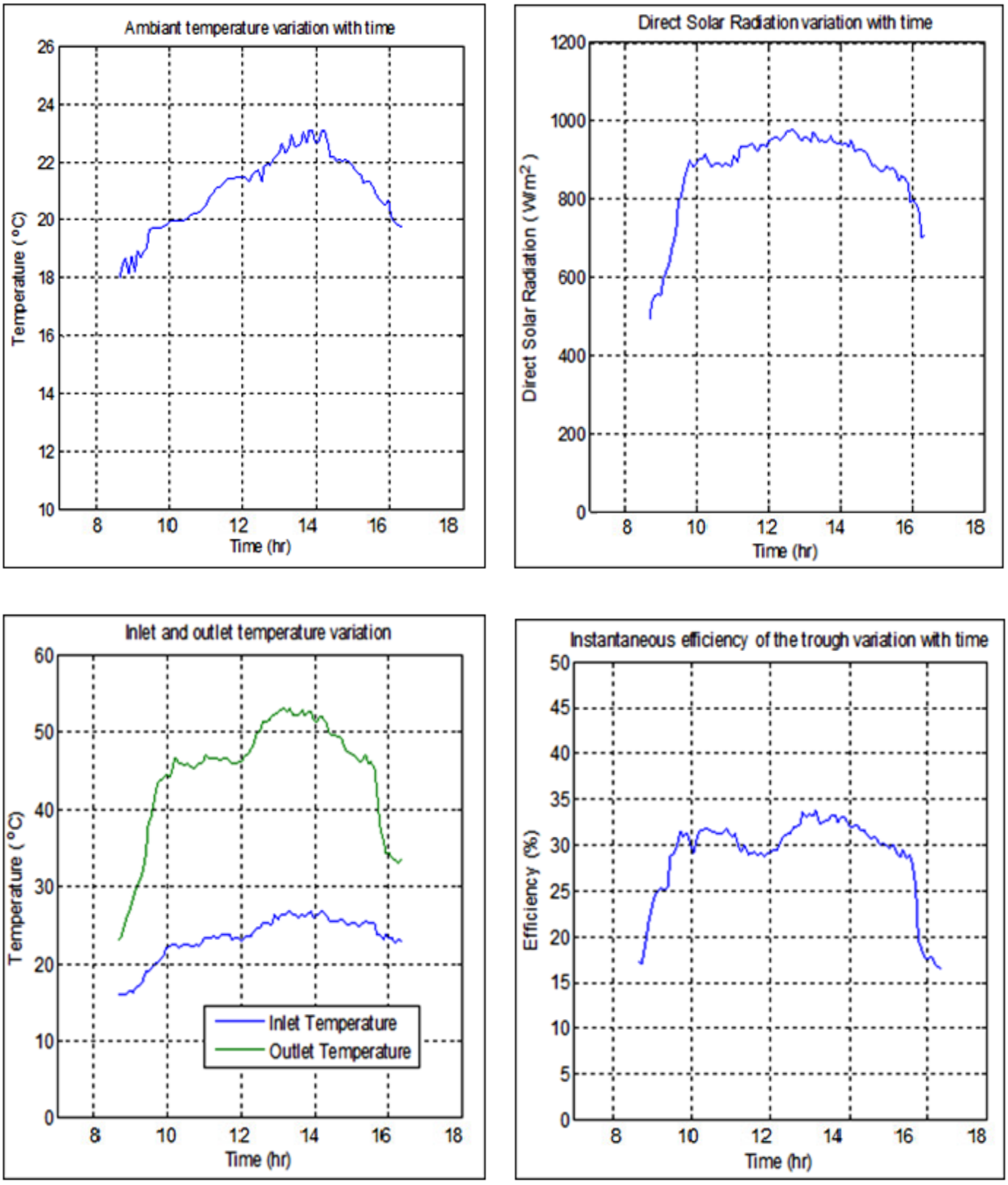

Figure A.3 Graphical representation of the test data collected on November 25, 2011

B. Ambient Temperature, Direct Solar Radiation, Inlet and Outlet Temperature of the Water and Efficiency Graphs for Aluminum Absorber Tube

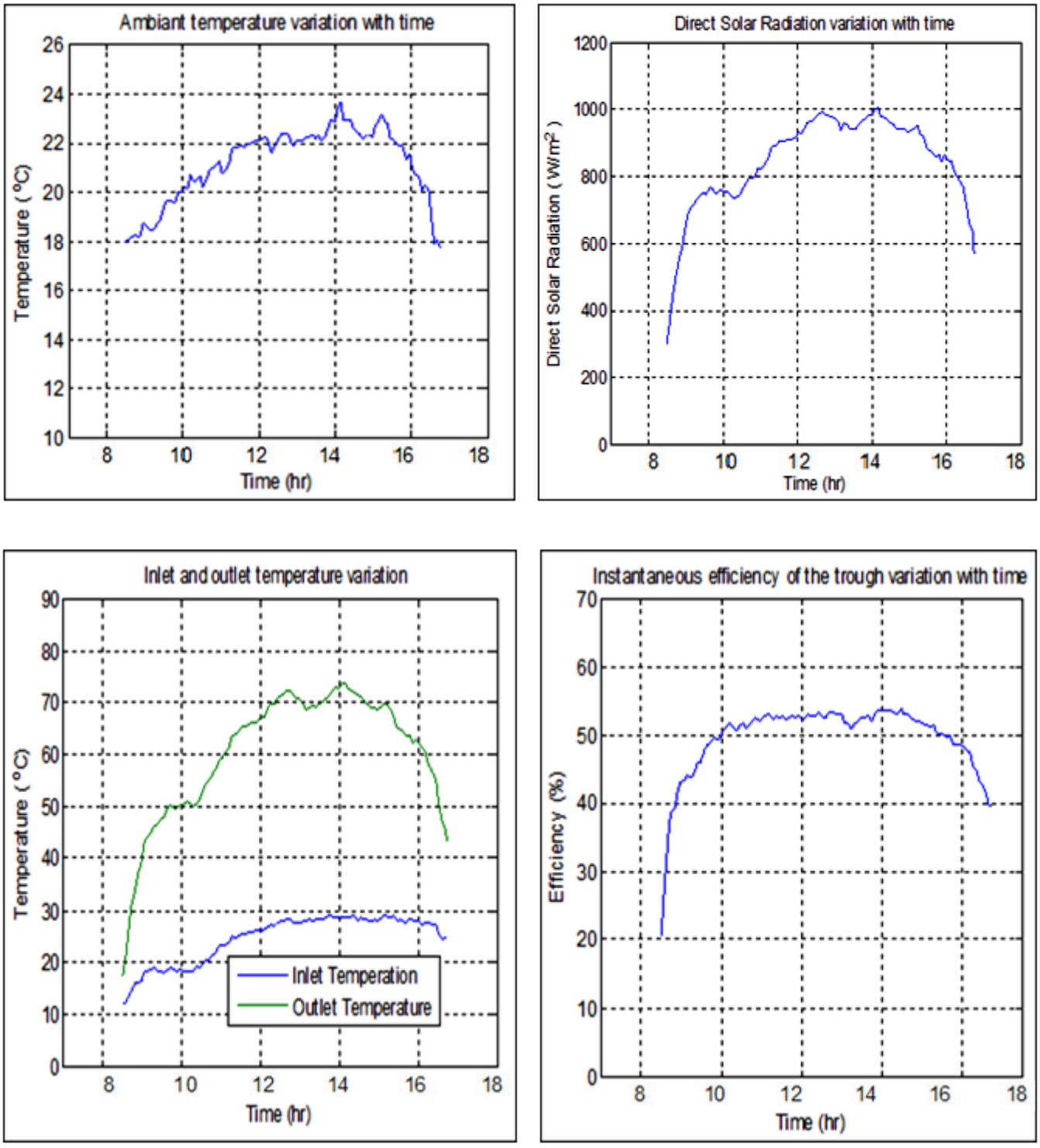

Figure B.1 Graphical representation of the test data collected on November 29, 2011

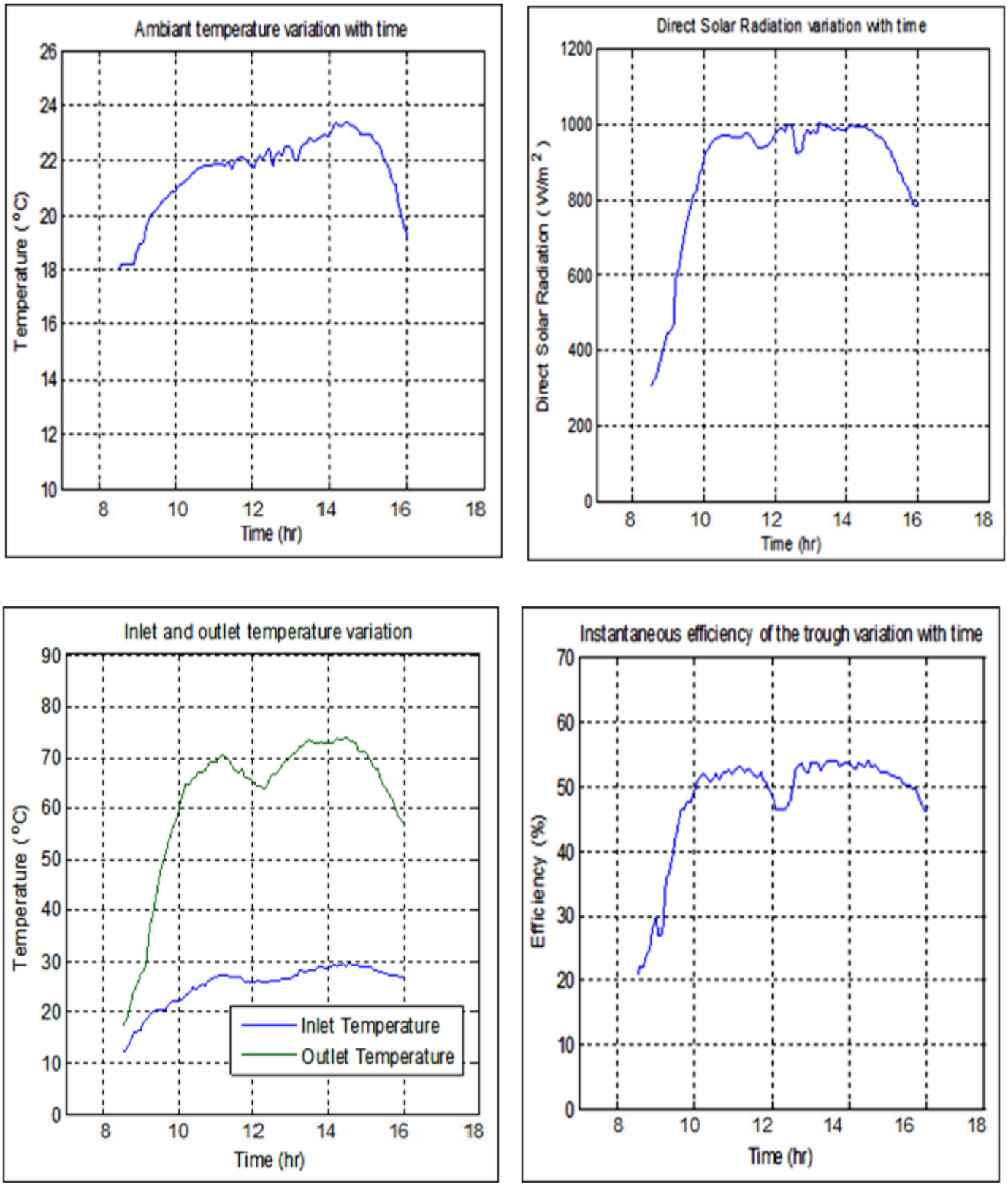

Figure B.2 Graphical representation of the test data collected on December 01, 2011

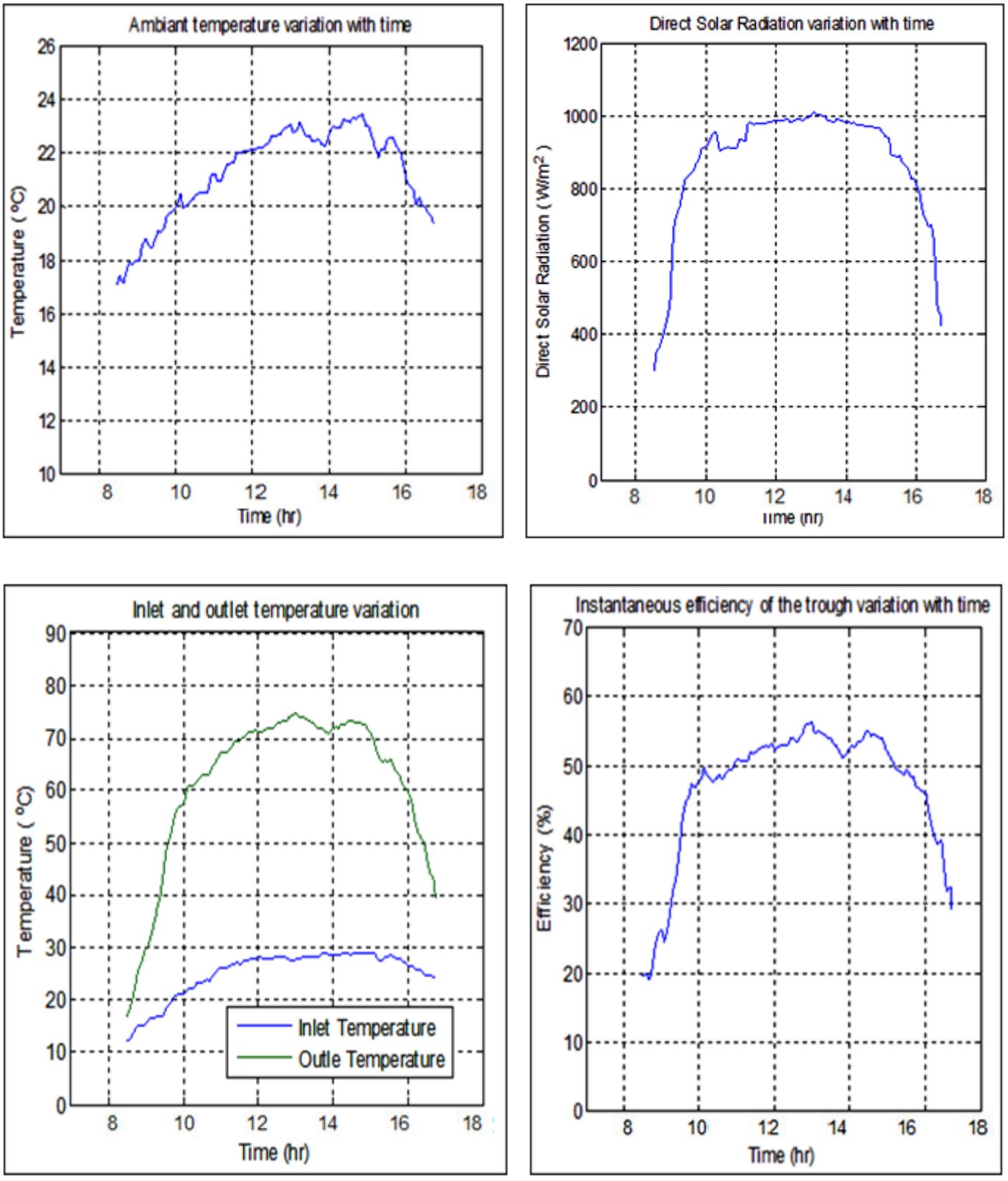

Figure B.3 Graphical representation of the test data collected on December 06, 2011

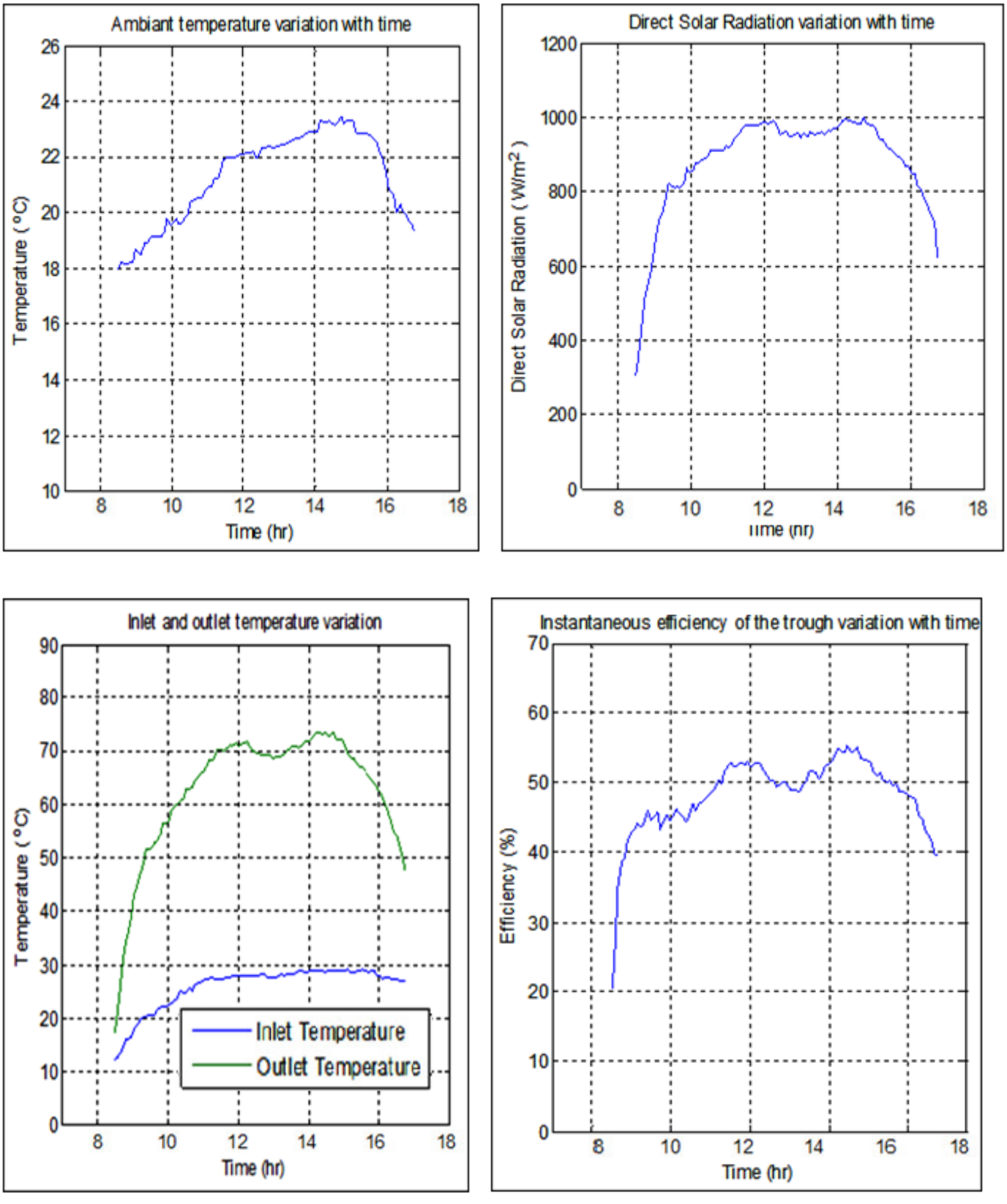

Figure B.4 Graphical representation of the test data collected on December 08, 2011

C. MATLAB Code for analytical analysis

```
%*************************************************************************
% Matlab program used to determine the outlet temperature of the
% parabolic %trough mathematically
%*************************************************************************

clear
clc
format short g

%*************************************************************************
%
% Measured time value in hours
%*************************************************************************

t=[2.5 2.5738 2.6558 2.7378 2.8198 2.9018 2.9838 3.0658 3.1478 3.2298...
   3.3118 3.3938 3.4758 3.5578 3.6398 3.7218 3.8038 3.8858 3.9678 4.0498...
   4.1318 4.2138 4.2958 4.3778 4.4598 4.5418 4.6238 4.7058 4.7878 4.8698...
   4.9518 5.0338 5.1158 5.1978 5.2798 5.3618 5.4438 5.5258 5.6078 5.6898...
   5.7718 5.8538 5.9358 6.0178 6.0998 6.1818 6.2638 6.3458 6.4278 6.5098...
   6.5918 6.6738 6.7558 6.8378 6.9198 7.0018 7.0838 7.1658 7.2478 7.3298...
   7.4118 7.4938 7.5758 7.6578 7.7398 7.8218 7.9038 7.9858 8.0678 8.1498...
   8.2318 8.3138 8.3958 8.4778 8.5598 8.6418 8.7238 8.8058 8.8878 8.9698...
   9.0518 9.1338 9.2158 9.2978 9.3798 9.4618 9.5438 9.6258 9.7078 9.7898...
   9.8718 9.9538 10.0358 10.1178 10.1998 10.2818 10.3638 10.4458 10.5278...
   10.6098 10.6918 10.741];

%*************************************************************************
% Measured inlet temperature value in degree centigrade
%*************************************************************************

Ti=[14.997918 17.230284 18.16999 18.199949 18.172738 18.242723 18.689153...
    19.527773 19.507773 19.877773 20.02467 20.068578 20.163765 20.334995...
    20.506225 20.621455 20.722685 20.823915 20.925145 21.02637 21.127605...
    21.228835 21.330065 21.447295 21.568525 21.689755 21.754985 21.78421...
    21.795445 21.806675 21.819905 21.851135 21.864365 21.865595 21.86682...
    22.352675 22.364105 22.375535 22.3109965 22.33313 22.3552825 22.3774...
    22.399568 22.421713 22.443854 22.465997 22.48814 22.510283 22.532426...
    22.5545695 22.57671 22.598855 22.620998 22.64314 22.665284 22.687427...
    22.7095705 22.73171 22.753856 22.775999 22.77814 22.780285 22.782428...
    22.784571 22.786714 22.788857 22.791000 22.79314 22.795286 22.797429...
    22.799572 22.801715 22.803858 22.806001 22.80814 22.810287 22.812430...
    22.814573 22.816716 22.818859 22.8210025 22.8231 22.843716 22.830284...
    22.811685 22.810342 22.78999 22.60065585 22.5031 22.200969 21.976264...
    21.502832 20.880386 20.732447 20.584508 20.00365 20.28863 20.0340691...
    19.927520 19.8209709 19.71442183 19.60787274];

%*************************************************************************
% Measured outlet temperature value in degree centigrade
%*************************************************************************

Tom=[14.80474576 21.65725608 28.53758312 32.64839732 32.55282328...
     33.93647752 36.64682232 37.75716712 37.96751192 39.37143256...
     42.04494576 42.87127816 43.99761056 42.98394296 45.83027536...
```

```
    46.00766078 47.92294016 47.85087256 48.30120496 49.05153736...
    49.50186976 48.65220216 50.30253456 50.86926696 50.31559936...
    51.09979318 51.50026416 52.00081397 52.0982929 51.498990145...
    52.31863376 51.55756616 51.96114986 52.20223096 52.90929634...
    53.37009576 53.14722816 53.52436056 53.90149296 54.23426254...
    54.35013578 54.49889016 54.20069223 54.60919553 54.77588736...
    54.56661976 55.06615216 55.03092846 55.13201696 55.23310547...
    55.7934194 55.53528247 54.73637098 54.537459482 55.23854799...
    55.35229944 55.39076161 55.40419772 55.11441858 55.32463944...
    55.42486031 55.95081171 55.3625302 55.28255229 55.19255806 ...
    55.39925529 55.22547829 55.15427151 55.3825376 55.27750529 ...
    54.37296417 55.16932223 55.05864347 54.94141723 54.62411948...
    54.76670058 54.52418922 54.20040778 54.37043665 54.33298551...
    53.97374375 53.55643239 53.22752102 53.30260965 53.24649829...
    52.79038692 51.15067555 51.33416419 50.68765282 49.63314146...
    48.95943009 48.69371872 48.23760736 46.40749599 46.50938463...
    45.49567326 44.18276189 44.43665053 43.62533916 41.5848278 ...
    38.36071643 38.02624961];

%************************************************************************
% Measured ambient temperature in degree centigrade
%************************************************************************

Ta=[17.997918 18.230284 18.16999 18.199949 18.172738 18.242723 18.689153...
    19.527773 19.507773 19.877773 20.024674 20.068578 20.163765 20.33499...
    20.506225 20.621455 20.722685 20.823915 20.925145 21.026375 21.12760...
    21.228835 21.330065 21.447295 21.568525 21.689755 21.754985 21.78421...
    21.795445 21.806675 21.819905 21.851135 21.864365 21.865595 21.86682...
    21.868055 21.899285 21.930515 21.961745 21.992975 22.024205 22.05543...
    22.086665 22.117895 22.149125 22.180355 22.211585 22.242815 22.27404...
    22.295275 22.316505 22.337735 22.358965 22.318415 22.359845 22.40127...
    22.442705 22.484135 22.525565 22.566995 22.608425 22.649855 22.69128...
    22.748715 22.830145 22.918575 22.901000 22.861435 22.905286 22.99742...
    22.929572 22.927155 22.958585 22.890015 22.7981445 22.96028 22.82430...
    22.8910873 22.97442 22.9840105 22.970579 22.8571475 22.8437 22.8302 ...
    22.8116853 22.810342 22.78999 22.600655 22.503127 22.200969 21.97626...
    21.5028325 20.880386 20.732447 20.584508 20.0036569 20.28863 20.0340...
    19.92752001 19.82097092 19.71442183 19.60787274];

%************************************************************************
% Measured direct solar radiation in watt per meter square
%************************************************************************

I=[302.32 350.31 390.56 410.52 445.63 490.123 510.24 590.32 620.9 640.85...
   760.52 790.59 799.85 810.23 845.23 850.23 862.35 879.32 892.5 906.972...
   905.54 910.748 915.74 920.497 915.481 922.256 956.876 960.342 956.23 ...
   987.54 990.87 992.45 993.34 1000.78 999.755 1001.736 1004.341 1011.58...
   1020.237 1016.7 1022.86 1019.775 1004.803 1026.089 1037.0605 1030.032...
   1029.003 1035.975 1030.946 1021.918 1022.889 1033.861 1040.83 1035.80...
   1046.7755 1045.74 1040.7185 1038.69 1030.66 1028.633 1032.60 1038.576...
   1041.5475 1049.519 1044.49 1040.462 1043.433 1044.405 1047.37 1043.34...
   1045.319 1040.29 1043.262 1042.234 1044.205 1040.17 1037.1485 1018.12...
   1020.0915 1028.063 1015.034 1002.006 989.977 999.949 992.9205 989.892...
   994.8635 989.835 986.8065 970.778 967.7495 975.721 948.6925 900.664  ...
   902.63 879.607 835.57 788.21 770.52 733.0463 700.517 667.98];
```

```
%*************************************************************************
% Constants Values
%*************************************************************************

Mw=0.2;           % Mass flow rate of the water in the absorber tube [Kg/s]
kp=16;            % Thermal Conductivity of Pipe Material (w/m.K)
emi=0.91;         % Emittantce of black coated  steel absorber tube
Vw=2.5;           % Wind speed [m/s]
kva=1.589*(10^-5);% Kinematic viscosity of wind [m^2/s]
Ka=0.0263;        % Thermal conductivity of air [W/mK]
sigma=5.67*10^-8; % Stefan  Boltzmann Constant [W/mK^4]
Ts=50;            % Maximum average absorber tube temperature [0C]
pra=0.707;        % prantle Number at ambient temperature
prt=0.7;          % prantle Number at pipe surface temperature

%*************************************************************************
% Properties of saturated liquid water
%*************************************************************************

cp=4181.8;        % Specific heat capacity [J/kgK]
rho=1000;         % Density [kg/m^3]
k=0.597;          % Thermal conductivity [W/mK]
pr=7.02;          % Prandle number
kvw=1.006*10^-6;  % Kinematic viscosity in m^2/s

%*************************************************************************
% Absorber tube size
%*************************************************************************

Dip=0.034;        % Inner Diameter of Pipe [m]
Dop=0.04;         % Outer Diameter of Pipe [m];
L=5;              % Overall Heat Transfer Length of the absorber tube [m]

%*************************************************************************
% Collector trough size
%*************************************************************************

Lc=5;             % Length of the collector field [m]
Wc=1.70;          % Width of the collector field [m]

%*************************************************************************
% Collector area calculation
%*************************************************************************

Ar=pi*Dop*L;      % Circumfrancial area of the Receiver tube
Ac=pi*(Dip^2)/4;  % Cross sectional  Flow area of absorber tube
Aa=(Wc-Dop)*Lc;   % Area of the collector field taking into account of
                  % shading of the absorber tube in the middle
```

```
%*************************************************************************
% Fluid velocity calculation
%*************************************************************************

V=Mw/(rho*Ac);

%*************************************************************************
% Reynolds number calculation for wind across absorber tube
%*************************************************************************

Rea=(Vw*Dop)/kva;

%*************************************************************************
% Nusselt number calculation
%*************************************************************************

% For flow of air across a single tube in the outdoor environment

if (Rea<40)
    Nua= 0.75*(Rea^0.4)*(pra^0.37)*(pra/prt)^0.25;
elseif (40<Rea<10^3)
        Nua= 0.51*Rea^0.5*pra^0.37*(pra/prt)^0.25;
elseif (10^3<Rea<2*10^5)
        Nua= 0.26*Rea^0.6*pra^0.37*(pra/prt)^0.25;
else
        Nua= 0.076*Rea^0.7*pra^0.37*(pra/prt)^0.25;
end

%*************************************************************************
% Wind convection coefficient
%*************************************************************************

haconv=Nua*(Ka/Dop);

%*************************************************************************
% Nusselt number for the water
%*************************************************************************

Nuw=4.36;

%*************************************************************************
% Water convection coefficient
%*************************************************************************

hwconv=Nuw*(k/Dip);

%*************************************************************************
% Convection heat transfer flux
%*************************************************************************

qconv=haconv*pi*Dop*(Ts-Ta);
```

```
%*************************************************************************
% Radiation heat transfer flux
%*************************************************************************

qrad=sigma*pi*Dop*emi*(Ts.^4-Ta.^4);

%*************************************************************************
% Heat trnsfer loss coeficent
%*************************************************************************

a=1./qconv+1./qrad;
U=1./a;

%*************************************************************************
% Over all heat transfer coeficent
%*************************************************************************

Uov=(1./U)+(Dop/(hwconv*Dip))+((Dop*log(Dop/Dip)/(2*kp)));

%*************************************************************************
% Collector efficency factor
%*************************************************************************

Fcef=(1./U)./Uov;

%*************************************************************************
% Collector removal factor
%*************************************************************************

b=(Mw*cp./(Ar*U));
c=(Ar.*U.*Fcef/(Mw*cp));
Fr=a.*(1-exp(-c));

%*************************************************************************
% The actual useful energy collected by fluid
%*************************************************************************

qab=I;
d=Aa*qab;
Ts=Ti*2;
e=Ar.*U.*(Ti-Ta);
qused=Fr.*((d-e)/L);

%*************************************************************************
% Exit temperature of the water
%*************************************************************************

To=Ti+(qused/(Mw*cp*3.9*10^-5));
```

```
%*************************************************************************
% Plot results
%*************************************************************************

plot(t,Tom,t,To);
grid on
axis tight
axis ([1 12 0 80])
xlabel('Time, (hr)');
ylabel('Temperature ( ^oC )');
title(' Comparition between the mathematical model and test rsult');
```

D. The parabolic trough dimension

Diameter	170.00
Depth	45.00
Focal Length	40.14
Volume	510705.16
Area	22698.01

X	Y
-85.00	45.00
-74.38	34.45
-63.75	25.31
-53.13	17.58
-42.50	11.25
-31.88	6.33
-21.25	2.81
-10.63	0.70
0.00	0.00
10.63	0.70
21.25	2.81
31.88	6.33
42.50	11.25
53.13	17.58
63.75	25.31
74.38	34.45
85.00	45.00

E. Dimension and Detail Drawing of the Experimental Setup Components

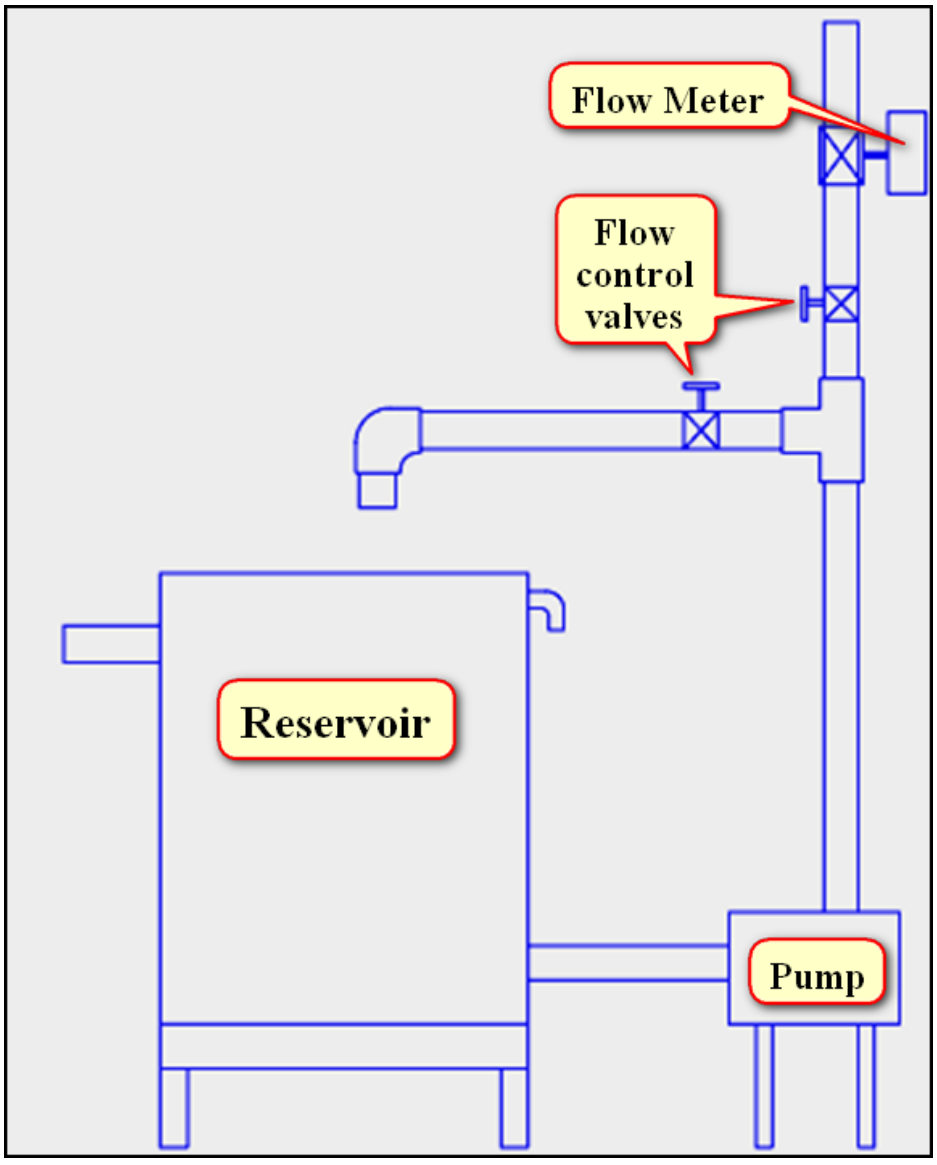

Figure C.1 Layout of the pumping and the flow control system

F. Subassembly Force Analysis of the Parabolic Support

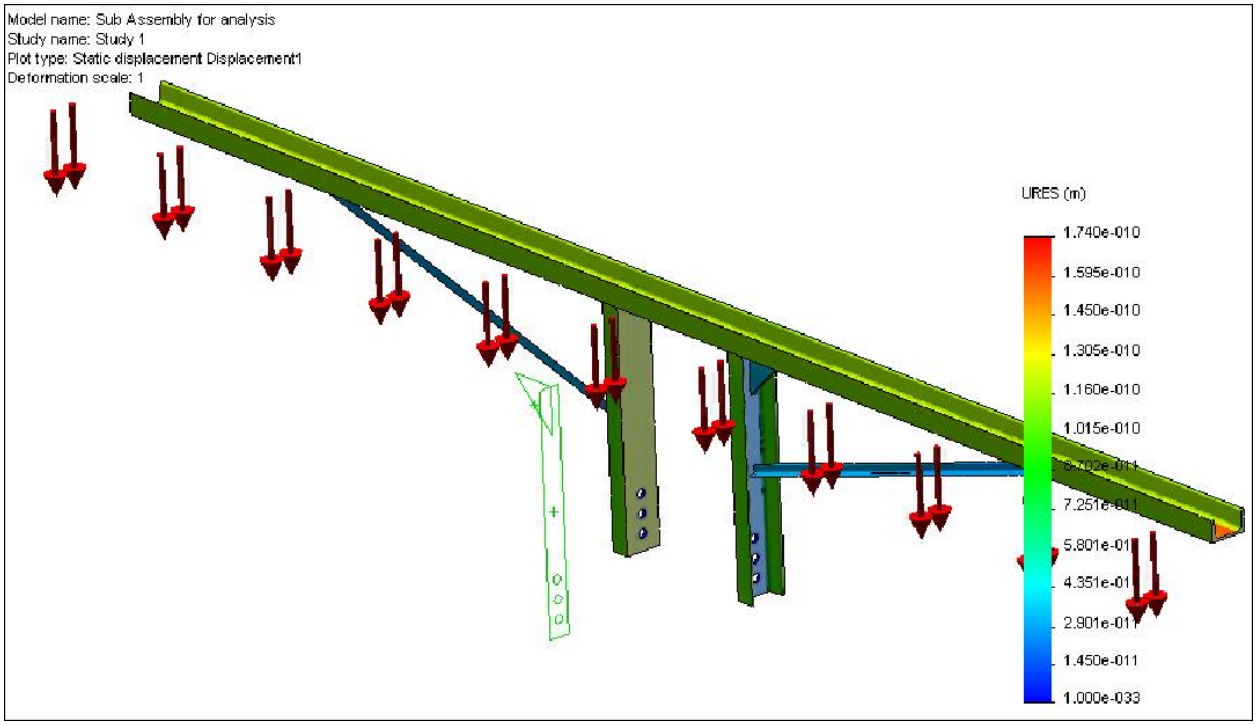

Figure E.1 Static distance displacement

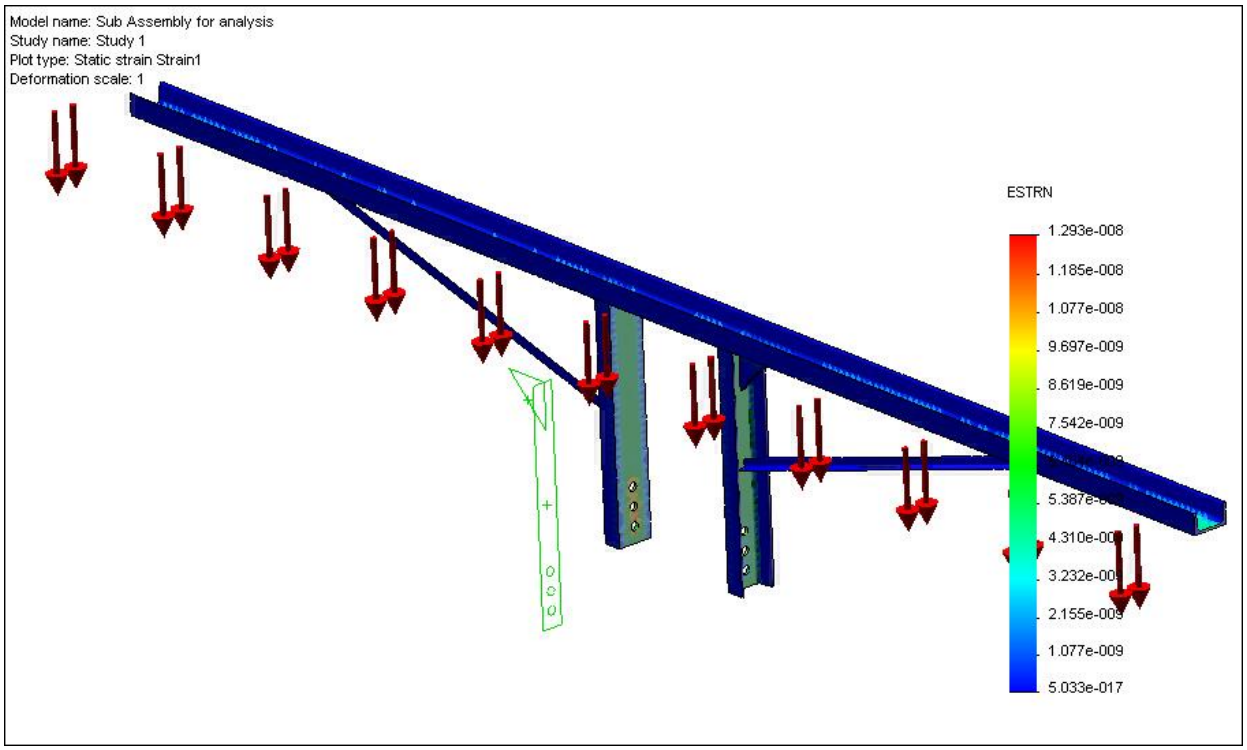

Figure E.2 Static strain

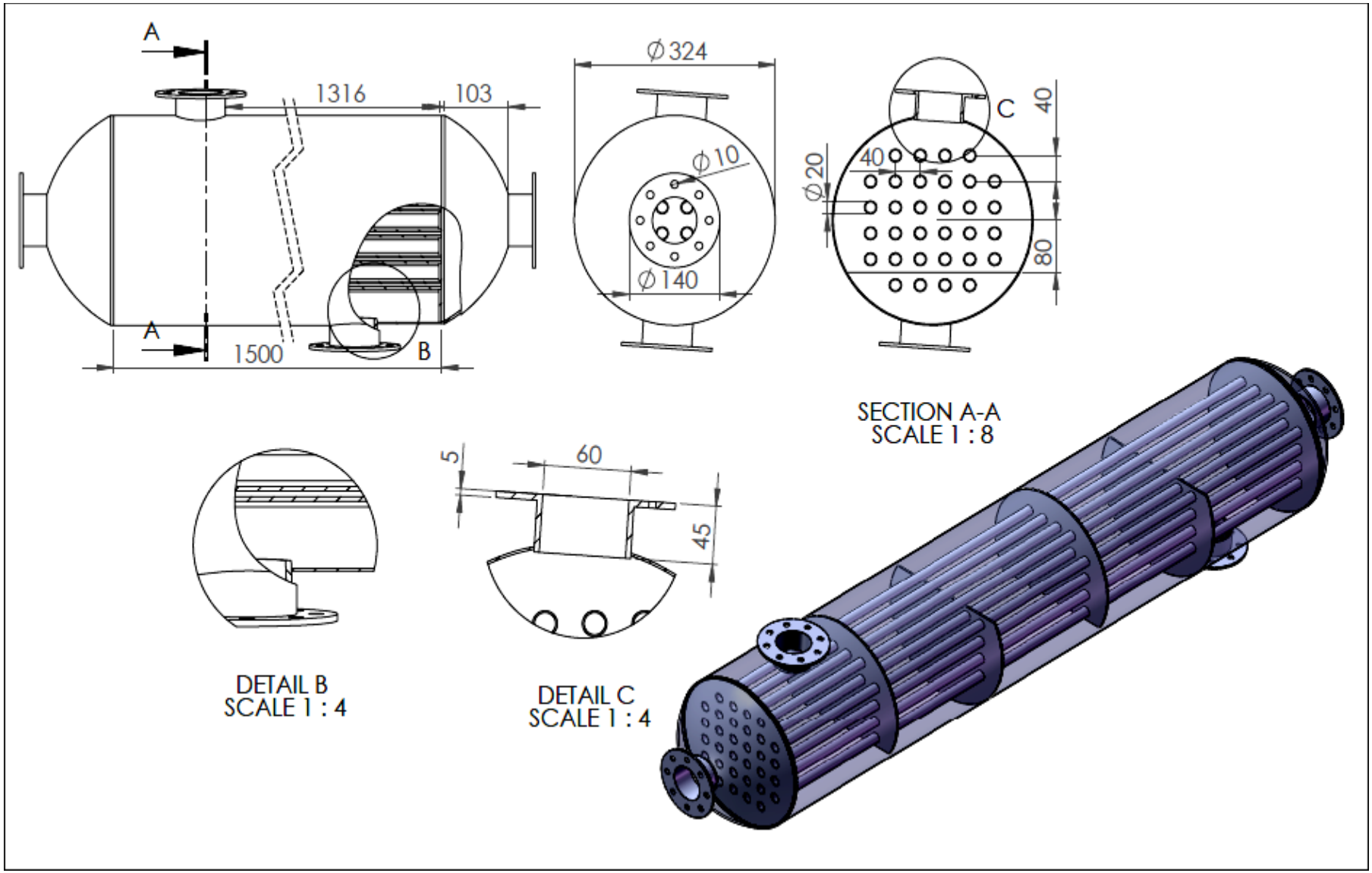

Figure C.2 Dimension and detail drawing of the heat exchanger

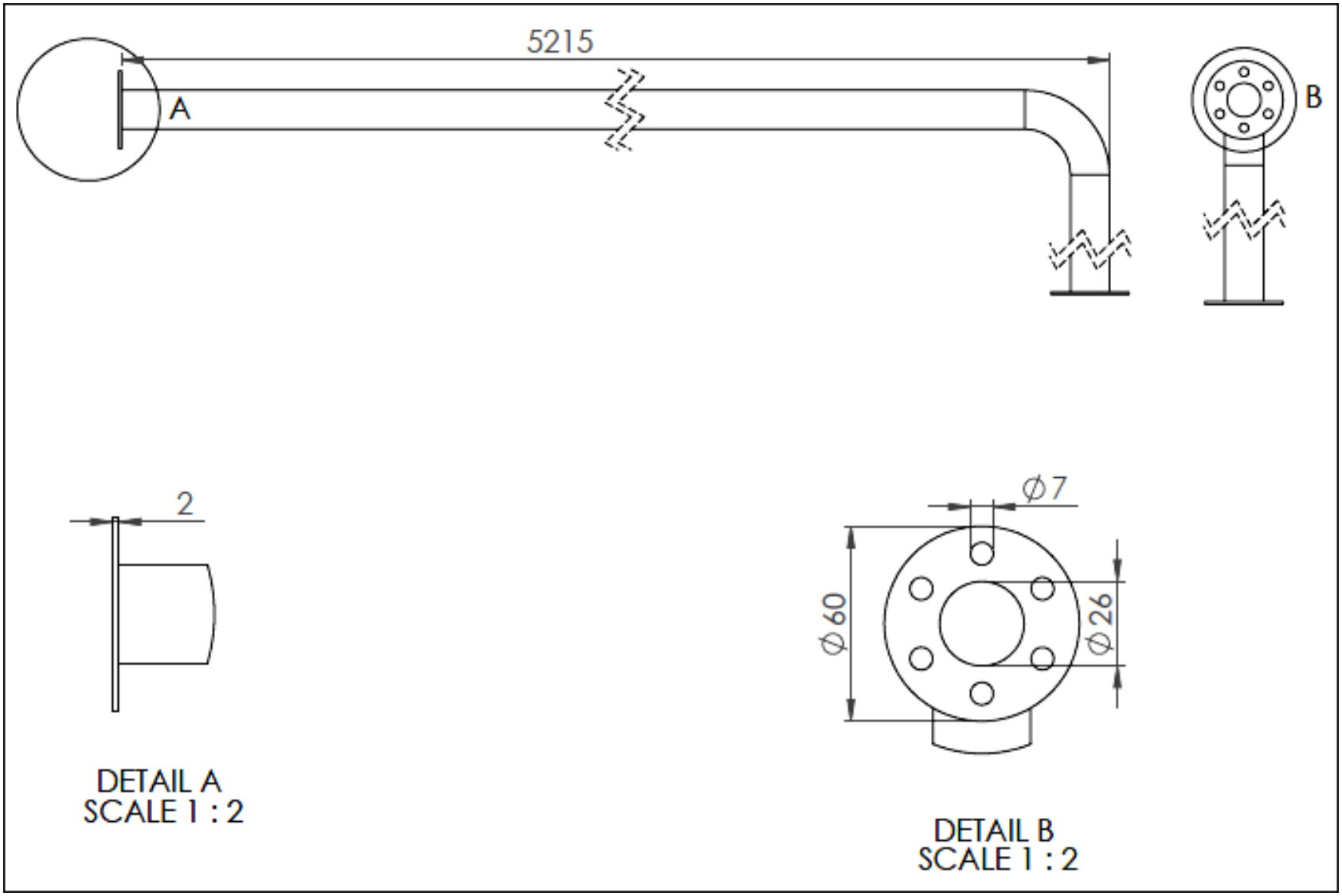

Figure C.3 Dimension and detail drawing of the absorber tube

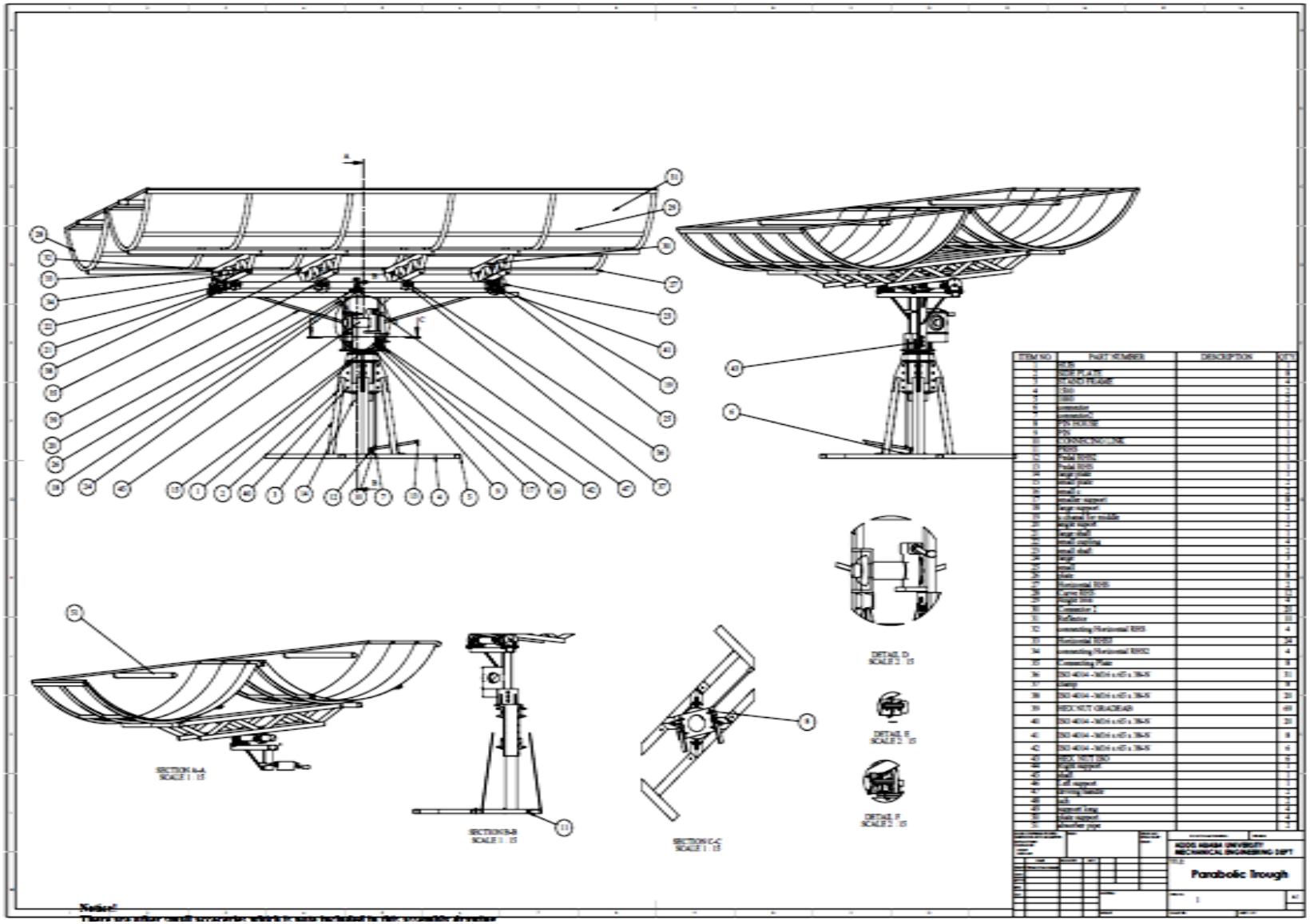

Figure C.4 Assembly drawing of the parabolic trough

Bibliography

1. **Development, Ethiopian Rural Energy.***Solar and Wind Energy Utilization and Project Development Scenarios.* October 2007.

2. **Energy, US department of.** Energy basics. *www.eere.energy.gov.* [Online] http://www.eere.energy.gov/basics/renewable_energy/solar_resources.html#.

3. **International, Pilkington Solar.***Status Report on Solar Trough Power Plants.* Cologne : Pilkington Solar International GmbH, 1996. ISBN 3-9804901-0-6.

4. **Prairie, M.***Overview of Solar Thermal Technology.* 200.

5. **Ruiz, Pablo Fernández.***European Research on.* Belgium : Luxembourg, 2004.

6. http://www.encyclopedia.com/article-1G2-3451200023/solar-energy.html. [Online]

7. **Church, William Conant.***The Life of John Ericsson.* New York : Charles, 1890.

8. *solar energy installations for pumping irrigation water.* **Pytlinski, JT.** 1978.

9. **Kreider JF, kreith F.***Solar energy handbook.* New York : McGraw Hill, 1981.

10. **LC, Spencer.***A comprehensive review of small solar-powered heat engines.* 1989.

11. *Terrestrial solar thermal power plants: on the verge of comercialization.* **Romero M, Martinez D, Zarza E.** 2004.

12. *Exergy analysis of low and high temperature.* **OZTURK, Murat.** Turkey : Department of Physics, Science-Literature Faculty, Suleyman Demirel University,.

13. **Sadik Kakac, Hongtan Liu.***Heat Exchangers: Selection, Rating and Thermal Design.* s.l. : CRC Press, 2002. ISBN0849309026..

14. **Perry, Robert H. and Green, Don W.***Perry's Chemical Engineers' Handbook.* s.l. : McGraw-Hill, 1984. ISBN 0-07-049479-7..

15. http://www.engineeringpage.com/technology/thermal/fouling_factors.html. *http://www.engineeringpage.com/.* [Online]

16. **DONALD R. PITTS, LEIGHTON E. SISSOM.***THEORY AND PROBLEMS of HEAT TRANSFER.* s.l. : McGraw-Hill, 1998.

17. **AMERICAN SOCIETY OF HEATING, REFRIGERATING AND air conditioing engineers.***method of testing to determine the thermal performance of solar collector.* Atlanta : tullier circle, 1991. issn 1041-2336.

18. **Frank M.White.***Fluid Mechanics.* Boston : McGraw-Hill, 1991.

19. *Ashrae Handbook 2001.*

20. **Solar Measuring Device.***MacSolar Manual.*

21. **DEVICES, DELTA-T.***User Manual for Temperature Probes.* Cambridge : s.n., Nov 1996.

22. **Corporation, National Instruments.***USER GUIDE AND SPECIFICATIONS NI cDAQ-9172.* Texas : s.n., 2008. 371747F-01.

23. **corporation, National instrument.***LabVIEW Fundamental.* Texas : s.n., 2007.

24. *Design, manufacture and testing of fiberglass reinforced.* **A. Valan Arasu *, T. Sornakumar.** 10, Tamilnadu, India : science direct, 2007, Vol. 81. ISSN: 0038092X.

25. **Forristall, R.***Heat Transfer Analysis and Modeling of a Parabolic Trough Solar Receiver Implemented in Engineering Equation Solver.* Colorado : s.n., 2003. DE-AC36-99-GO10337.

26. **Witt, Frank P. Incopera David P. De.***Fundamental of heat and Mass Transfer.*

27. **VELAUTHAM, SANJAYAN.***RENEWABLE ENERGY POWERED ORGANIC RANKINE CYCLE.* 2006.

28. *A Concept for Future Parabolic Trough Based Solar Thermal Power Plants.* **Jürgen Birnbaum a, Markus Eck b, Markus Fichtner a, Tobias Hirsch b,.** Berlin : ICPWS XV, 2008.

29. *Solar Parabolic Trough* . 1988.

31. http://en.wikipedia.org/wiki/Parabolic_trough. [Online]

32. http://thefraserdomain.typepad.com/energy/2005/09/about_parabolic.html. [Online]

33. **Norton, Brian.** http://www.thermopedia.com/content/1136/. *SOLAR ENERGY.* [Online]